INVESTIGATION OF VIBRATIONAL ENERGY TRANSFER IN CONNECTED STRUCTURES

FINAL REPORT

NOR 73-105 JULY 1973

Prepared for
George C. Marshall Space Flight Center
National Aeronautics and Space Administration
Huntsville, Alabama

NASA Contract NAS8-28171
(March 1972 - June 1973)

NORTHROP CORPORATION, AIRCRAFT DIVISION
3901 West Broadway
Hawthorne, California 90250

Chintsun Hwang, W. S. Pi (Authors)

INVESTIGATION OF VIBRATIONAL ENERGY TRANSFER IN CONNECTED STRUCTURES

FINAL REPORT

NOR 73-105 JULY 1973

Prepared for
George C. Marshall Space Flight Center
National Aeronautics and Space Administration
Huntsville, Alabama

NASA Contract NAS8-28171
(March 1972 - June 1973)

NORTHROP CORPORATION, AIRCRAFT DIVISION
3901 West Broadway
Hawthorne, California 90250

Chintsun Hwang, W. S. Pi (Authors)

CONTENTS

LIST OF ILLUSTRATIONS

LIST OF ILLUSTRATIONS (continued)

SUMMARY

The report covers the results of an analytical and experimental investigation on the vibrational energy transfer between connected substructures under random excitation. In the analytical area, the basic foundation and assumptions of the Statistical Energy Analysis (SEA) method, a major tool in random response analysis of structures, were examined and reviewed. A new SEA formulation based on the strong coupling condition of the substructures was carried out and presented. Also presented were the results of vibration energy transfer study based on the wave equations applied to connected structures. In the experimental phase, three simple structural models were fabricated and tested. Additional tests were performed on selected substructures which formed parts of the test models. The test results were presented and evaluated against the analytical data.

The work described in this report was carried out at Northrop Corporation under the sponsorship of NASA Marshall Space Flight Center. The contract number was NAS8-28171. The program was monitored by Drs. Hugo Steiner and Rudolph Glaser of NASA, under the overall direction of Mr. Richard Schock. The experimental work was carried out by Mr. Paul Finwall of Northrop. Dr. Paul Seide participated in the analytical work which is described in the Appendices of the report.

INTRODUCTION

This report covers the analytical and experimental results obtained in the conduction of the Contract NAS8-28171 entitled "Investigation of Vibrational Energy Transfer in Connected Structures." The purposes of the subject program are (1) to investigate the high-frequency energy transfer mechanism between two connected structures, (2) to determine the major parameters that affect the energy transfer, and (3) to determine the parameters and their influences to the application of the statistical energy analysis (SEA) method to the structures. To accomplish the program tasks, coordinated experimental and analytical methods were applied. Specifically, conditions were established under which the SEA method can be used to predict the vibrational energy transmission in two connected structures. Guidelines were established. A new analytical formulation was introduced to cover the cases where the substructure intercoupling was strong. In addition, analytical and experimental definitions of the key parameters relating to the application of SEA were examined and applied to structures under high-intensity acoustic or random mechanical loads.

The statistical energy analysis (SEA) method was first applied to the structural vibration problem as an extension of the room acoustics approach in acoustic engineering. Developed in the past decade by Lyon, Smith, Dyer and associates (References 1-15), the method considers the linear responses of multimodal structures and the resulting energy flow among the modes of two or more sets of substructures. The modes of a substructure are called a subset. Because of the complexity of the high-frequency modal data of structures and the desire to have a simple tool for engineering application, a number of assumptions are made in the formulation of the SEA. These assumptions, together with the related parameters which affect the validity of the assumptions, are considered to be the key points in determining the applicability of the SEA method to high-frequency vibrational energy transfer problems for connected structures.

In addition to the fundamental derivations of Lyon and associates described above, Zeman and Bogdanoff presented an elaborate formulation of SEA using technical terms and analytical procedures commonly used by structural dynamicists (Reference 16). Zeman's derivation deviates from the original SEA formulation in some details relating to the coefficients of dissipation functions, etc. While the end results are essentially the same as compared to the Lyon and Maidanik derivation (References 1, 11), Zeman's derivation and its reasoning are helpful in making the SEA method more comprehensible to the structural dynamicists.

The SEA is based on the power flow between groups of linear oscillators. Between two groups, the power flow is established by a set of dynamic equations. Each equation represents the mode response of one oscillator and its weak coupling with one or more oscillators from the other group. The coupling parameters are classified into inertia, damping, and spring types. For a stationary process, the assumption that the damping coupling parameters for any two oscillators are equal in magnitude and opposite in sign gives rise to a condition called gyroscopic coupling. Specifically, a gyroscopic coupling element is defined as one which produces a negative coupling force on Oscillator No. 2 due to a positive velocity of Oscillator No. 1 if the velocity results in a positive force on Oscillator No. 1 due to a positive velocity of Oscillator No. 2 (Reference 11). The gyroscopic coupling force on Oscillator No. 2 due to a positive velocity of Oscillator No. 1 if it results in a positive force on Oscillator No. 1 due to of the power flow coefficient under the weak gyroscopic coupling condition.

Consider a narrow frequency band for which the modal density of the substructure may be determined either experimentally or analytically. In SEA, it is assumed that the input power spectrum is fairly flat within the frequency band. Each linear oscillator which is directly excited by the external source is considered to be subject to a "thermal bath." Under this condition, the modal energies of all the oscillators whose natural frequencies lie within the narrow band are fairly equal and may be represented by an average value. A final formulation of the SEA involves the response levels of two or more substructures (which may be either connected substructures or a structure and a reverberant acoustic field) based on the average modal energies of the externally excited and the coupled oscillators.

The SEA method has the potential of being a powerful engineering tool because of its generality and, specifically, its averaging technique, where the structural and response details are considered only in a broad sense. The method may also be misused if applied indiscriminately. In view of this background, the subject program investigates the key factors affecting the SEA, and specially the high frequency vibration energy transmission, so that the applicability of the method may be clearly defined. Furthermore, new analytical derivations are established which tend to clarify certain aspects relating to the formulation and application of the SEA.

As part of the engineering method development, a user-oriented preliminary test procedure is developed in the application of SEA. The purpose of the preliminary procedure is to ensure that the structural model and the substructure definition implemented by the user will satisfy the basic assumptions of SEA. The same procedure also yields guideline indications when the limits of the application of SEA have been surpassed due to such factors as substructure design, the operating frequency range, and the like.

In the experimental phase of the investigation, three structural models were fabricated and tested in order to extract the maximum amount of information from the test program. The models were designed to consist of connected substructures with typical variations in interface configurations, modal density distributions, vibrational energy transmission paths, and degrees of modal energy diffusion.

The remaining text of this report follows the logical sequence of development. After a general discussion, the basic formulation of SEA is presented where the degree of coupling of the connected structural sets is discussed. This is followed by a new derivation on the SEA applicable to the strong coupling case. The subsequent sections cover the user guidelines for SEA and the analytical formulations involving various types of connected structures. The text is concluded with the presentation and discussion of the experimental data.

DISCUSSION OF THE PROBLEM

The current investigation emphasizes a detailed understanding of the mechanism of energy transmission at the interface of connected structures. In general, the high-frequency energy transmission is in the form of bending and shear waves for thin-skinned space vehicle structures. The tension/compression waves may be involved in the picture, but they are considered to contribute minimally to energy transfer. The major parameters affecting the magnitudes and modes of energy transfer include the makeup of the substructures, their boundary conditions, the interface configurations (length, geometry, method of fabrication, etc.), the substructure and coupling loss factors, the relative amplitudes of the modal densities of the connected substructures, and the location and type of loading. In order to sort out the various parameters and to reach a rational solution of the complex problem, a number of simple test models featuring certain basic similarities were used. The details of the models will be described in a later section.

In a given connected structure, the degree of modal diffusion depends greatly on the wave length relative to the characteristics dimensions of the substructure and, for a thin-skinned substructure, on its thickness. As the stress waves propagate in the structure, they meet the structural boundaries and interfaces where the waves are partially or totally reflected according to the boundary geometry and the constraint conditions. The infinitely many possibilities of these wave propagations and reflections cause a randomly distributed wave pattern (i.e., a high degree of modal diffusion). For waves of medium or long length, the degree of diffusion will affect the energy transfer through an interface because the directional properties of the waves determine the amount of energy transmitted to the neighboring structure. The effect is believed to be less pronounced for shorter-length waves.

To confirm the energy transfer mechanism in a structural interface, analytical methods are applied using the classical equations of wave propagation. In a previous work by Lyon and Eichler (Reference 4), a set

of flexural wave equations was established. Simplified boundary conditions were applied to the interface. The energy transfer rate through the interface was estimated based on the assumption of thoroughly diffused waves.

In the current program, more elaborate equations (e.g., those given by Mindlin in Reference 50) and more complicated interface configurations are used. For shell-type structures, the curvature effect and the proper constraint at the interface are considered. Typical applications of the wave equations are described later in the report.

In previous work on the application of SEA, it was found that the weak coupling conditions are not always satisfied, depending on the frequency range and other pertinent factors (Reference 49). In addition to establishing the applicability of the SEA method for specific structures, alternative approaches are investigated and reported where non-weak intercouplings of substructures are involved.

To make the SEA method a usable tool for practicing engineers dealing with high-frequency vibrations of connected aerospace structures, it is desirable to have available general guidelines on the proper application of the method. The guidelines presented in this report take into consideration such structural parameters as coupling loss factors, damping loss factors, modal densities, etc. These guidelines also include preliminary test procedures which can be followed by practicing engineers. In the subsequent sections, the basic foundation of the SEA method, the applicability of the method to strongly coupled structures, and the guidelines and preliminary test procedures to the proper application of the SEA method are described in detail.

BASIC ASSUMPTIONS OF THE SEA METHOD

The theoretical foundation of the statistical energy approach to vibration analysis is that the steady-state time-average power flow from one mode to another is proportional to the difference between the time-average kinetic energies of the two modes provided that the following conditions are satisfied (References 1, 11):

1. The coupling between the two modes which satisfy the following set of equations is linear, weak, and conservative (gyroscopic).

$$\begin{aligned} m_1 (\ddot{y}_1 + \beta_1 \dot{y}_1 + \omega_1^2 y_1) + A \ddot{y}_2 + B_2 \dot{y}_2 + C y_2 &= f_1 \\ m_2 (\ddot{y}_2 + \beta_2 \dot{y}_2 + \omega_2^2 y_2) + A \ddot{y}_1 + B_1 \dot{y}_1 + C y_1 &= f_2 \end{aligned} \qquad (1)$$

   where m, β, ω are the mass, damping coefficient, and the natural frequency of the oscillators, respectively. The modal displacements are denoted by y. In Equation (1), the coupling parameters A and C represent the inertial and stiffness couplings, respectively. The coupling parameters B_1 and B_2 represent the gyroscopic coupling when $B_1 = -B_2$.

2. The forces f_1 and f_2 (see Equation (1)) acting on the two modes are uncorrelated and have spectra that are relatively flat within the frequency band encompassed by the resonances of the coupled system.

Furthermore, the steady-state time-average power flow from one set of modes to another is proportional to the difference between the set average modal kinetic energies of the two sets provided that either:

1. The mode-to-mode coupling is the same for all mode pairs, or,
2. All modes in each set have equal time-average kinetic energies. (Note that the members of each set are not coupled to each other.)

The coupling factor, applicable to set-to-set power flow is equal to the sum of all the mode-to-mode coupling factors.

For a given connected structure, the SEA method can be applied to predict the response levels under high frequency excitation. For this case, it is further required that the wave patterns are diffused, and the major wave lengths of interest are small compared with the characteristic dimension of the structure. Based on the above, the prerequisite conditions of applicability of the SEA to a connected structure may be restated in terms of the analytical formulations given below:

1. The generalized coordinates of displacements of the connected structural system satisfy the following set of equations:

$$\begin{cases} m_i(\ddot{x}_i + \beta_i\dot{x}_i + \omega_i^2 x_i) + \sum_{k=1}^{\bar{N}}\left[A_{ki}\ddot{y}_k + B_{ki}\dot{y}_k + C_{ki}y_k\right] = f_i \quad i = 1, \ldots,N \\ \bar{m}_j\,(\ddot{y}_j + \bar{\beta}_j\dot{y}_j + \bar{\omega}_j^2 y_j) + \sum_{\ell=1}^{N}\left[A_{\ell j}\ddot{x}_\ell + B_{\ell j}\,\dot{x}_\ell + C_{\ell j}x_\ell\right] = \bar{f}_j \quad j = 1, \ldots,\bar{N} \end{cases} \tag{2}$$

   where $A_{ji} = A_{ij}$ and $C_{ji} = C_{ij}$

2. The coupling is gyroscopic, i.e., $B_{ij} + B_{ji} = 0$. (3)

3. The coupling is weak, $|A_{ij}|, |A_{ji}| \ll m_i, m_j$;

   $|B_{ij}|, |B_{ji}| \ll m_i\beta_i, \bar{m}_j\bar{\beta}_j; |C_{ij}|, |C_{ji}| \ll m_i\omega_i^2, \bar{m}_j\bar{\omega}_j^2$. (4)

In addition to conditions noted in Equations (2), (3), and (4), other conditions such as uncorrelated modal forces, equal modal energies, etc., are also needed in order to apply the SEA to the connected structure.

In general, for a given connected structure, it is not always clear whether the values of the coupling parameters A, B, and C satisfy conditions contained in Equations (2), (3), and (4).

In the following, the degree of coupling of a connected system used by Lyon and Eichler is examined.

In Reference 4, Lyon and Eichler treated analytically the coupled system shown in Figure 1, namely, a mass-spring resonator attached to a finite thin plate. The same configuration is used here to examine the magnitude of the coupling parameters of the coupled system. The transverse displacement w of the plate satisfies the following equation:

$$K_P^2 \, C_P^2 \, \nabla^4 \, w + \ddot{w} + \beta_P \, \dot{w} = \frac{1}{\rho_s} \left[r(x, t) - f(t) \, \delta(x - x_o) \right] \tag{5}$$

where K_P is the radius of gyration of the cross section, C_P is the longitudinal wave velocity in the thin plate, β_P is the damping coefficient related to the loss factor η_P by $\beta_P = \eta_P \, \omega$, ρ_s is the mass per unit area, r(x, t) represents the random loads per unit area, and f is the reaction force produced by the resonator which is attached to the plate. The corresponding modal response equations are:

$$\ddot{\xi}_m + \beta_P \, \dot{\xi}_m + \omega_m^2 \, \xi_m + \frac{1}{\rho_s} \, \Psi_m^o \, f = F_m(t) \tag{6}$$

where ξ_m = modal amplitude of m^{-th} mode

ω_m = natural frequency of m^{-th} mode

Ψ_m^o = m^{-th} mode shape at $x = x_o$

F_m = modal force corresponding to m^{-th} mode

Using the reaction force as the dependent variable, the equation of motion for the resonator of Figure 1 is:

$$\ddot{f} + \beta_o \, \dot{f} + \omega_o^2 \, f - K \sum_m \Psi_m^o \, \ddot{\xi}_m = \omega_o^2 \, f_s(t) \tag{7}$$

where $\beta_o = \frac{r}{M}$ and $\omega_o^2 = \frac{K}{M}$. The exciting force on the resonator mass is $f_s(t)$. The reaction force f is related to the displacement of resonator d by the following relation:

$$K(d - w_o) = -f = K(d - \sum_m \Psi_m^o \, \xi_m) \tag{8}$$

The corresponding power balance equations for the system are:

$$\begin{aligned} &\beta_P < \rho_s \dot{\xi}_m^2 > + \Psi_m^o < f \, \dot{\xi}_m > = \rho_s < F_m \, \dot{\xi}_m > \\ &\beta_o < f^2/K > - \sum_m \Psi_m^o < f \, \dot{\xi}_m > = \frac{1}{M} < f_s \int f dt > \approx - < f_s \, \dot{d} > \end{aligned} \tag{9}$$

The above equations show that the coupling of the system is conservative. Since the equation of motion for the resonator is in a special form, Lyon and Eichler introduced the following new variables:

$$\begin{aligned} \theta &= (K\ \rho_s)^{-\frac{1}{4}}\ f \\ \nu_m &= (K\ \rho_s)^{\frac{1}{4}}\ \dot{\xi}_m \\ \psi_m &= (K/\rho_s)^{\frac{1}{2}}\ \Psi_m \end{aligned} \tag{10}$$

Based on the above, a new set of equations are obtained as follows:

$$\begin{aligned} &\ddot{\nu}_m + \beta_p\ \dot{\nu}_m + \omega_m^2\ \nu_m + \psi_m^{\circ}\ \dot{\theta} = (K\ \rho_s)^{\frac{1}{4}}\ \dot{F}_m(t) \\ &\ddot{\theta} + \beta_0\ \dot{\theta} + \omega_0^2\ \theta - \sum_m \psi_m^{\circ}\ \dot{\nu}_m = \omega_0^2\ \epsilon_s(t) \end{aligned} \tag{11}$$

Comparing with Equation (1), Equation (11) satisfies the following conditions:

$$\begin{aligned} A_{1m} &= A_{m1} = 0 \\ B_{1m} &= -B_{m1} = \psi_m^{\circ} \\ C_{1m} &= C_{m1} = 0 \end{aligned} \tag{12}$$

The above conditions establish the gyroscopic coupling of the system and the applicability of the SEA method. Based on Equation (11) and the formulas given in Reference 1, the amount of energy transfer through the spring resonator and the finite thin plate may be computed. Consider a simply supported square plate with a resonator attached at the center. We have:

$$\Psi_m^{\circ} \equiv \frac{2}{a},\ B_{1m} = \psi_m^{\circ} = \frac{2}{a}\sqrt{\frac{K}{\rho_s}} = 2\omega_0\sqrt{\frac{M}{a^2\rho_s}} = 2\omega_0\sqrt{\frac{M}{M_p}} \tag{13}$$

where a is the edge length of the plate and M_p is the mass of the plate. In the narrow frequency band with center frequency ω_o, the ratio of B/β_p is:

$$\frac{B}{\beta_p} = \frac{2}{\pi_p}\sqrt{\frac{M}{M_p}} \tag{14}$$

Figure 9 of Reference 4 shows $\eta_p \simeq 0.0005$ for a 0.145 cm (0.057") steel plate. So we have:

$$\frac{B}{\beta_p} \simeq 4000\sqrt{\frac{M}{M_p}} \tag{15}$$

It is noted that for the case described above, m_i of Condition (4) is equal to unity. In other words, the weak coupling Condition (4) is now $B/\beta_p << 1$, which may be restated as: $M << M_p/(16 \times 10^6)$. Since the latter condition is not satisfied in a typical set-up, we conclude that the resonator-plate arrangement is not a weak coupling case. In the following section, new formulation of vibrational energy transfer involving strong coupling of sub-structures is described.

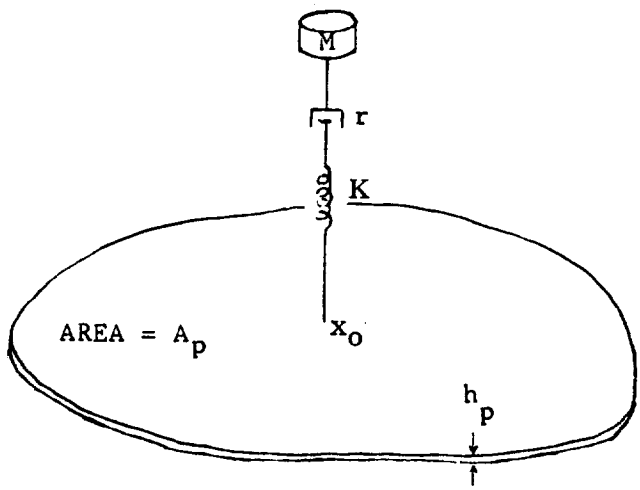

FIGURE 1 DIAGRAM OF PLATE WITH ATTACHED RESONATOR

THE EXTENSION OF THE SEA METHOD TO STRONGLY COUPLED STRUCTURES

A major item of interest in the application of the Statistical Energy Analysis is the degree of coupling of connected structures. Previous work at Northrop indicated that the weak coupling condition assumed by the original workers of SEA was not always satisfied in typical structures. Our present effort is to determine the extent of coupling of practical aerospace structures and to explore the additional formulation in structural responses based on the condition that the substructure coupling is not weak. Our findings are described below.

Power Flow between Two Modes

The average net power transferred between two linearly strongly coupled oscillators which satisfy the set of Equations (1) is derived below. The mean value function equations of Reference 1 are the starting point of this derivation. Thus, the sources f_1 and f_2 are assumed to be statistically independent and to have power spectra which are flat as compared to the admittance spectra of the two oscillators. Suppose an impulse "a" occurs from source f_1 only, then by Equation (1)

$$\begin{cases} m_1 \Delta\dot{y}_1 + A\Delta\dot{y}_2 = a, \\ A\Delta\dot{y}_1 + m_2 \Delta y_2 = 0. \end{cases} \tag{16}$$

Accordingly,

$$\begin{cases} \Delta\dot{y}_1 = a m_2/(m_1 m_2 - A^2) \\ \Delta\dot{y}_2 = -aA/(m_1 m_2 - A^2) \end{cases} \tag{17}$$

From the nature of f_1, subsequent increments of $\Delta\dot{y}_1$ and $\Delta\dot{y}_2$ (due to different impulses) are independent increments of velocity, and therefore in one second the amounts of energy gained by oscillator 1, 2 are

$$\begin{cases} m_1 \langle \dot{y}_1^2 \rangle \Big|_{1 \text{ sec.}} = m_1 m_2^2 \, D_1/(m_1 m_2 - A^2)^2 \\ m_2 \langle \dot{y}_2^2 \rangle \Big|_{1 \text{ sec.}} = m_2 A^2 \, D_1/(m_1 m_2 - A^2)^2 \end{cases} \tag{18}$$

where D_1 is the spectral density of f_1.

Thus, the power from source 1 is

$$\langle f_1\dot{y}_1\rangle = D_1m_2(m_1m_2 + A^2)/(m_1m_2 - A^2)^2 \tag{19}$$

and similarly,

$$\langle f_2\dot{y}_2\rangle = D_2m_1(m_1m_2 + A^2)/(m_1m_2 - A^2)^2 \tag{20}$$

also, since $\Delta\dot{y}_2 = -A\Delta\dot{y}_1/m_2$ one has

$$\langle f_1\dot{y}_2\rangle = -D_1A(m_1m_2 + A^2)/(m_1m_2 - A^2)^2 \tag{21}$$

and

$$\langle f_2\dot{y}_1\rangle = -D_2A(m_1m_2 + A^2)/(m_1m_2 - A^2)^2 \tag{22}$$

Since an impulse produces no immediate increment of displacement,

$$\langle f_1y_1\rangle = \langle f_2y_2\rangle = \langle f_1y_2\rangle = \langle f_2y_1\rangle = 0$$

The above covariances between the sources, displacements, and velocities define the statistical properties of the sources. The effective force which the motion of oscillator 1 causes to be produced on oscillator 2 is seen from equations (1)

$$f_{12} = -A\ddot{y}_1 - B_1\dot{y}_1 - Cy_1 \tag{23}$$

Thus, for stationary ergodic process the average net power flow delivered from oscillator 1 to mode 2 is

$$P_{12} = \langle f_{12}\dot{y}_2\rangle = -A\langle\ddot{y}_1\dot{y}_2\rangle - B_1\langle\dot{y}_1\dot{y}_2\rangle - C\langle y_1\dot{y}_2\rangle \tag{24}$$

Similarly, the net power transferred from oscillator 2 to 1

$$P_{21} = \langle f_{21}\dot{y}_1\rangle = -A\langle\dot{y}_1\ddot{y}_2\rangle - B_2\langle\dot{y}_1\dot{y}_2\rangle - C\langle y_2\dot{y}_1\rangle$$

For a stationary process

$$\begin{cases}\langle\ddot{y}_1\dot{y}_2\rangle = -\langle\dot{y}_1\ddot{y}_2\rangle \\ \langle y_1\dot{y}_2\rangle = -\langle\dot{y}_1y_2\rangle\end{cases} \tag{25}$$

and therefore we may write

$$P_{21} = A\langle \ddot{y}_1 \dot{y}_2 \rangle - B_2 \langle \dot{y}_1 \dot{y}_2 \rangle + C \langle y_1 \dot{y}_2 \rangle \tag{26}$$

In order to evaluate the moments involved in Equations (24) and (26) the following set of equations may be obtained from stochastic equations (1)

$$\begin{bmatrix}
m_1\beta_1 & 0 & 0 & 0 & 0 & B_2 & -C & -A \\
0 & m_2\beta_2 & 0 & 0 & 0 & B_1 & C & A \\
0 & B_2 & 0 & 0 & 0 & m_1\beta_1 & m_1\omega_1^2 & m_1 \\
B_1 & 0 & 0 & 0 & 0 & m_2\beta_2 & -m_2\omega_2^2 & -m_2 \\
-m_1 & 0 & m_1\omega_1^2 & 0 & C & -A & B_2 & 0 \\
0 & -m_2 & 0 & m_2\omega_2^2 & C & -A & -B_1 & 0 \\
0 & -A & 0 & C & m_1\omega_1^2 & -m_1 & m_1\beta_1 & 0 \\
-A & 0 & C & 0 & m_2\omega_2^2 & -m_2 & m_2\beta_2 & 0
\end{bmatrix}
\begin{Bmatrix}
\langle \dot{y}_1^2 \rangle \\
\langle \dot{y}_2^2 \rangle \\
\langle y_1^2 \rangle \\
\langle y_2^2 \rangle \\
\langle y_1 y_2 \rangle \\
\langle \dot{y}_1 \dot{y}_2 \rangle \\
\langle y_1 \dot{y}_2 \rangle \\
\langle \ddot{y}_1 \dot{y}_2 \rangle
\end{Bmatrix}
=
\begin{Bmatrix}
\langle f_1 \dot{y}_1 \rangle \\
\langle f_2 \dot{y}_2 \rangle \\
\langle f_1 \dot{y}_2 \rangle \\
\langle f_2 \dot{y}_1 \rangle \\
0 \\
0 \\
0 \\
0
\end{Bmatrix} \tag{27}$$

Equation (27) may be solved explicitly and the results used to obtain power flow P_{12}, etc. This is accomplished if the coupling is conservative (gyroscopic coupling $B_1 = -B_2 = B$).

$$P_{12} = -P_{21} = g_{12}(\theta_1 - \theta_2) \tag{28}$$

where P_{ij} = the average net power delivered from oscillator i to oscillator j.

θ_i = the stored energy in system i = $\langle f_i \dot{y}_i \rangle / \beta_i$

$g_{12} = g_{21}$ = the power flow coefficient

$$= (m_1 m_2 \beta_1^2 \beta_2^2 \{A^2 [\beta_1 \omega_2^4 + \beta_2 \omega_1^4 + \beta_1 \beta_2 (\beta_1 \omega_2^2 + \beta_2^2 \omega_1^2)]$$
$$+ (B^2 - 2AC)(\beta_1 \omega_2^2 + \beta_2 \omega_1^2)$$
$$+ C^2(\beta_1 + \beta_2)\} + B^2 \beta_1 \beta_2 \{A^2 [\beta_1 \omega_2^4 + \beta_2 \omega_1^4 - \beta_1 \beta_2 (\beta_1 \omega_2^2$$
$$+ \beta_2 \omega_1^2)] - (B^2 + 2AC)(\beta_1 \omega_2^2 + \beta_2 \omega_1^2) + C^2 (\beta_1 + \beta_2)\}) .$$

$$\{m_1 m_2 \beta_1 \beta_2 (\omega_1^2 - \omega_2^2)^2 + (m_1 m_2 \beta_1 \beta_2 - B^2 - 2AC) \cdot (\beta_1 + \beta_2)(\beta_1 \omega_2^2 + \beta_2 \omega_1^2) + (\beta_1 + \beta_2)^2 C^2 + (\beta_1 \omega_2^2 + \beta_2 \omega_1^2)^2 A^2 \}^{-1} (B^2 + m_1 m_2 \beta_1 \beta_2)^{-1} \quad (29)$$

For the special case of weak coupling between two oscillators, ($|A| \ll m_1, m_2$; $|C| \ll m_1 \omega_1^2$, $m_2 \omega_2^2$; $|B| \ll m_1 \beta_1$, $m_2 \beta_2$ and $m_1 = m_2 = 1$), Equation (29) may be reduced to the form which is identical to the result of Reference 1, Equation (3,4).

Equation (28) shows the fact that the steady-state time-average power flow from one mode to another is proportional to the difference between the time-average modal energies even though the coupling between the two modes is strong, provided that all other requirements to apply the SEA method are satisfied.

In the following subsection, the power flow between two strongly coupled sets of modes is described.

Power Flow between Two Strongly Coupled Sets of Modes

Consider two sets of modes. Within each set, the modes are uncoupled to each other. The power flows between modes of the two sets are assumed to be proportional to the modal energy difference. The modal displacements of the oscillators, which are denoted by x_i, y_j respectively, satisfy Equations (2) and (3). Furthermore, assuming a stationary process, the time average of a function is denoted by a pair of brackets $\langle \ \rangle$ around the function. The power balance equations may then be expressed as follows:

$$\begin{cases} m_i \beta_i \langle \dot{x}_i^2 \rangle = \beta_i \theta_i - \sum_{k=1}^{\bar{N}} g_{ik} (\theta'_{ik} - \bar{\theta}'_{ki}) & i = 1, \ldots, N \quad (30) \\ \bar{m}_j \bar{\beta}_j \langle \dot{y}_j^2 \rangle = \bar{\beta}_j \bar{\theta}_j + \sum_{\ell=1}^{N} g_{\ell j} (\theta'_{\ell j} - \bar{\theta}'_{j\ell}) & j = 1, \ldots, \bar{N} \quad (31) \end{cases}$$

or

$$\begin{cases} m_i \beta_i \left\langle \dot{x}_i^2 \right\rangle = \beta_i \theta'_{ij} - g_{ij}(\theta'_{ij} - \bar{\theta}'_{ji}) & (32) \\ \bar{m}_j \bar{\beta}_j \left\langle \dot{y}_j^2 \right\rangle = \bar{\beta}_j \bar{\theta}'_{ji} + g_{ij}(\theta'_{ij} - \bar{\theta}'_{ji}) & \\ \qquad\qquad i = 1, \cdots, N;\ j = 1, \cdots, \bar{N} & (33) \end{cases}$$

where θ'_{ij}, $\bar{\theta}'_{ji}$ are called the equivalent modal energies as defined below:

$$\theta'_{ij} = \theta_i - \sum_{k \asymp j}^{\bar{N}} g_{ik} \, (\theta'_{ik} - \bar{\theta}'_{ki}) \, / \beta_i \qquad (34)$$

$$\bar{\theta}'_{ji} = \bar{\theta}_j + \sum_{\ell \asymp i}^{N} g_{\ell j} \, (\theta'_{\ell j} - \bar{\theta}'_{j\ell}) \, / \bar{\beta}_j \qquad (35)$$

and

$$\theta_i = \left\langle f_i \dot{x}_i \right\rangle / \beta_i \qquad (36)$$

$$\bar{\theta}_j = \left\langle \bar{f}_j \dot{y}_j \right\rangle / \bar{\beta}_j \qquad (37)$$

Thus, the expression of the mode-to-mode power flow and the relation between coupling parameters and g are as shown below:

$$\langle P_{ij} \rangle = g_{ij} \, (\theta'_{ij} - \bar{\theta}'_{ji}) = - A_{ij} \langle \ddot{x}_i \dot{y}_j \rangle - B_{ij} \langle \dot{x}_i \dot{y}_j \rangle - C_{ij} \langle x_i \dot{y}_j \rangle \qquad (38)$$

where the power flow coefficient g_{ij} is defined by Equation (29). Equations (34), (35) and (38) are used for defining the energy terms. Based on this formulation, the power flow diagram for a typical mode (x_i) and the mode (y_j) is shown in Figure (2a). The steady-state time-average power flow from one set of modes to another may be expressed as

$$P_{IJ} = \sum_{i=1}^{N} \sum_{j=1}^{\bar{N}} g_{ij} \, (\theta'_{ij} - \bar{\theta}'_{ji}) \qquad (39)$$

Taking the summation of the terms of Equation (33) with respect to index "i" from 1 to N yields

$$N \bar{m}_j \bar{\beta}_j \left\langle \dot{y}_j^2 \right\rangle = \bar{\beta}_j \sum_{i=1}^{N} \theta'_{ji} + \sum_{i=1}^{N} g_{ij} \, (\theta'_{ij} - \bar{\theta}'_{ji}) \qquad (40)$$

Insertion of Equation (31) into Equation (40) gives the following expression

$$\sum_{i=1}^{N} \overline{\theta}'_{ji} = \overline{\theta}_j + (N - 1) \overline{m}_j \langle \dot{y}_j^2 \rangle \tag{41}$$

In Equations (40) and (41) the unknown $\overline{\theta}'_{ji}$ may be represented in terms of $\langle \dot{y}_j^2 \rangle$ and $\langle \dot{x}_i^2 \rangle$. This is accomplished by solving the simultaneous equations (32) and (33).

$$\theta'_{ij} = \left[\overline{m}_j (1 - g_{ij}/\beta_i) \langle \dot{y}_j^2 \rangle - m_i (g_{ij}/\overline{\beta}_j) \langle \dot{x}_i^2 \rangle\right] / \Delta_{ij} \tag{42}$$

$$\overline{\theta}'_{ji} = \left[m_i (1 - g_{ij}/\overline{\beta}_j) \langle \dot{x}_i^2 \rangle - \overline{m}_j (g_{ij}/\beta_i) \langle \dot{y}_j^2 \rangle\right] / \Delta_{ij} \tag{43}$$

where

$$\Delta_{ij} = 1 - (\beta_i^{-1} + \overline{\beta}_j^{-1}) g_{ij} \tag{44}$$

Substituting Equations (42) and (43) into Equation (39), the following expression is reached

$$P_{IJ} = \sum_{i=1}^{N} \sum_{j=1}^{\overline{N}} g_{ij} \left[m_i \langle \dot{x}_i^2 \rangle - \overline{m}_j \langle \dot{y}_j^2 \rangle\right] / \Delta_{ij} \tag{45}$$

It may be concluded from Equation (45) that the set-to-set power flow is proportional to the difference between the set-average modal energies of the two sets provided that either or both of the following two conditions are true: (1) the mode-to-mode coupling is the same for all mode pairs; (2) all modes in a set have equal time-average energies . Furthermore, Equation (45) may be rewritten as

$$P_{IJ} = \left(\sum_{i=1}^{N} \sum_{j=1}^{\overline{N}} g_{ij}/\Delta_{ij}\right) \left(\frac{M \langle V^2 \rangle}{N} - \frac{\overline{M} \langle \overline{V}^2 \rangle}{\overline{N}}\right) \tag{46}$$

where the M, N, $\langle V^2 \rangle$ are the mass, the mode count, and the mean square velocity of Set I; and $\overline{M}$, $\overline{N}$, $\langle \overline{V}^2 \rangle$ are the corresponding functions for the Set J. The energy flow diagram of two coupled sets is shown in Figure (2b).

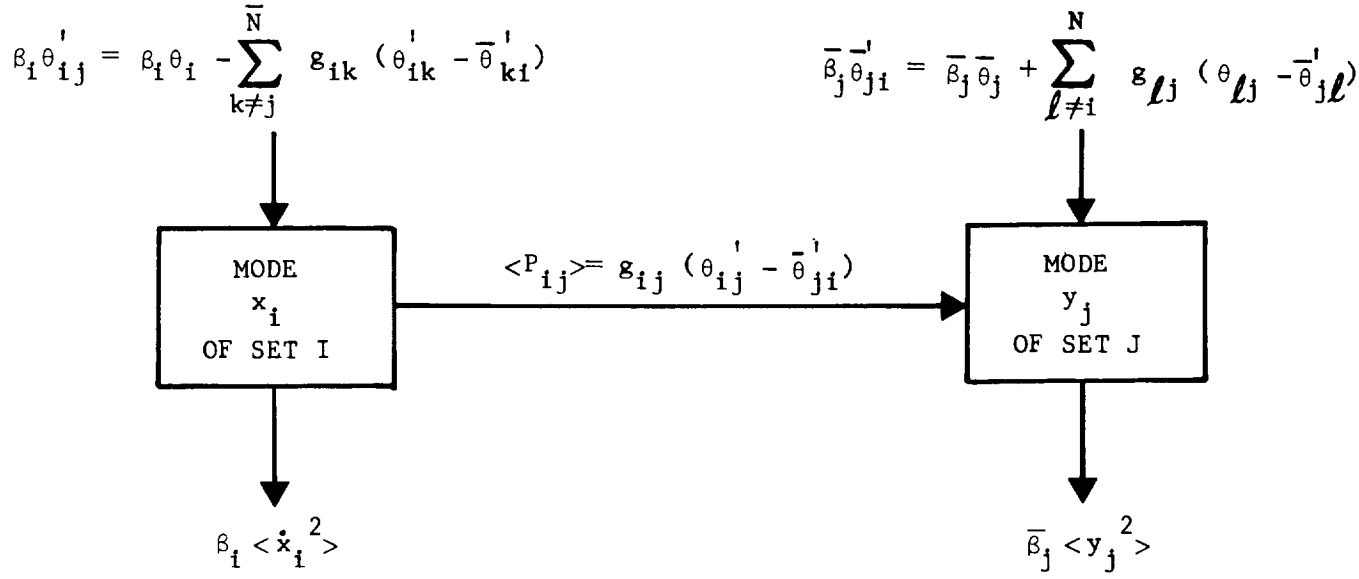

(a)

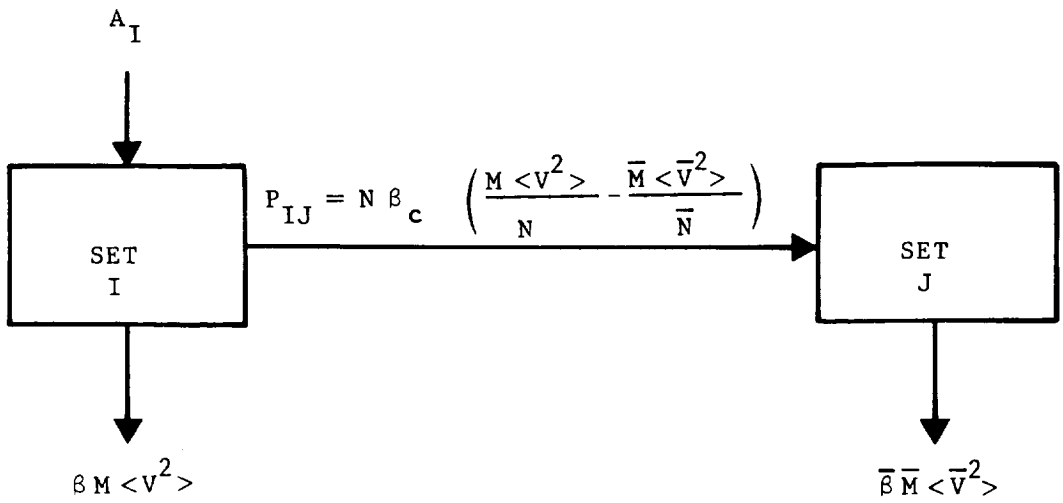

(b)

FIGURE 2 ENERGY FLOW IN TWO COUPLED MODE SETS

In Reference 11, a term called coupling loss factor of Set I is defined to describe the loss of mechanical energy from Set I, the energy being transferred to set J through the interface:

$$\eta_c = \eta_{IJ} = \frac{P_{IJ}}{\omega_o M \langle V^2 \rangle} \Bigg|_{\langle \bar{V}^2 \rangle = 0} = \frac{1}{\omega_o} \frac{1}{\bar{N}} \left(\sum_{i=1}^{N} \sum_{j=1}^{\bar{N}} g_{ij}/\Delta_{ij} \right) \quad (47)$$

where ω_o is the center circular frequency of the narrow band excitation. The condition $\langle \bar{V}^2 \rangle = 0$ in Equation (47) is imposed in order to make this loss factor independent of the modal energies of the system receiving energy inflow.

It is noted that the coupling loss factor $\bar{\eta}_c = \eta_{JI}$ of set J is generally not the same as the loss factor $\eta_c = \eta_{IJ}$ of Set I. Instead, we have

$$N \eta_c \omega_o = \bar{N} \bar{\eta}_c \omega_o = \sum_{i=1}^{N} \sum_{j=1}^{\bar{N}} g_{ij}/\Delta_{ij} \quad (48)$$

Ways to determine the coupling loss factors analytically and experimentally for various connected structures will be discussed later in the report.

Estimation of the Response Ratio of Two Connected Structures When One Is Directly Excited

In the SEA method, an important application is to estimate the response ratio when the primary structure of the connected structural system is randomly excited in a narrow frequency band. The response ratio may be estimated by inserting equation (43) into Equation (41) and setting $\bar{\theta}_j \equiv 0$ (Set J is excited through attachment only):

$$m_j \langle \dot{y}_j^2 \rangle = \frac{\sum_{i=1}^{N} (g_{ij}/\Delta_{ij})\, m_i \langle x_j^2 \rangle}{\bar{\beta}_j + \sum_{i=1}^{N} g_{ij}/\Delta_{ij}} \quad (49)$$

The above result may be expressed in the following simplified form

$$\langle \bar{V}^2 \rangle / \langle V^2 \rangle = \frac{M\bar{N}}{\bar{M}N} \quad \frac{\bar{\beta}_c}{\bar{\beta} + \bar{\beta}_c} \tag{50}$$

where $\bar{\beta}$ is the average damping coefficient of the coupled structure J and $\bar{\beta}_c$ is the coupling damping factor defined below:

$$\bar{\beta}_c = \text{mean of} \sum_{i=1}^{N} g_{ij}/\Delta_{ij} \quad \text{for all j's} \tag{51}$$

$$\cong \bar{\eta}_c \omega_o = \eta_{JI}^c \omega_o$$

Equation (50) conforms to the general formulation of SEA (see Equation 101, Reference 11). Furthermore, a term called the apparent loss factor η_{IJ}^a is introduced in Reference 11 (Equation 103). The apparent loss factor is the value of the dissipation loss factor ascribed to set I (on the basis of measurements performed on Set I) if the observer is not aware that the set is coupled to Set J, i.e.,

$$\eta_{IJ}^a = \eta + \frac{\eta_{IJ}\bar{\eta}}{\eta_{JI} + \bar{\eta}} = \eta + \frac{\eta_c \bar{\eta}}{\left(\frac{N}{\bar{N}}\right)\eta_c + \bar{\eta}} \tag{52}$$

where η and $\bar{\eta}$ denote the loss factors of Set I and J respectively. It is evident from equation (52) that the apparent loss factor η_{IJ}^a is always greater than the actual dissipative loss factor

Based on the above equation, the mean square of response ratio of the two mode sets (Equation (52)) may be reduced to:

$$\langle \bar{V}^2 \rangle / \langle V^2 \rangle = \frac{M}{\bar{M}} \quad \frac{\eta_{IJ}^a - \eta}{\bar{\eta}} \tag{53}$$

Conservation of energy requires the following conditions.

$$A_I = \eta \omega_o M \langle V^2 \rangle + P_{IJ} \tag{54a}$$

$$= \eta^a_{IJ} \omega_o M \langle V^2 \rangle \tag{54b}$$

$$P_{IJ} = N \eta_c \left(\frac{M \langle V^2 \rangle}{N} - \frac{\bar{M} \langle \bar{V}^2 \rangle}{\bar{N}} \right) \tag{55a}$$

$$= \bar{\eta} \omega_o \bar{M} \langle \bar{V}^2 \rangle \tag{55b}$$

where A_I is the time-average power supplied to Set I (Figure 2b). Equation (55a) is an alternate form of Equation (46).

In Reference 4, Lyon and Zichler applied Equation (50) to two coupled plates (Figure 3a) using the apparent loss factor:

$$\eta^a_{IJ} = \eta + \eta_c \tag{56}$$

Comparing the above with Equation (52), it may be concluded that Equation (56) is true only when the weak coupling condition is satisfied. The weak coupling condition is:

$$\eta_{JI} = \bar{\eta}_c \ll \bar{\eta} \quad , \text{ or } \quad \eta_{IJ} \ll \frac{\bar{N}}{N} \bar{\eta} \tag{57}$$

In Equations (56) and (57), Set I denotes the vertical plate while the set J denotes the base plate of the two-plate system.

In the test phase of the program the loss factors and the apparent loss factor were measured experimentally for various structural models. The acquired data and the conclusion drawn from these data will be given in a later section.

GUIDELINES AND PRELIMINARY TEST PROCEDURES TO THE PROPER APPLICATION OF SEA METHOD

In order to make the SEA method a usable tool dealing with high-frequency vibrations of connected aerospsce structures, it is desirable to have general guidelines on the proper application of the method. The guidelines described here include a preliminary test procedure which can be followed conveniently by practicing engineers. The purpose of the preliminary procedure is to ensure that the structural model and the sub-structure definition implemented by the user satisfies the basic assumptions of SEA. The same procedure also yields guideline indications when the limits of the application of SEA have been surpassed. The procedure is formulated below.

The theoretical foundation of SEA in vibration analysis demonstrates that under certain conditions, the average rate of flow of energy between two sets of modes (representing groups of modes of two coupled systems in a given frequency band) is proportional to the difference in the set-average modal energies (Equation (46))

$$P_{IJ} = N \bar{N} \bar{g}_{IJ}\left(\frac{M\langle V^2\rangle}{N} - \frac{\bar{M}\langle \bar{V}^2\rangle}{\bar{N}}\right) \tag{58}$$

where g_{IJ} denotes the average value of the power flow coefficients from a mode of set "I" to a mode of set "J." Equating Equations (55b) and (58) yields

$$\frac{\langle \bar{V}^2\rangle}{\langle V^2\rangle} = \frac{M \bar{N}}{\bar{M} N} \frac{N \bar{g}_{IJ}}{\bar{\eta}\omega_o + N\bar{g}_{IJ}} \tag{59}$$

The above equation is equivalent to Equation (50) where "J" represents the substructure excited through the connecting interface only. Furthermore, by means of Equation (48) we have

$$\bar{g}_{IJ} = \eta_c \omega_o / \bar{N} \tag{60}$$

For a connected structural system, if all the basic assumptions of SEA are satisfied, it may be concluded from the above equations that

$$\bar{g}_{IJ} = \bar{g}_{JI} > 0 \tag{61}$$

The proposed test procedure will check whether $\bar{g}_{IJ}$ (Set "I" excited) is approximately equal to $\bar{g}_{JI}$ (Set "J" excited) for all frequency bands of interest. (The ways to determing $\bar{g}$ values will be described later in the discussion.) It is expected that the test results will fall into one of the two categories given below:

1. The values of $\bar{g}_{IJ}$ differ substantially from the values of $\bar{g}_{JI}$. It indicates that the SEA method cannot be applied to the connected structural model under test.

2. The values of $\bar{g}_{IJ}$ are approximately equal to the values of $\bar{g}_{JI}$. It indicates that the coupling between the connected structures is conservative and the SEA method may be applied.

For typical structural elements, mass M and modal density n are known quantities. The dissipation loss factor η may be determined based on the measurement of the decay time. Another test method called the Q-method may be applied to determine η. The total number of modes N in a set may be determined as the product of modal density n and the frequency band of excitation $\Delta\omega$. For a connected structural system after the substructure data M, N, η, $\bar{M}$, $\bar{N}$, $\bar{\eta}$ are determined, the values of $\bar{g}_{IJ}$ may be determined by either one of the following approaches:

1. Excite primary structure "I" of the system at points chosen at random and measure the response levels $< V^2 >, < \bar{V}^2 >$. The values of $\bar{g}_{IJ}$ will be computed based on Equation (59).

2. Compute $\bar{g}_{IJ}$ based on equation (60). The values of the coupling loss factor η_c may be obtained as a function of η, $\bar{\eta}$, η^a_{IJ} by solving equation (52).

$$\eta_c = \frac{\bar{\eta}(\eta^a_{IJ} - \eta)}{\bar{\eta} - N(\eta^a_{IJ} - \eta)/\bar{N}} \tag{62}$$

The loss factor η^a_{IJ} may be determined either experimentally or analytically (Reference 4).

The aforementioned test procedures were performed on the three fabricated test specimens which are described in a later section of the report. The same procedures may be used to various types of connected structures. It will yield guideline information when the limits of the application of SEA have been surpassed due to such factors as structural element designs, the operating frequency range, etc.

In the following section, analytical methods are applied to investigate the energy transfer mechanism in the structural interface of two types of connected structural systems.

VIBRATIONAL ENERGY TRANSFER MECHANISM IN TWO CONNECTED STRUCTURES

In this section, the mechanism of energy transmission at the interface of two connected structures is investigated analytically. For this purpose, the classical equations of wave propagation are employed based on the assumption of thoroughly diffused waves. The results developed are compared with the test data given in a later section. Two typical structural models are considered:

1. A two-plate system considering rotatory inertia and transverse shear.
2. An infinite flat plate with an integrally attached half circular cylindrical shell.

Two-Plate System Considering Rotatory Inertia and Transverse Shear

The classical two dimensional theory of flexural motions of elastic plates is good only for waves which are long in comparison with the thickness of the plate. In case of transient loads with a sharp front, the significant frequencies of modes of vibration are of a high order. The flexural wave lengths of interest may reach the order of the plate thickness. An improved theory, which takes into account the effects of transverse shear deformation and rotatory inertia, should be used. In the following, the more elaborate plate equations of Mindlin (Reference 50) are used to determine analytically the energy transfer mechanism at the interface of a two-plate structure (Figure I-1) which was investigated by Lyon and Eichler (Reference 4) using the Bernoulli-Euler plate equation. In the approach, the base plate is assumed to be continuous and supported along the interface in such a way that the normal deflection vanishes and the twisting moment is continuous. The vertical plate hypothetically extends to the middle surface of the base plate where it is fastened along the interface. The detailed formulation of the flexural

wave propagation is given in Appendix I. If the effects of the transverse shear deformation and rotatory inertia are omitted, the result is identical to that obtained by Lyon and Eichler in Reference 4.

In Reference 27, Heckl used an analogy of architectural acoustics to characterize the localized boundaries of plates in terms of absorption coefficients. The absorption coefficient γ is defined as the ratio of the outgoing wave energy rate per unit length of the junction line vs. the incoming wave energy rate in the other plate. The absorption coefficient γ may be related to the difference between the apparent loss factor η^a and the loss factor η as shown below:

$$(\eta^a - \eta)\,\omega_0 = \frac{\gamma C_g L}{\pi S} \tag{63}$$

where S is the area of the plate, L is the total length of the boundary, and C_g is the group velocity for bending waves on the plate.

In Appendix II, the effect of the coupling of the flexural and tangential waves on energy transmission is investigated analytically. In Appendix III, the transmission of a flexural wave in an infinite plate with an integrally attached half cylindrical shell is analyzed. The end results of Appendices I through III are applied in Appendix IV where the energy transfers in various structural systems are formulated. Specifically, Appendix IV of the report shows the energy transfer mechanism in the two structural systems as previously mentioned. The expressions of the average input power and the transmitted power are formulated. It also shows generally the orthogonality relationships for the average power expressions. In other words, the average power involved in the forces of one mode of motion moving through the displacements of another mode is zero.

For the two-plate system to be considered, as shown in Reference 4, the junction absorption coefficient may be computed as the total absorbed power averaged over all angles of incidence ϕ_1 (Figure I-1) and divided by the averaged incident power. In the following, the expression of γ for the incoming wave in the vertical plate is formulated and simplified. All the symbols used are defined in Appendix I.

Based on Equation (IV-7) of Appendix IV, the average input power per unit width at an angle of incidence ϕ_1 is given by

$$P_i = \frac{\omega^4 D_1}{2 c_1^3} \cos \phi_1 \left[\left(1 - \frac{c_1^2 \rho_1}{G_1'} \right)^2 + \frac{c_1^4}{\omega^2} \frac{\rho_1 h_1}{D_1} \right] \tag{64}$$

The corresponding average transmitted power per unit width is given by Equation (IV-32) as

$$P_o \equiv 2 | A_2^+ |^2 \cos \phi_2 \frac{\omega^4 D_2}{2 c_2^3} \left[\left(1 - \frac{c_2^2 \rho_2}{G_2'} \right)^2 + \frac{c_2^4}{\omega^2} \frac{\rho_2 h_2}{D_2} \right] \tag{65}$$

If $\sin \phi_2 = \frac{c_2}{c_1} \sin \phi_1 > 1$, the outgoing power vanishes.

By definition, the absorption coefficient γ may be expressed in the following form

$$\gamma = \frac{\int_{-\pi/2}^{\pi/2} P_o \, d\phi_1}{\int_{-\pi/2}^{\pi/2} P_i \, d\phi_1} \tag{66a}$$

$$= \frac{H_2 \rho_2 h_2 c_2^*}{h_1 \rho_1 h_1 c_1^*} \int_{-\pi/2}^{\pi/2} | A_2^+ |^2 \cos \phi_2 \, d\phi_1 \tag{66b}$$

where

$$H_i = \frac{1 - g_i \sqrt{1 + g_i} + g_i^2}{\left[\sqrt{1 + g_i^2} + s_i \right]^{\frac{1}{2}}} \tag{67}$$

$$g_i = \frac{1}{2} \Phi_i \left(1 - \frac{1 - \nu_i}{2} \kappa^2 \right) \tag{68a}$$

$$s_i = \frac{1}{2} \Phi_i \left(1 + \frac{1 - \nu_i}{2} \kappa^2 \right) \tag{68b}$$

$$\Phi_i = \rho_i c_i^{*2} / G_i' \tag{68c}$$

Substituting Equations (I-17c) - (I-17f) into Equation (66) yields

$$\gamma = 2r \frac{(1 + g_1^2 - 2g_1\sqrt{1+g_1^2})(1+g_1^2)}{\left[(\sqrt{1+g_1^2}+s_1)(\sqrt{1+g_2^2}+s_2)\right]^{\frac{1}{2}}(1+g_2^2)} \frac{(1+g_2^2 - g_2\sqrt{1+g_2^2})}{(1+g_1^2 - g_1\sqrt{1+g_1^2})}$$

$$\int_{-\pi/2}^{\pi/2} \frac{\cos\phi_1 \cos\phi_2}{|\bar{\Delta}|^2} \, d\phi_1 \tag{69}$$

where

$$|\bar{\Delta}|^2 = \left[\bar{\alpha}_1 + \frac{\phi_1}{\bar{\alpha}_1'} \frac{\bar{\alpha}_1\bar{\alpha}_1' - 2\sqrt{1+g_1^2}\sin\phi_1}{\sqrt{1+g_1^2} - s_1} + r\sqrt{\frac{1+g_1^2}{1+g_2^2}}(\bar{\alpha}_2 + \frac{\phi_2}{\bar{\alpha}_2'} \frac{\bar{\alpha}_2\bar{\alpha}_2' - 2\sqrt{1+g_2^2}\sin\phi_2}{\sqrt{1+g_2^2} - s_2}\right]^2 + \left[\frac{\sqrt{1+g_1^2} - g_1}{(\sqrt{1+g_1^2}+s_1)^{\frac{1}{2}}}\cos\phi_1 + r\sqrt{\frac{1+g_1^2}{1+g_2^2}} \frac{(\sqrt{1+g_2^2} - g_2)}{(\sqrt{1+g_2^2}+s_2)^{\frac{1}{2}}}\cos\phi_2\right]^2 \tag{70}$$

$$r = \frac{D_1 C_2^*}{2 D_2 C_1^*} \tag{71}$$

In general, for a thin plate with thickness h = 0(0.2 cm.) and the interested frequency range f < 20 K Hz. The values of ϕ^2, g^2, s^2 as defined in Equation (68) are much smaller than unity. Under this condition, Equations (69) and (70) may be simplified as follows:

$$\gamma = 2r \frac{(1 - 2g_1)}{(1+s_1)(1+s_2)} \frac{(1-g_2)}{(1-g_1)} \int_{-\pi/2}^{\pi/2} \frac{\cos\phi_1 \cos\phi_2 \, d\phi_1}{|\bar{\Delta}|^2} \tag{72}$$

$$|\bar{\Delta}^2| \simeq \left[\frac{\bar{\alpha}_1(1+g_1)}{(1-s_1)} + r\,\frac{\bar{\alpha}_2\,(1+g_2)}{(1-s_2)}\right]^2 + \left[\frac{(1-g_1)}{\sqrt{1+s_1}}\cos\phi_1 + r\,\frac{1-g_2}{\sqrt{1+s_2}}\cos\phi_2\right]^2 \tag{73}$$

The expressions for $\bar{\alpha}_i$ and ϕ_2 may be represented as

$$\sin\phi_2 = \frac{c_2^*}{c_1^*}\sqrt{\frac{1+s_1}{1+s_2}}\sin\phi_1 \tag{74}$$

$$\bar{\alpha}_i \simeq \sqrt{1+\sin^2\phi_i}\left[1 - \frac{s_i\cos^2\phi_i}{2(1+\sin^2\phi_i)}\right] \tag{75}$$

Two simple cases of γ of special interest to the present program are described below. The plates are assumed of the same material.

1. $h_1 = h_2$

$$\gamma = \frac{2}{9}\,\frac{(1-2g)(1-s)}{\phi(1+s)}\left[-1 + \frac{1+a}{\sqrt{a}}\sin^{-1}\frac{\sqrt{a}}{\sqrt{1+a}}\right]\Bigg|_{a\,=\,2\phi/(1-s)} \tag{76}$$

2. $h_1 \ll h_2$

Let $b = h_1/h_2 \ll 1$, then

$$\gamma = \frac{\pi}{4}\,b^3\,\frac{(1-2bg_2)(1-g_2)}{(1-bg_2)\sqrt{1+s_2+b\,s_2}}\sqrt{\frac{1+s_2}{1+bs_2}} \tag{77}$$

After the absorption coefficient is obtained, the corresponding loss factor data may be computed based on Equation (63).

Flat Plate with an Integrally Attached Half Circular Cylindrical Shell

In the analytical work on the wave propagation between two perpendicular plates (Appendix I), the junction line has been assumed to remain straight and the coupling between flexural and extensional waves was ignored. Since flexural and extensional waves are always coupled in the cylindrical shell equations of motion, an analysis was performed where coupling between flexural and extensional waves is taken into account. The results are given in Appendix II. The formulation indicates that there is a range of angles of flexural wave incidence for which coupling effects are important. These results also indicate that the proper boundary conditions should be used for the plate-cylinder structural systems.

The detailed formulation of the wave propagation in an infinite plate to which an infinite half circular cylindrical shell is integrally joined along the diametrically opposite generators (Figure III-1) is given in Appendix III. A harmonic flexural wave is assumed to be produced in the plate with the angle of incidence ϕ which is scattered by the half cylindrical shell. For this case, in order to simplify the problem, rotatory inertia and transverse shear deformations are neglected in both the plate and the cylindrical shell. The proper boundary conditions, in which the coupling between flexural and extensional waves is taken into consideration, are used.

The expression of the average input power per unit width and the average transmitted power in the half cylindrical shell are defined in Appendix IV, by Equations (IV-4C) and (IV-34) respectively. Some analytical computation based on the formulation of Appendices III and IV is given in the following section dealing with experimental results.

EXPERIMENTS ON VARIOUS STRUCTURAL SYSTEMS

In the current program, a combined experimental and analytical investigation was performed on the random vibration and energy transfer in connected structures. In the following, the experimental results are described. The description starts with the model fabrication and testing procedures. The test data acquired from the different models are illustrated and compared with the analytical results.

Model Fabrication and Testing Procedures

Three simply connected structural models and three separate components were fabricated in the performance of this experimental investigation. The specimens were fabricated from Gage 16 (.16 cm) and Gage 22 (.081 cm) Type 304 stainless steel plate stock. Electron beam welding techniques were employed to fabricate the simply connected structures to minimize warping of the specimens. The first model has an irregular shaped vertical plate welded to a rectangular base plate. The second model has a half cylindrical shell welded lengthwise to the base plate along the longitudinal boundaries of the shell. The third model consists of welding an open-end circular cylindrical shell to the base plate. All three models were supported at the corners of the 16-gage rectangular base plate. The three components fabricated were duplicates of the model No. 1 vertical plate, Model No. 2 half cylindrical shell, and a base plate which was common to all three models. The three models are illustrated in Figure 3 and photographs of the models are shown in Figures 4 - 6. Also shown in Figure 4 is a typical deformation pattern (center frequency 2668 Hz, half wave length 1.5 inches) yielded by the visualization technique through the use of lightweight polyvinyl chloride particles.

For each of the simply connected structural models and the components, the following test procedure was employed. A Goodman 390A shaker was attached

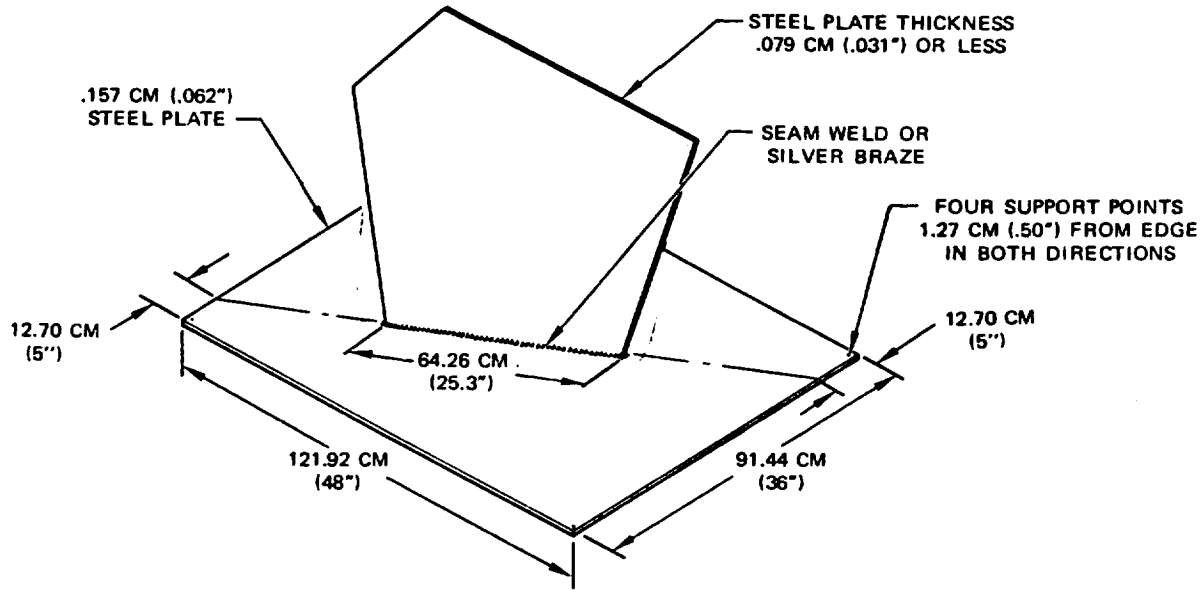

(a) MODEL NO. 1
DIMENSIONS ARE TYPICAL FOR ALL THREE MODELS

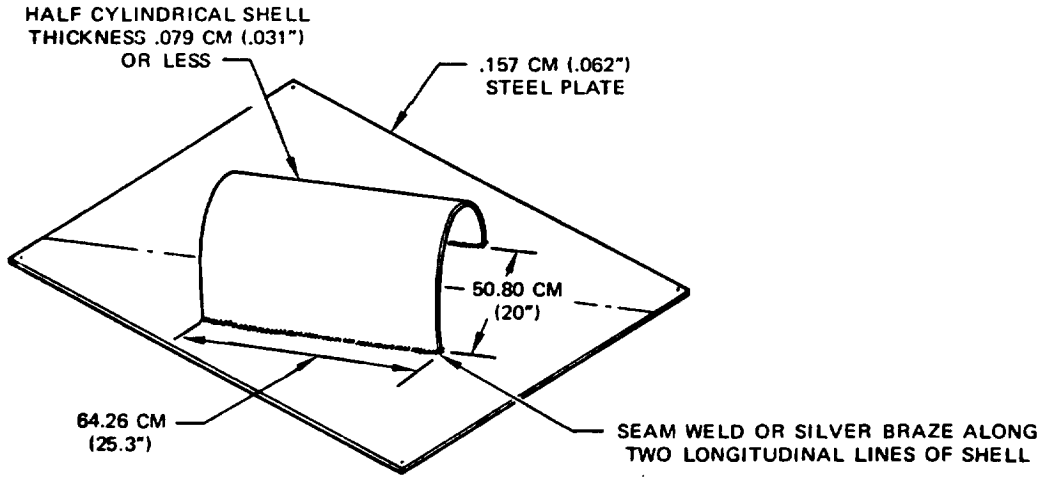

(b) MODEL NO. 2

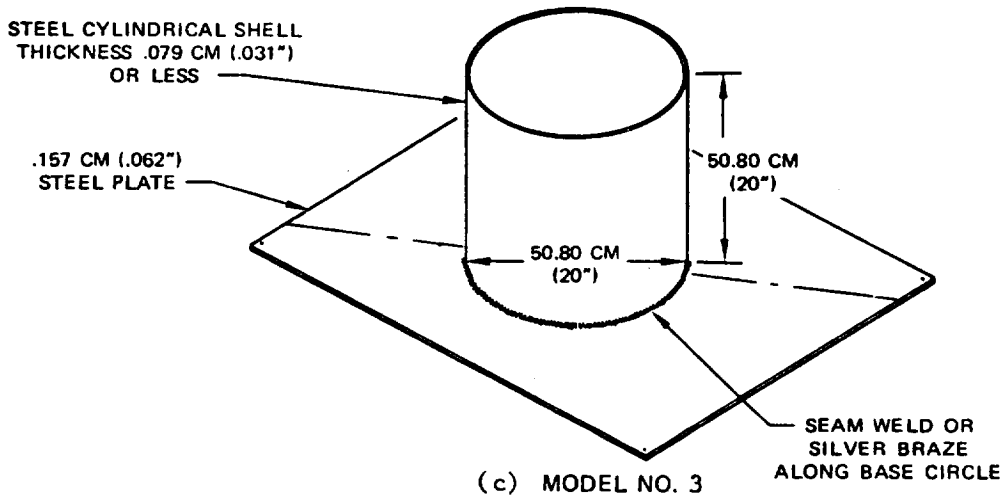

(c) MODEL NO. 3

FIGURE 3 SKETCHES OF TEST MODELS

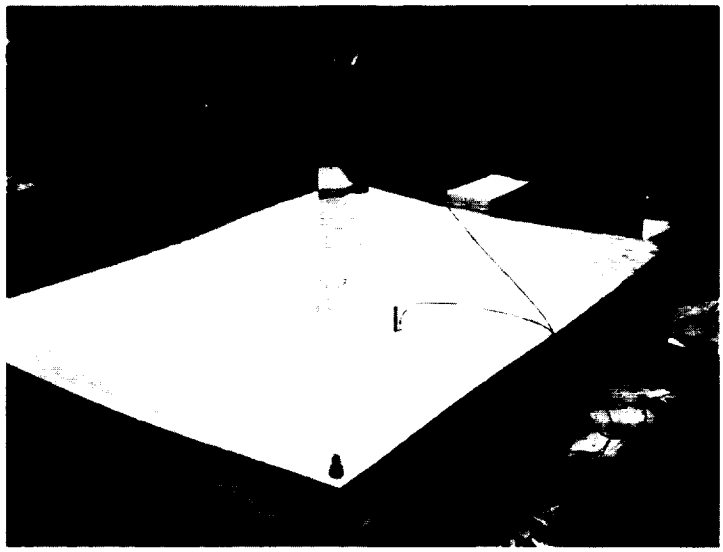

FIGURE 4 TEST MODEL NO. 1 AND THE TYPICAL DEFORMATION PATTERN OF THE BASE PLATE WITH CENTER FREQUENCY f = 2668 Hz, HALF WAVE LENGTH = 3.8 cm.

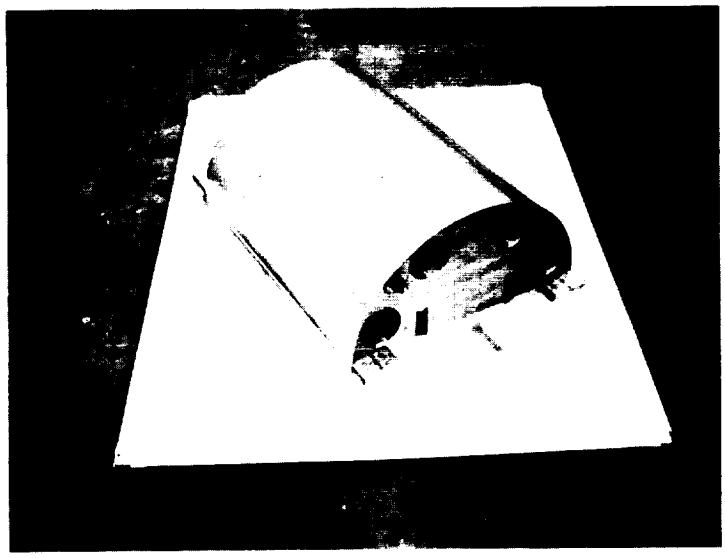

FIGURE 5 TEST MODEL NO. 2

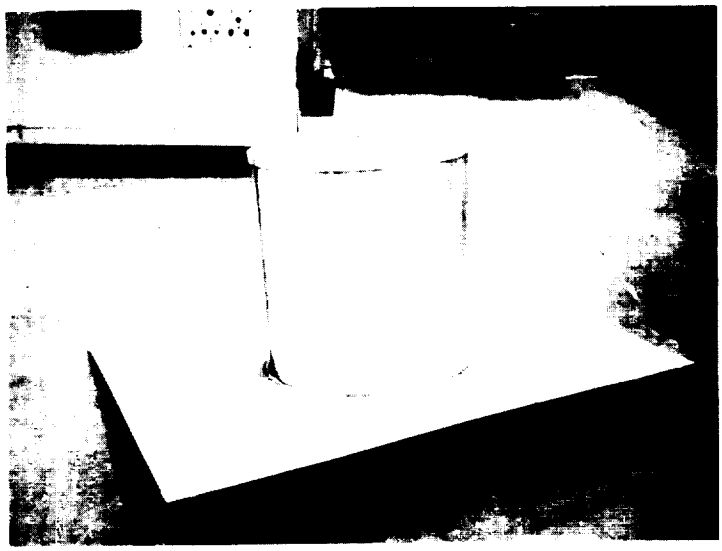

FIGURE 6 TEST MODEL NO. 3

through a Kisstler 931A force transducer to a selected point on the model. Endevco Model 2222B accelerometers were then cemented to the surfaces of the test specimen at selected locations. The specimen was then excited in 1/3 octave bands ranging in center frequency from 250 Hz to 16K Hz. During random excitation in each 1/3 octave band, the rms response acceleration was recorded for selected locations on the specimen surface(s). In addition, power spectral density plots of input and response functions were recorded. This was conducted using a spectral dynamics Model 301c real time analyzer. A SD 302c ensemble averager was used in conjunction with the 301c to provide a time-averaged value of power spectral density. The time-averaged value of power spectral density were used in evaluating the modal density of the specimen. In averaging, the discrete frequency components of the response function are enhanced while purely random components diminish. Resolution of data in the frequency domain was obtained by the use of a SD 107 low frequency translator. The translator provided a means of analyzing a narrow band of data at any frequency.

After completion of tests to determine the response ratios and the modal density under narrow band random excitation, each specimen was subjected to sinusoidal input of constant force. The force level was maintained by a SD 105 servo amplitude controller. A very stable SD 104-5 oscillator was used as a function generator and a Hewlett Packard Model 5323A electronic counter provided an accurate means of frequency readout. The counter displays the frequency to seven place accuracy in .4 sec. At the major modes of frequency response on the structure being excited, the 3 db bandwidth was obtained as a measure of damping. Several criteria were established for the selection of frequencies where damping was measured:

1. The frequencies represented major modes of the surface being excited.
2. No other modes existed close to the selected frequency.
3. The 3 db down points were nearly equally spaced about the selected natural frequency.

A block diagram of the typical instrumentation is shown in Figure 7. For tests of the three simply connected structural models and the base plate, the specimens were supported at the four corners of the rectangular base plate. The supporting structure was non-resonant up to 2kc. However, some motion was detected at the attachment above this frequency. Between 2kc and 6kc the amplitude of the attached corners was less than one tenth the input level. At frequencies above 6kc, corner motion reached unity with respect to the input excitation level. The overall effect of corner motion at high frequencies was not examined. However, it is expected that the high damping values measured above 6kc were in part attributed to the attachment.

The vertical plate and the half cylindrical shell components were tested separately by suspending them from light strings. No problems related to the means of suspension were detected.

In each test condition the shaker was in turn, attached through a .635 cm (.25 inch) diameter hole to each surface of the specimens. Models No. 1, No. 2, and No. 3 were first excited at the base plate with response ratios, spectral density measurements and damping ratios determined. The shaker was then suspended by shock cord and attached to the vertical plate, cylindrical half-shell, and open-end cylindrical shell, respectively, and a similar set of tests were repeated.

Test Data of Model No. 1

The first model (Figure 3a) has an irregularly shaped vertical plate welded to the base plate. The general configuration is similar to the model tested by Lyon and Eichler (Reference 4) except that the plate thicknesses are reduced.

The measured values for loss factors ($= 2c/c_r$) were averaged within each 1/3 octave frequency band. The apparent loss factor η^a_{tb} of the top plate, measured at the top plate of the two-plate system when the top plate is excited, is plotted in Figure 8 vs. 1/3 octave band center frequency. Also plotted in the figure is the dissipative loss factor η_t of the top plate component. Similarly, Figure 9 shows the plots of the apparent loss

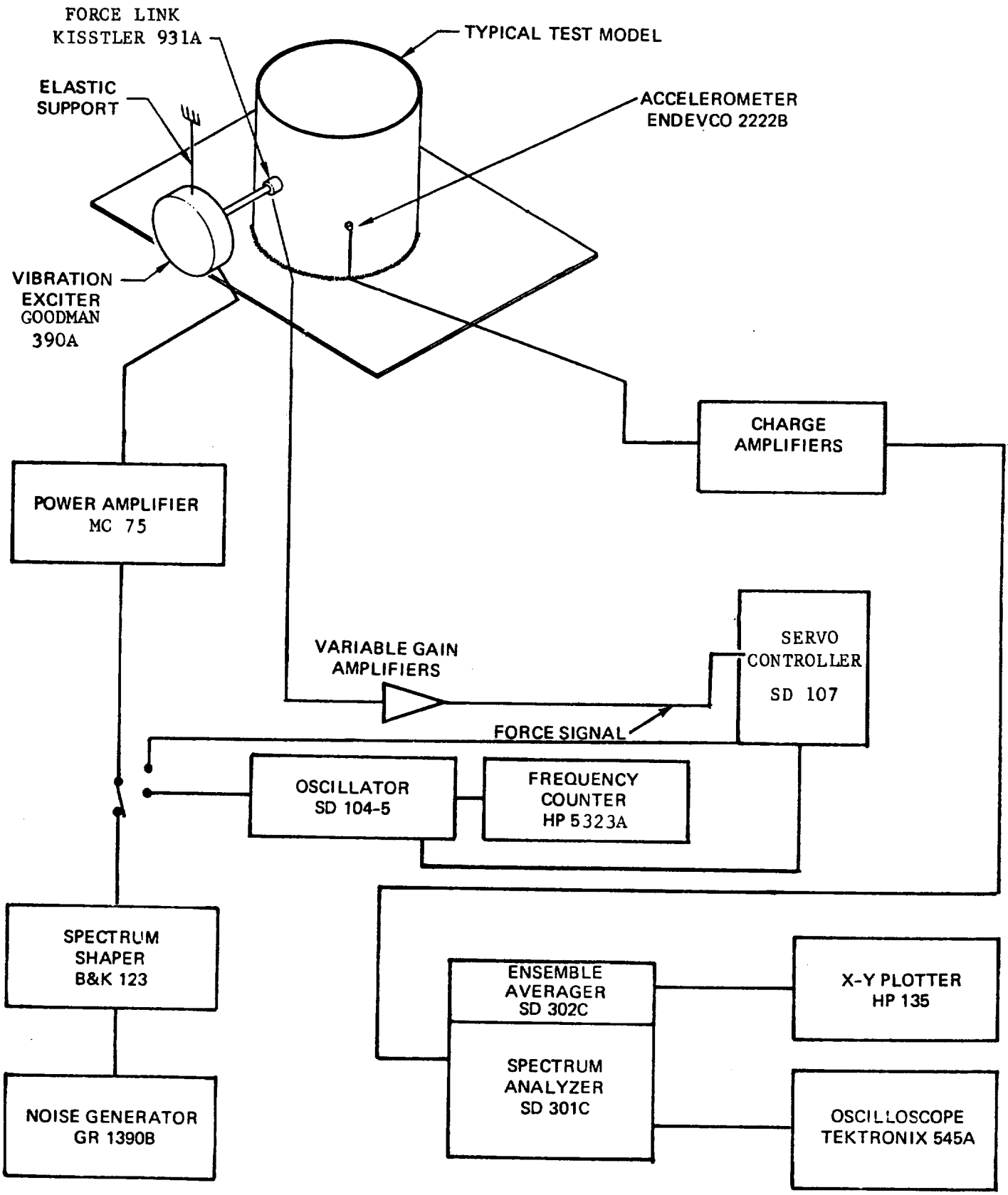

FIGURE 7 INSTRUMENTATION BLOCK DIAGRAM FOR MEASURING STEADY-STATE RESPONSE

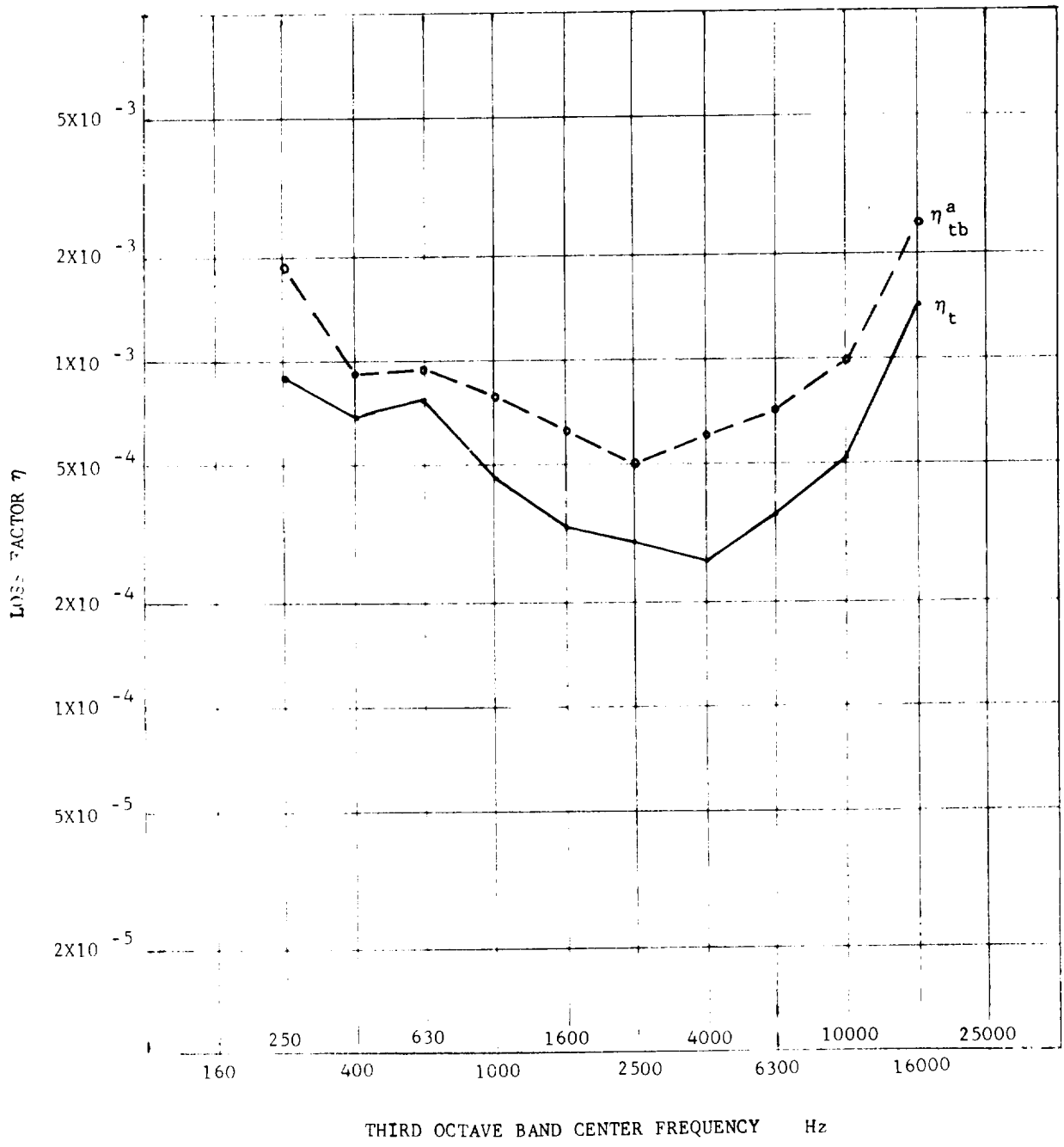

FIGURE 8 LOSS FACTORS MEASURED AT TOP PLATE OF MODEL NO. 1 WHEN TOP PLATE IS EXCITED

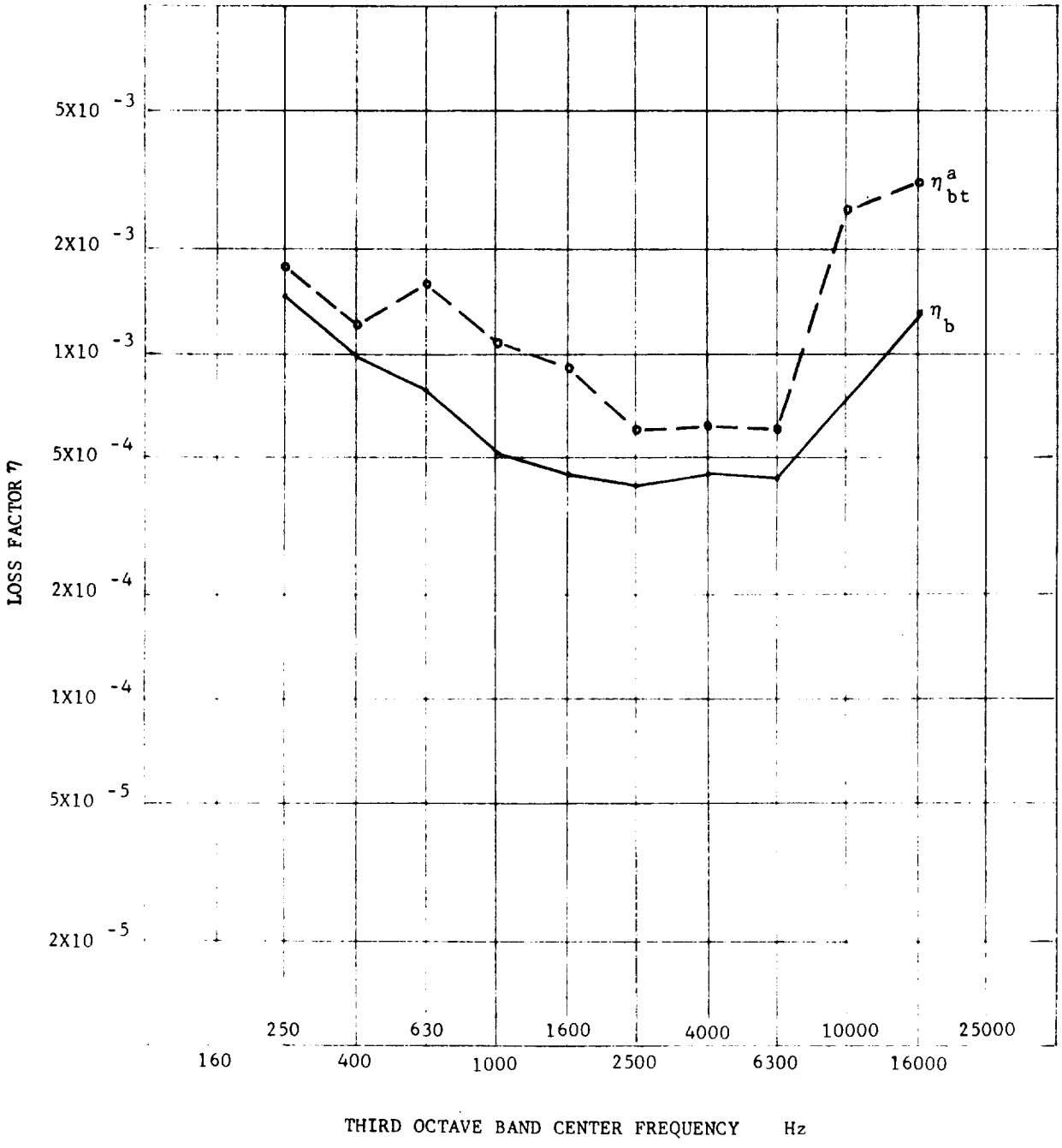

FIGURE 9 LOSS FACTORS MEASURED AT BASE PLATE OF MODEL NO.1 WHEN BASE PLATE IS EXCITED

factor η_{bt}^{a} of the base plate for the two-plate system and the dissipative loss factor η_b of the base plate component. For most cases, the apparent loss factors are greater than the corresponding component loss factor. This is as it should be, as indicated by Equation (52) previously. The few data points which do not satisfy the above condition are considered unreliable and are rejected. For the steady-state response measurements the specimen was excited with 1/3 octave frequency band random force, and the rms response acceleration was recorded at selected locations on the specimen surfaces. Typical input PSD plot with center frequency at 630 Hz is shown in Figure 10, while the corresponding response is shown in Figure 11. The ratios of the measured mean square values of average response $<V_t^2>/<V_b^2>$ when the base plate was excited were plotted in Figure 12 vs. center frequency of excitation (broken line). Also plotted in the figure are two sets of estimated response ratio data based on:

1. Strong coupling assumption: using Equation (53) and measured loss factors η_{bt}^{a}, η_b, η_t:

$$\frac{<V_t^2>}{<V_b^2>} = \frac{M_b}{M_t} \frac{\eta_{bt}^{a} - \eta_b}{\eta_t} \tag{78}$$

2. Weak coupling assumption: using equations (50), (56), and measured loss factors η_{tb}^{a}, η_t:

$$\frac{<V_t^2>}{<V_b^2>} = \frac{M_b}{M_t} \frac{N_t}{N_b} \frac{\eta_{tb}^{a} - \eta_t}{\eta_{tb}^{a}} \tag{79}$$

In Figure 12, a line corresponding to

$$\frac{<V_t^2>}{<V_b^2>} = \frac{M_b}{M_t} \frac{N_t}{N_b}$$

was plotted. This line serves as an upper bound of the actual $<V_t^2>/<V_b^2>$ ratio for the weak coupling case in view of Equation (79). It may also be stated that the line represents a condition where the average modal energies

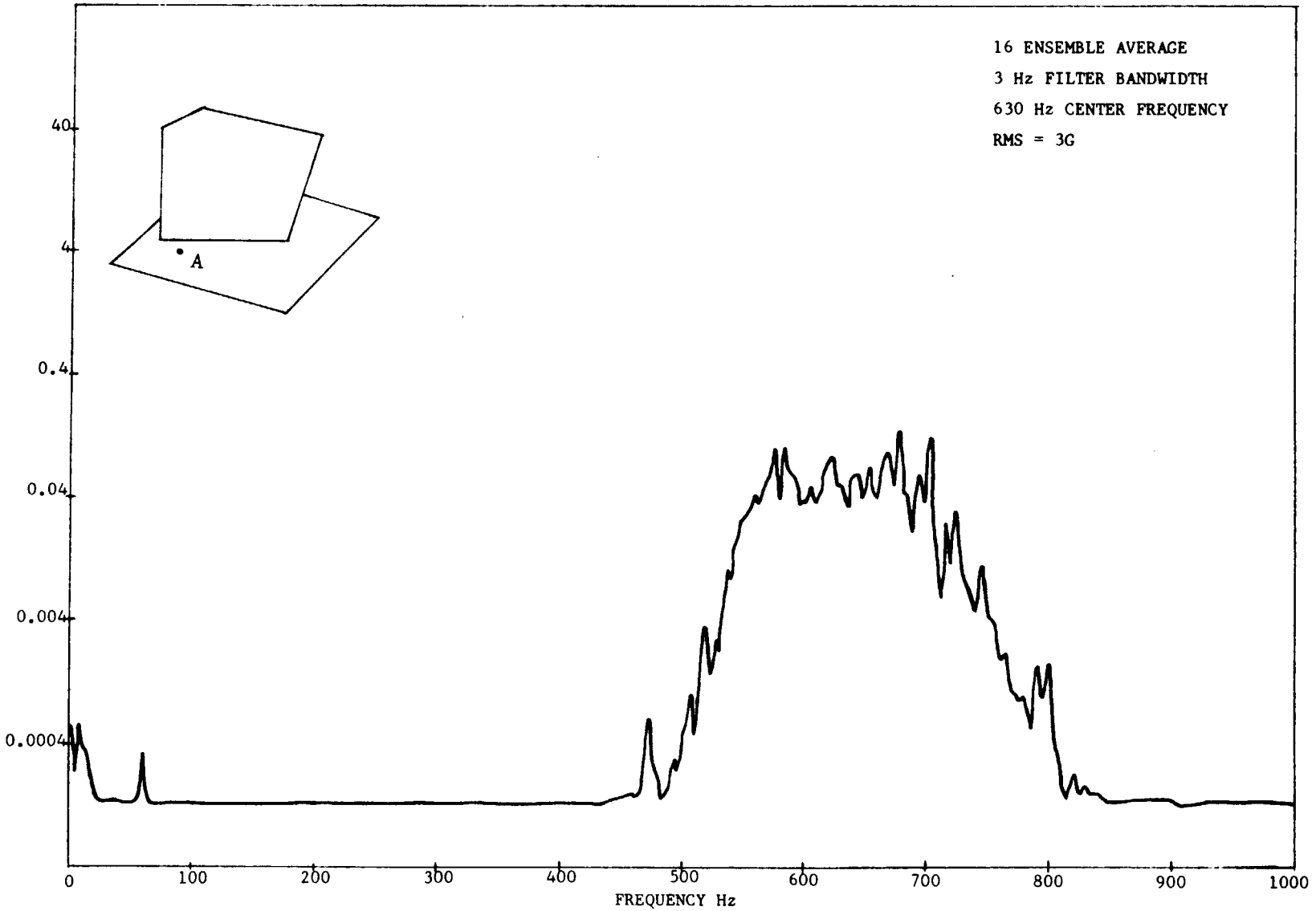

FIGURE 10 TYPICAL 1/3 OCTAVE 630 Hz CENTER FREQUENCY INPUT PSD AT LOCATION A

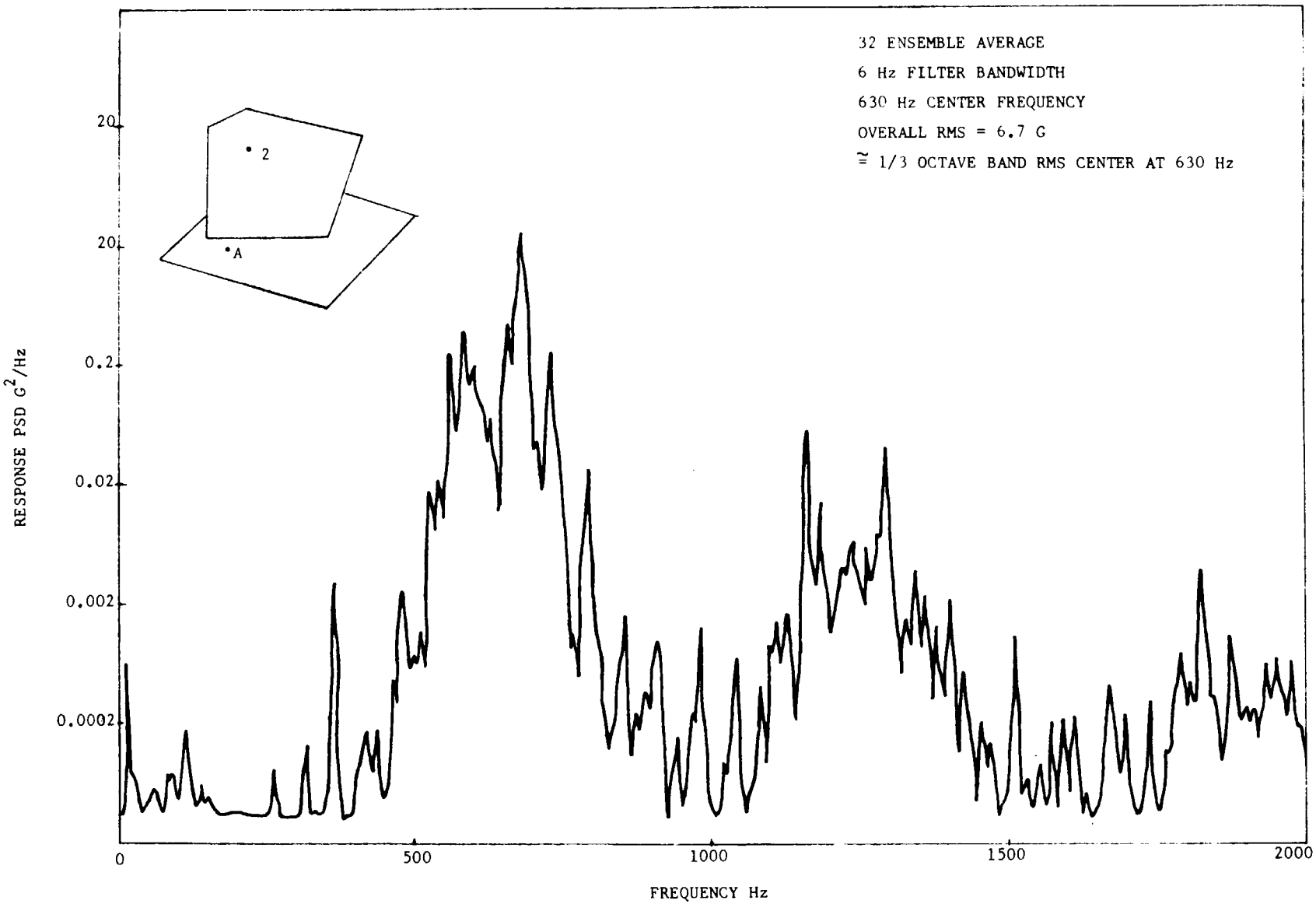

FIGURE 11 TYPICAL RESPONSE PSD AT POINT 2 DUE TO 630 Hz CENTER FREQUENCY INPUT AT A

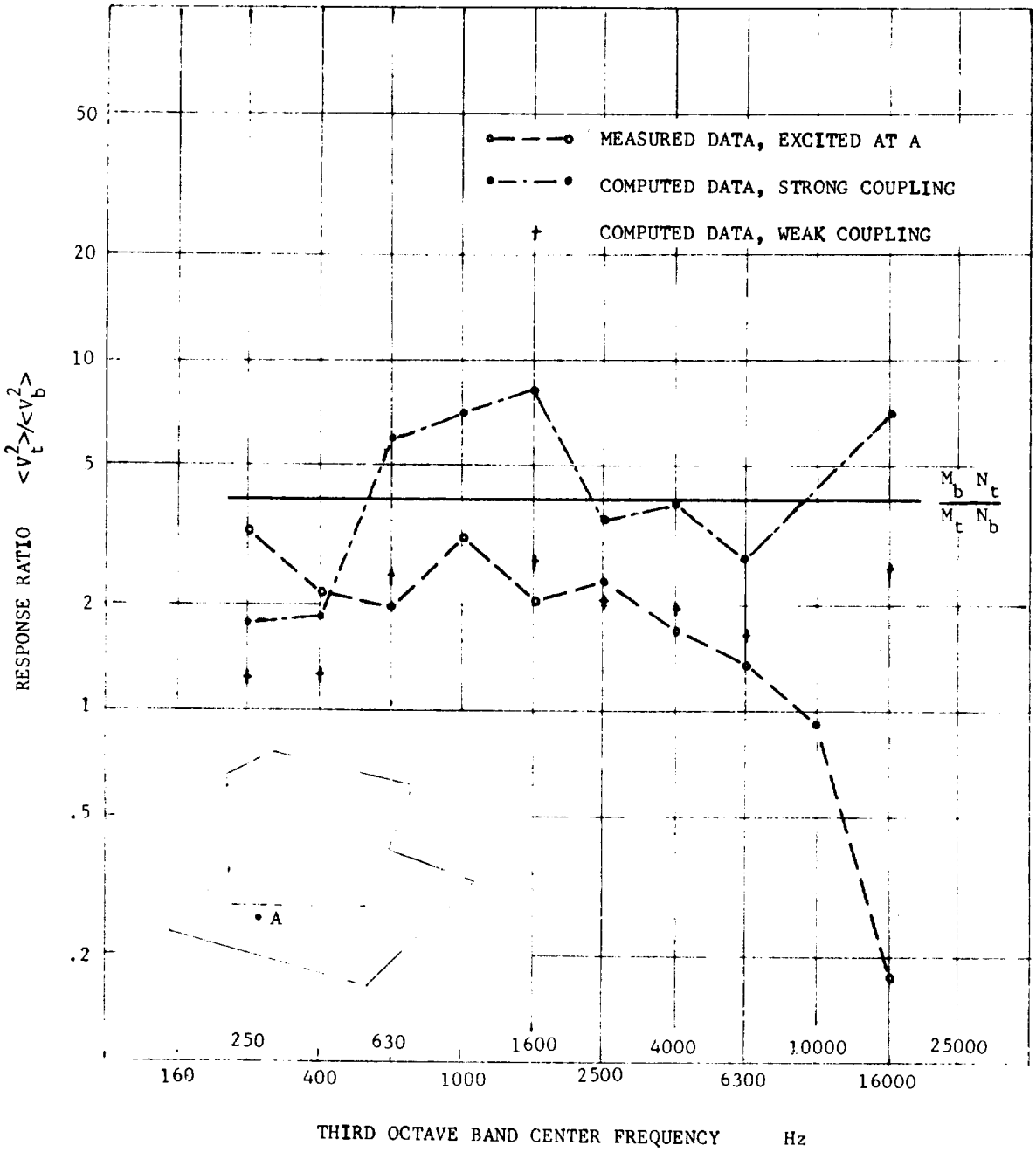

FIGURE 12 RESPONSE RATIOS OF THE TWO-PLATE SYSTEM WHEN BASE PLATE IS EXCITED

in the directly excited substructure and the indirectly excited substructure become equal. This condition makes it necessary that g_{ij} has to approach infinity in order for SEA to be applicable (see Equation (39)). Referring to Figure 12, the data seem to indicate that for the major portion of the frequency range, the computed response ratios based on the measured damping factors of a weak coupling case are more close to the actual measured ratio, while the computed ratios based on the strong coupling case are higher except in the low frequency end. The difference in the computed ratio data is believed due to the fact that the lower thickness of the top plate yields a low η_t which gives rise to a high $<V_t^2>/<V_b^2>$ ratio based on Equation (78). As will be shown later, the trend is reversed (i.e., strong coupling equation gives better fit), when the top plate is excited. Our conclusion is that in this case, the top plate is virtually cantilevered, the measured mean value $<V_t^2>$ is sensitive to the locations where the measurements are made. In the high frequency end (e.g., 16,000 Hz), the large deviation in the measured and computed results indicates the uncertainty in damping measurements based on which data Equations (78), (79) are applied.

When the top plate was excited, the estimated response ratio $<V_b^2>/<V_t^2>$ may be obtained by using Equation (53) with the measured loss factors η^a_{tb}, η_b, and η_t. In addition, instead of using measured values of $(\eta^a_{tb} - \eta_t)$, it may be evaluated analytically through the use of Equation (63) and the absorption coefficient γ. For the test model considered, the values of γ may be computed based on Equation (77). The results of γ/γ_o are plotted vs. one third octave band center frequency in Figure 13. As shown in the figure, the straight line result is based on the Kirchhoff plate theory and the curved line is based on the Mindlin theory. Similar to Figure 12, Figure 14 shows the measured and computed values of the response ratio $<V_b^2>/<V_t^2>$ when the top plate was excited. The dotted line represents the response ratios computed based on the theoretical absorption coefficient γ as given in Figure 13. The computed response ratios based on Equations (78), (79) are also plotted in Figure14. In this case, Equation (78), based on the strong coupling assumption, yields data which are closer to the measured response ratio data.

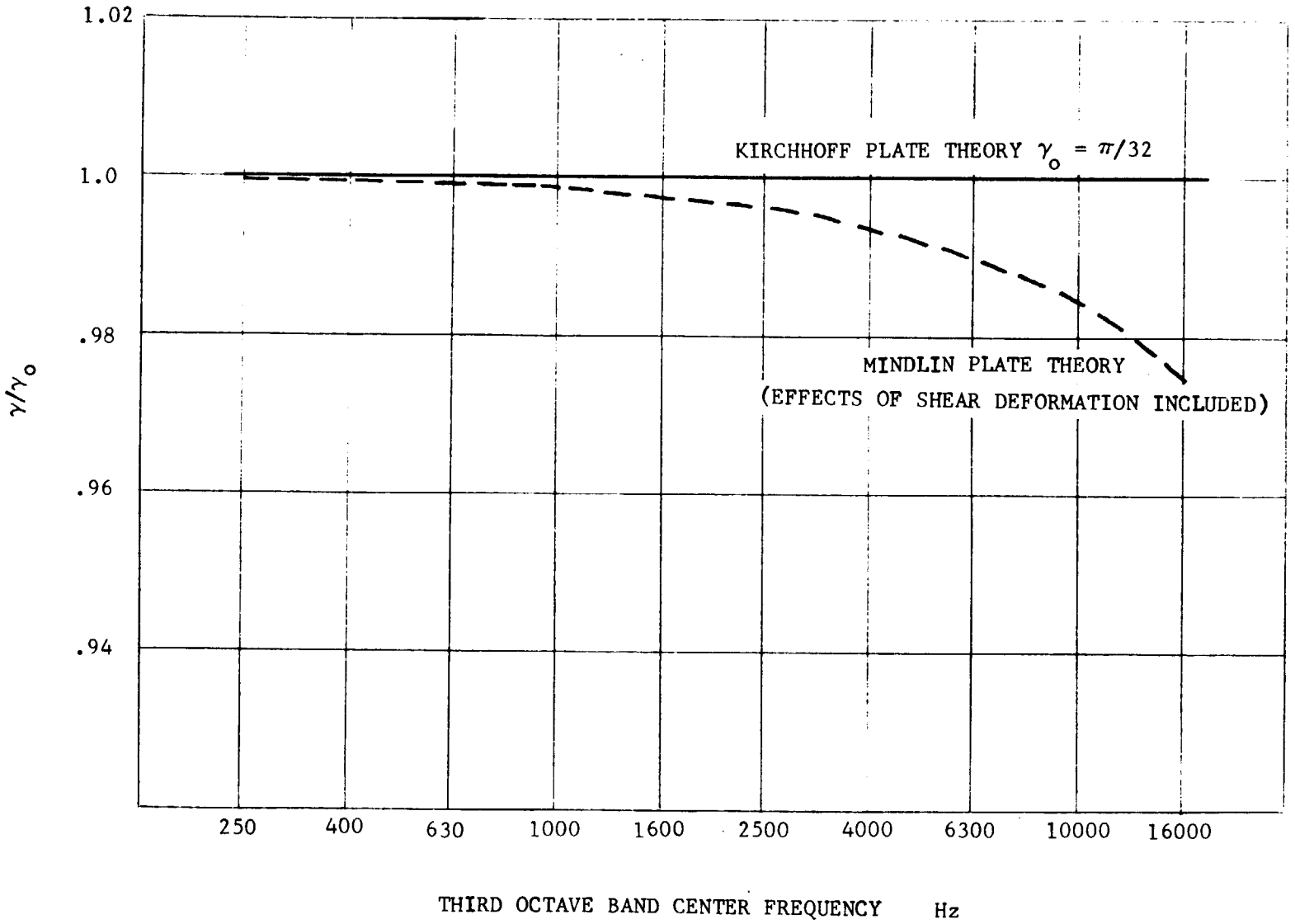

FIGURE 13. ABSORPTION COEFFICIENTS OF THE TWO-PLATE SYSTEM WHEN TOP PLATE IS EXCITED

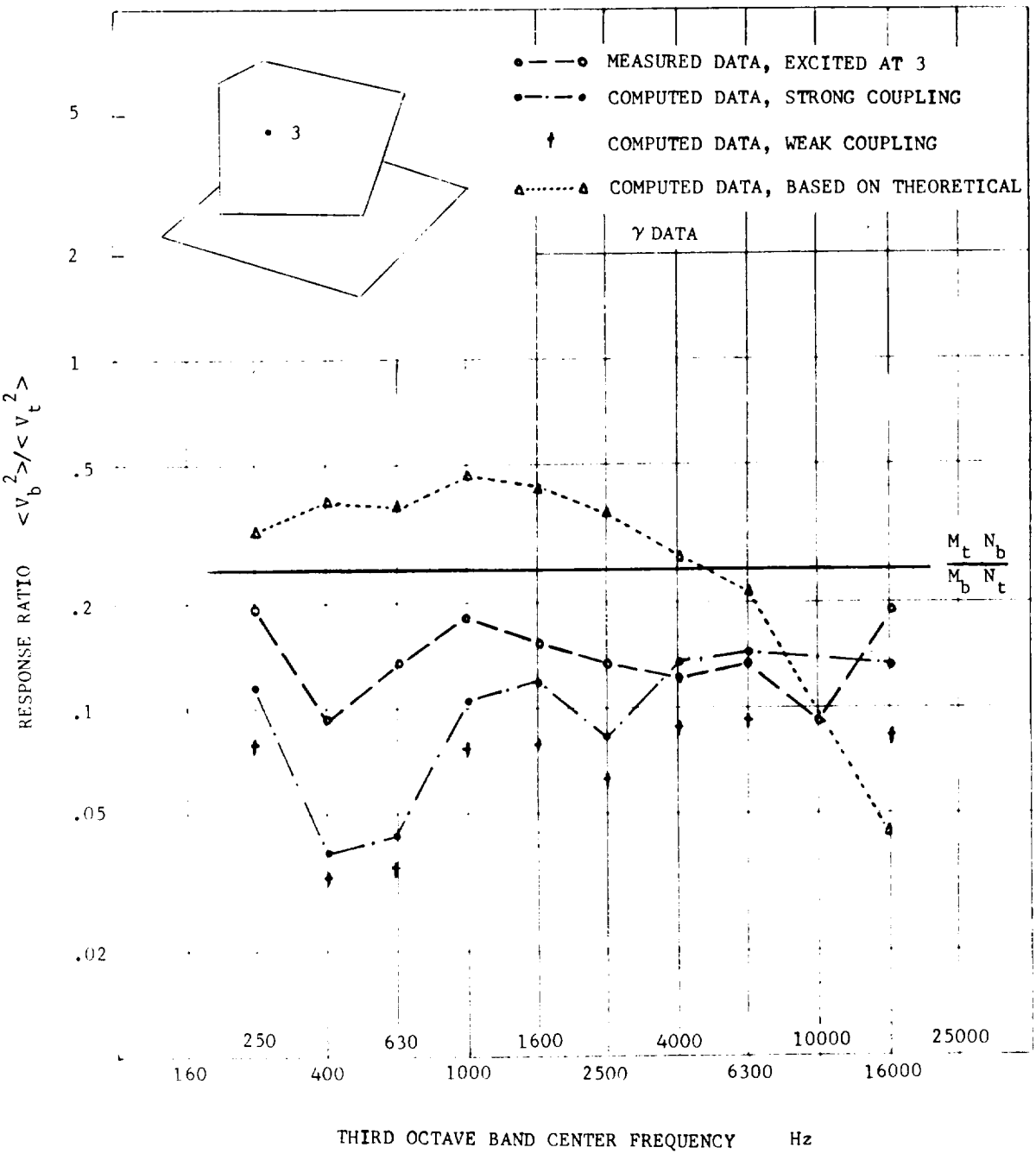

FIGURE 14 RESPONSE RATIOS OF THE TWO-PLATE SYSTEM WHEN TOP PLATE IS EXCITED

In order to evaluate the average mode-to-mode power flow coefficient $\bar{g}$ using Equations (47) and (50), the modal density is an important physical parameter. The modal density of a plate is given as:

$$n_p(f) = \sqrt{3}\ (1-\nu^2)\ A_p/C_p h_p \qquad (80)$$

where A_p is the area of the plate, h_p the plate thickness, ν the Poisson's ratio, and C_p the longitudinal wave speed of the plate material. Equation (80) gives $n_p(f) = .232$ mode/Hz for the base plate and $n_c(f) = 0.1605$ mode/Hz for the vertical plate. The analytical modal density data may be compared with the PSD peak count data in a high resolution PSD plots such as those generated by the real time analyzer. Typical PSD plot of the vertical plate component covering the frequency range (580-680 Hz) is shown in Figure 15. The mode count yields 15 modes in 100 Hz band at the center frequency of 630 Hz, which compares well with the modal density data quoted above.

It has been shown previously (Inequality (61)) that in order for the SEA method to be applicable in a connected structure, it is required that the two-way average power flow coefficients between the mode sets be equal and positive. This condition is now examined based on the measured and computed response ratio data. The values of the average mode-to-mode power flow coefficients $\bar{g}$ may be obtained as follows:

1. $\bar{g}_{bt}$ -- using Equation (59) with measured data of response ratio $\langle V_t^2\rangle / \langle V_b^2\rangle$ when the base plate was excited, and η_t.
2. $\bar{g}_{tb}$ -- using Equation (59) with measured data of response ratio $\langle V_b^2\rangle / \langle V_t^2\rangle$ when top plate was excited, and η_b.
3. $\bar{g}'_{bt}$ -- using Equations (60) and (62) with the measured loss factors η_t, η_b, and η^a_{bt} or using Equation (59) with computed data of response ratio $\langle V_t^2\rangle / \langle V_b^2\rangle$ as shown in Figure 12.
4. $\bar{g}'_{tb}$ -- using Equations (60) and (62) with measured loss factors η_t, η_b, and η^a_{tb} or using Equation (59) with computed data of $\langle V_b^2\rangle / \langle V_t^2\rangle$ as shown in Figure 14.

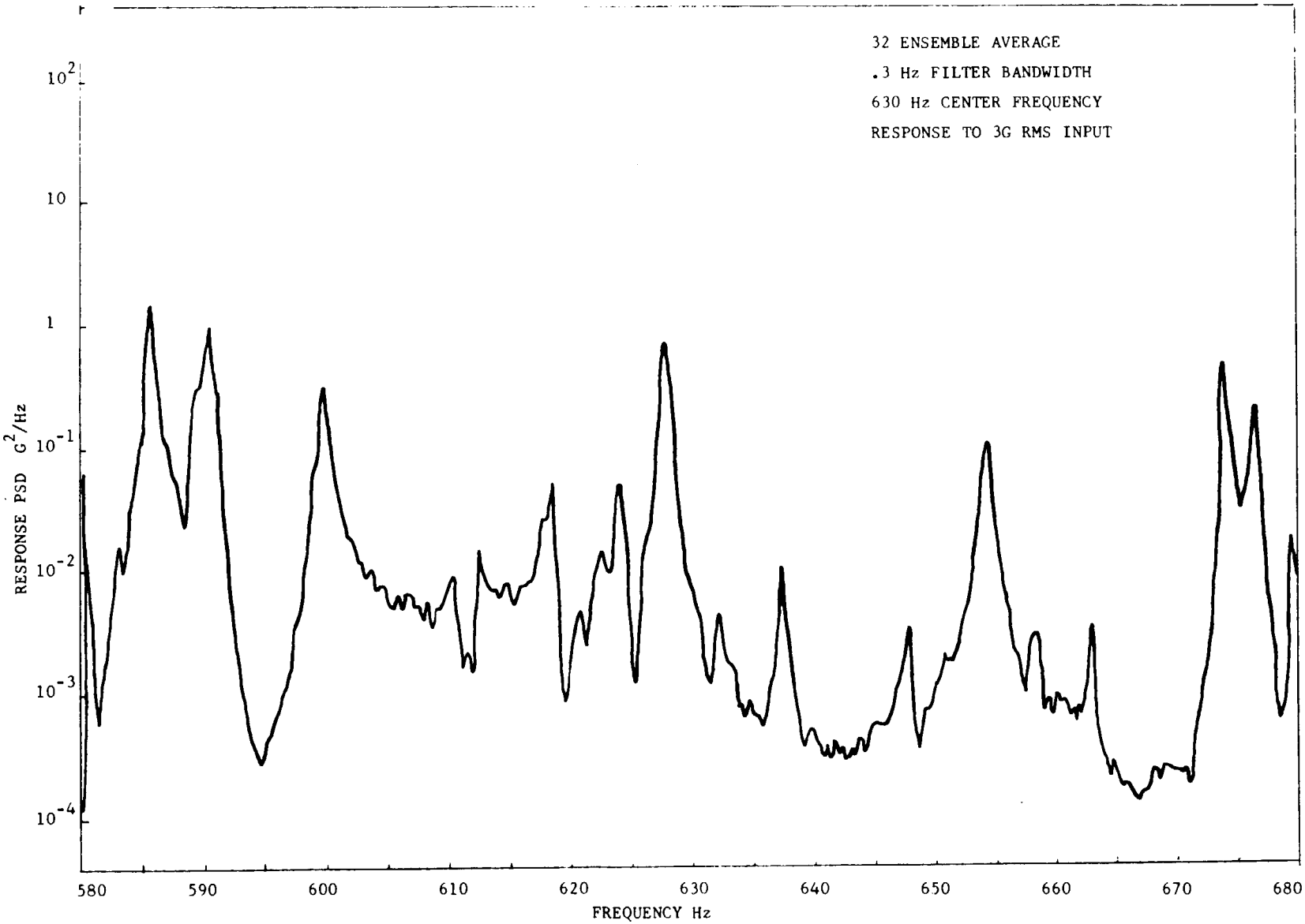

FIGURE 15 TYPICAL MODAL MAKEUP PLOT OF THE VERTICAL PLATE COMPONENT

The results of $\bar{g}_{bt}$ and $\bar{g}_{tb}$ are plotted in Figure 16 while $\bar{g}'_{bt}$ and $\bar{g}'_{tb}$ are plotted in Figure 17. As described above, $\bar{g}'_{bt}$ is computed based on Equations (60) and (62). Referring to Equation (62), η_c and $\bar{g}'_{bt}$ are negative if the numerator on the right side of (62) is positive and the denominator is negative. In other words, $\bar{g}'_{bt}$ is negative (and thus unacceptable in the physical sense) if the following is true:

$$\eta_t - \frac{N_b}{N_t} (\eta^a_{bt} - \eta_b) < 0 \qquad (81)$$

For the two-plate system, it was found that in the frequency range (630-1600 Hz), condition (81) is true. As a result, $\bar{g}'_{bt}$ data are not shown in Figure 16 corresponding to this frequency range.

Test Data of Model No. 2

The second model has a half cylindrical shell welded lengthwise to the base plate along the longitudinal boundaries of the shell (Figure 3b). The average values of the apparent loss factor η^a_{cb} of the half shell of model Number 2, as well as the dissipative loss factor η_c of the half shell component, are plotted in Figure 18. (Note that Figure 18 also includes one apparent loss factor plot for model No. 3, to be discussed later in the report.) The average values of the apparent loss factor η^a_{bc} of the base plate of model No. 2 are plotted in Figure 19.

The response ratio plots for model No. 2 are given in Figures 20 and 21. Figure 20 shows the values of $\langle V_c^2 \rangle / \langle V_b^2 \rangle$ when the base plate was excited. Also plotted in the figure are the computed data based on Equation (53) and the measured loss factor data. The response ratio plots $\langle V_b^2 \rangle / \langle V_c^2 \rangle$ when the top shell was excited are given in Figure 21, where one curve corresponds to the measured data, and the other curve corresponds to the computed data based on Equation (53).

The analytical expressions of the average input power per unit width in the plate and the average transmitted power in the half cylindrical shell are defined in Appendix IV by Equations (IV-4c) and (IV-34) respectively.

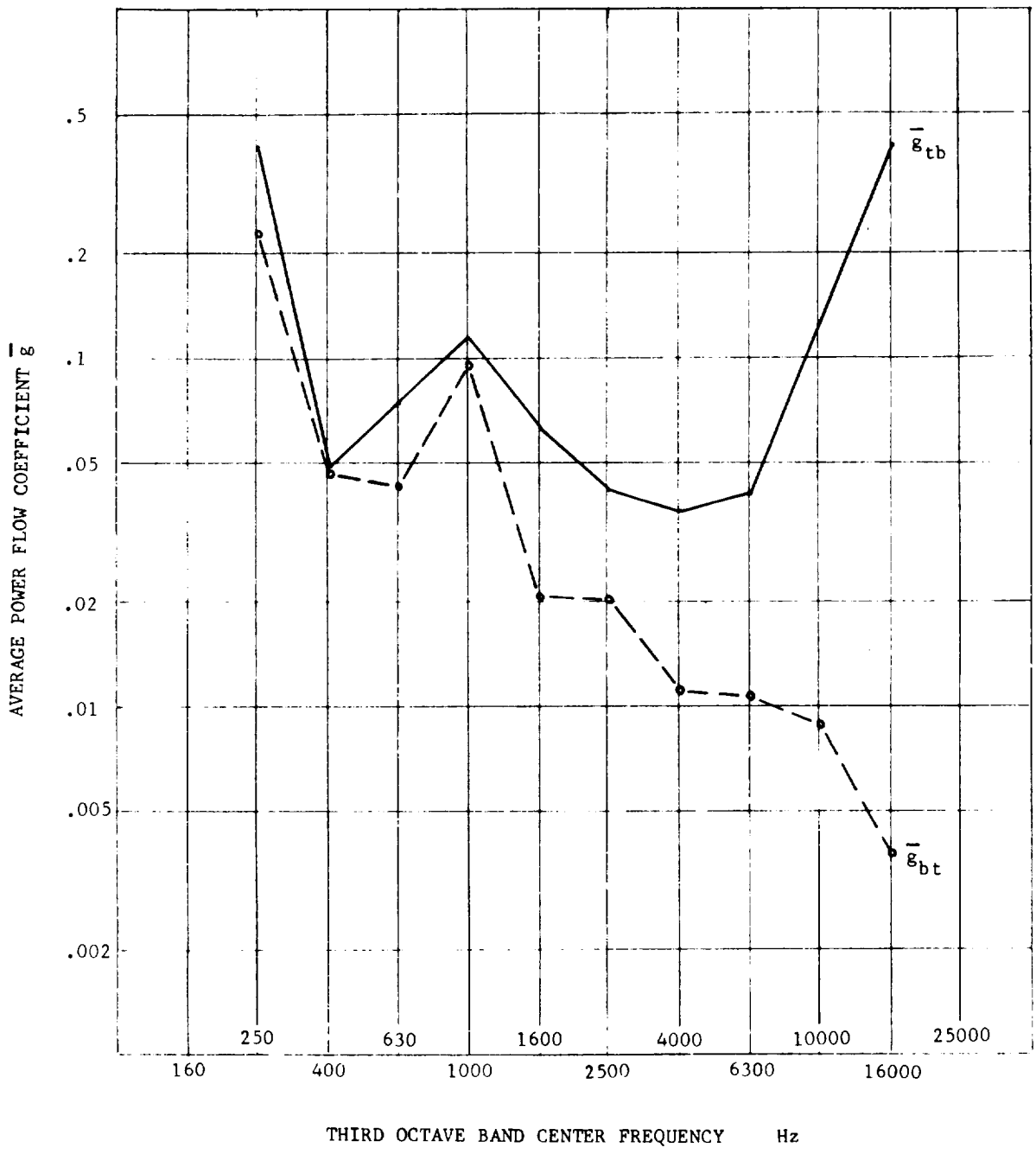

FIGURE 16 AVERAGE POWER FLOW COEFFICIENTS OF THE TWO-PLATE SYSTEM BASED ON MEASURED RESPONSE RATIO DATA

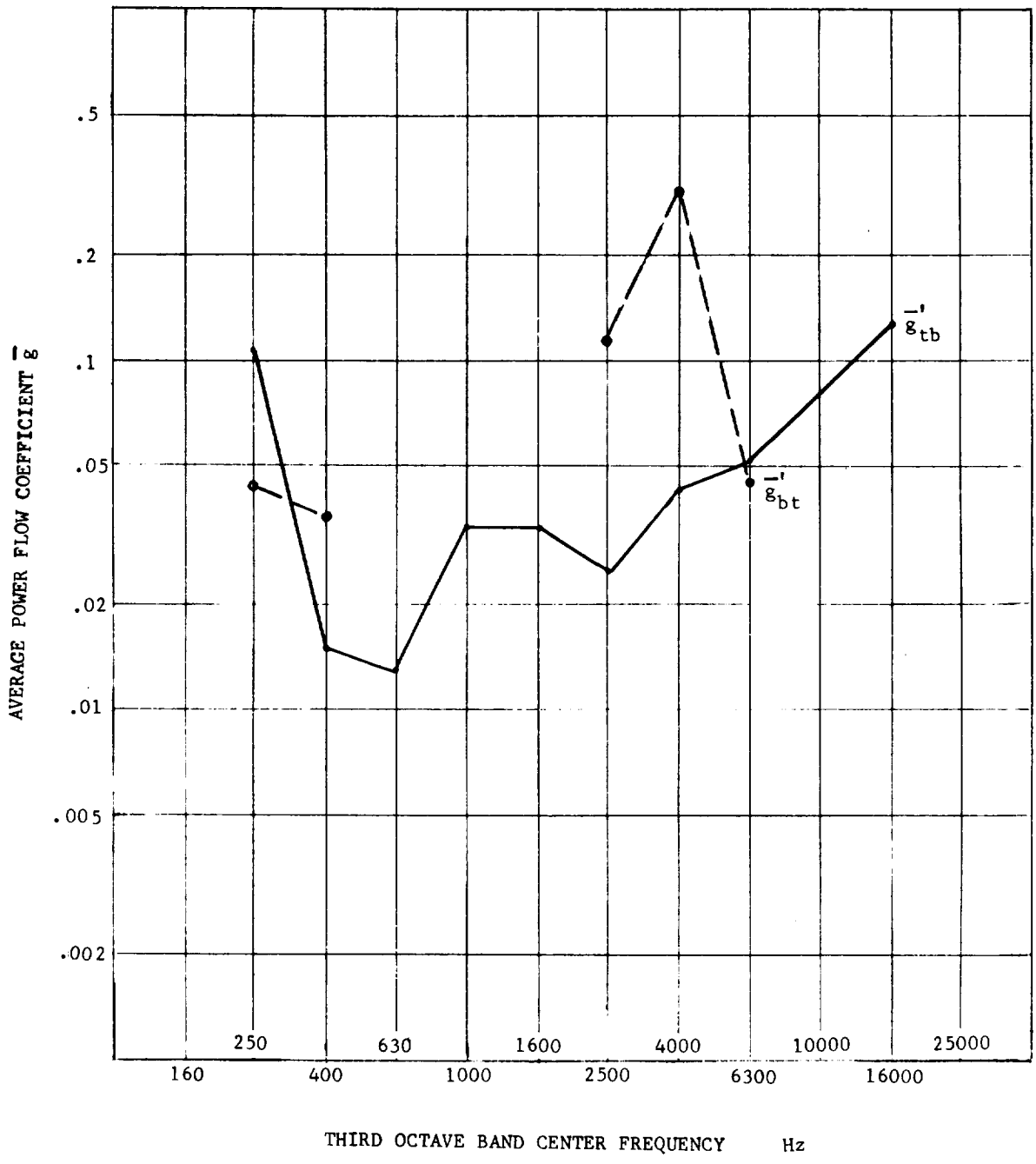

FIGURE 17 AVERAGE POWER FLOW COEFFICIENTS OF THE TWO-PLATE SYSTEM BASED ON COMPUTED RESPONSE RATIO DATA

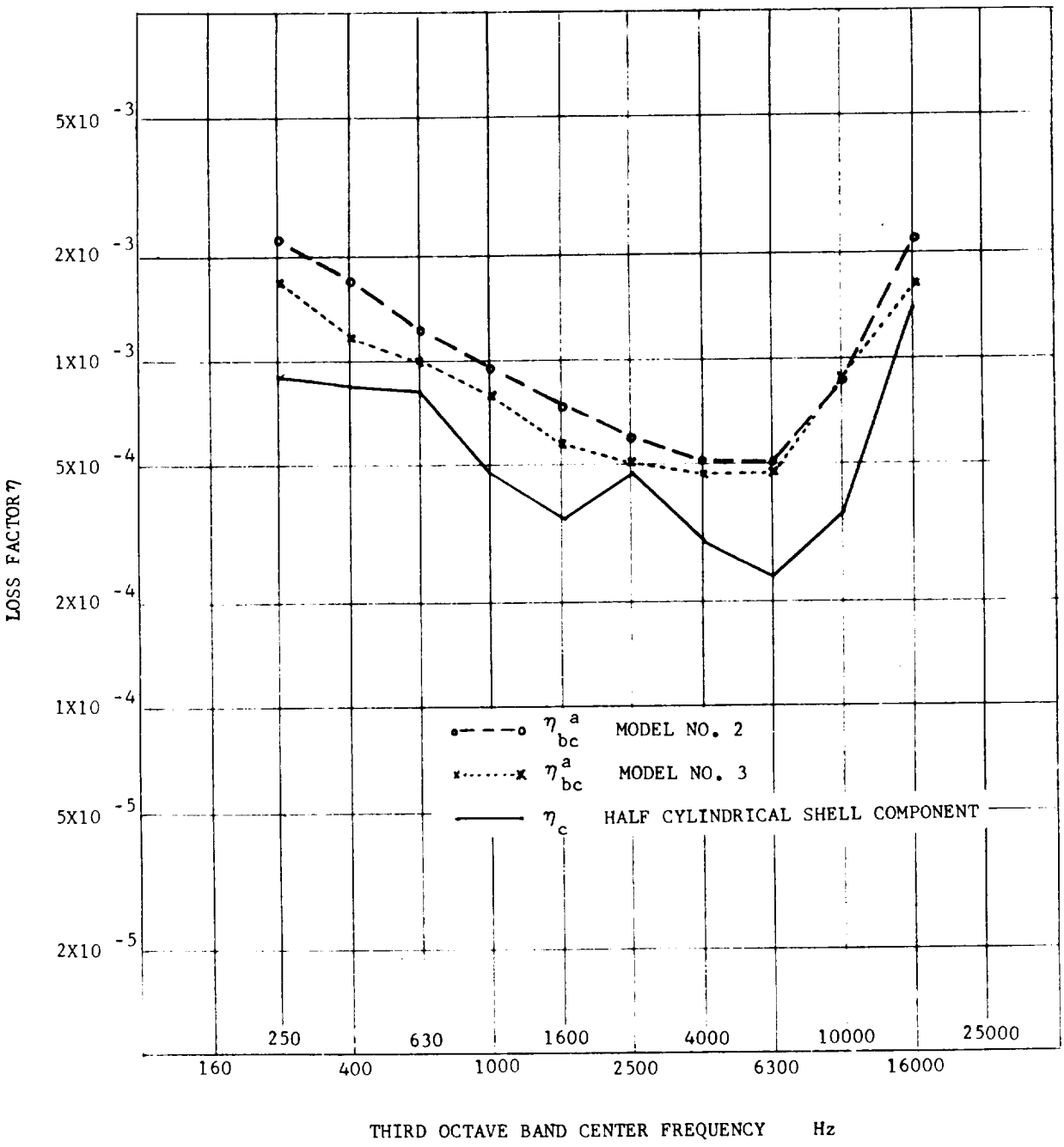

FIGURE 18 LOSS FACTORS MEASURED AT THE TOP SHELL OF MODELS NO. 2 AND 3 WHEN TOP SHELL IS EXCITED

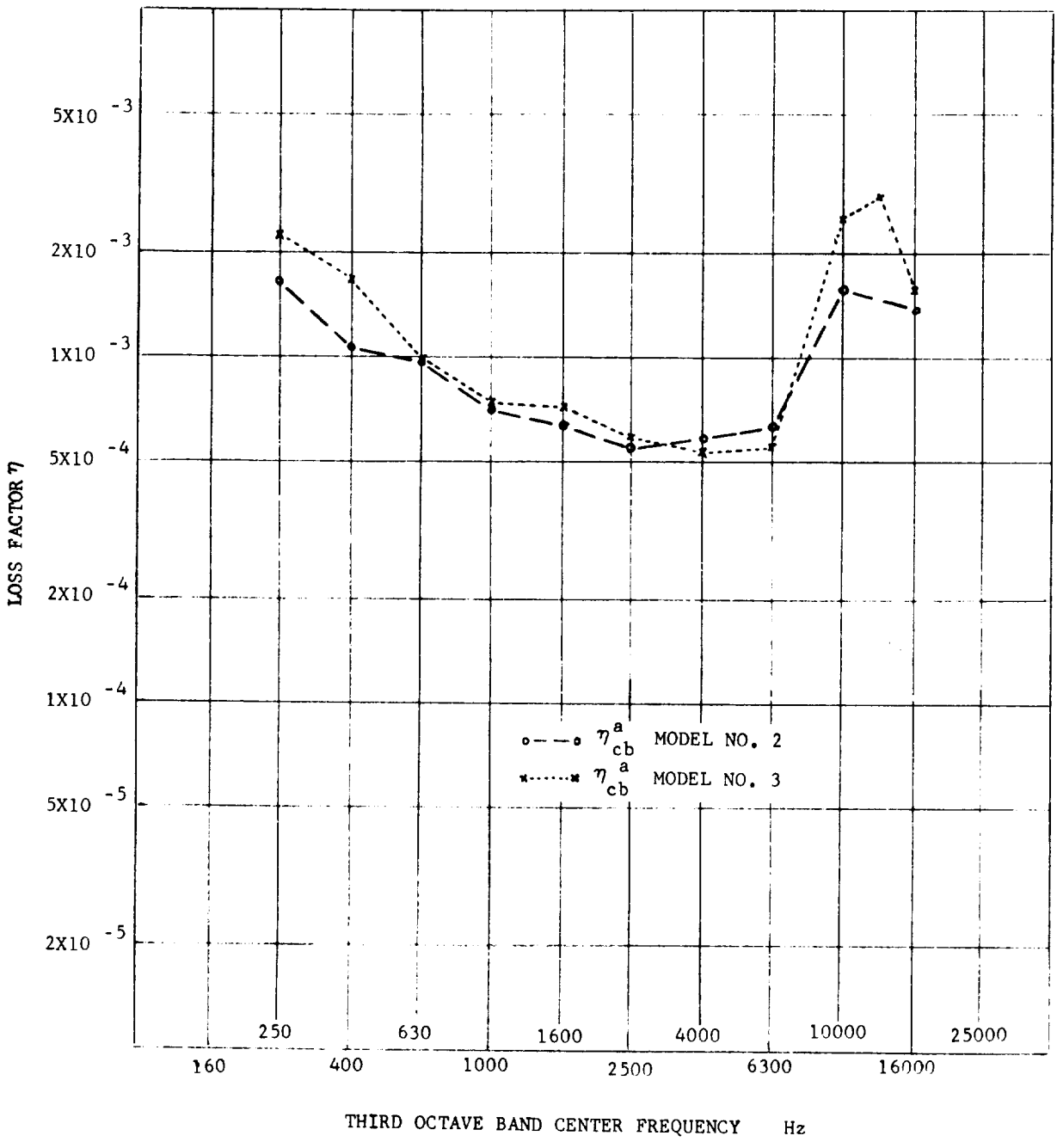

FIGURE 19 LOSS FACTORS MEASURED AT THE BASE PLATE OF MODELS NO. 2 AND 3 WHEN BASE PLATE IS EXCITED

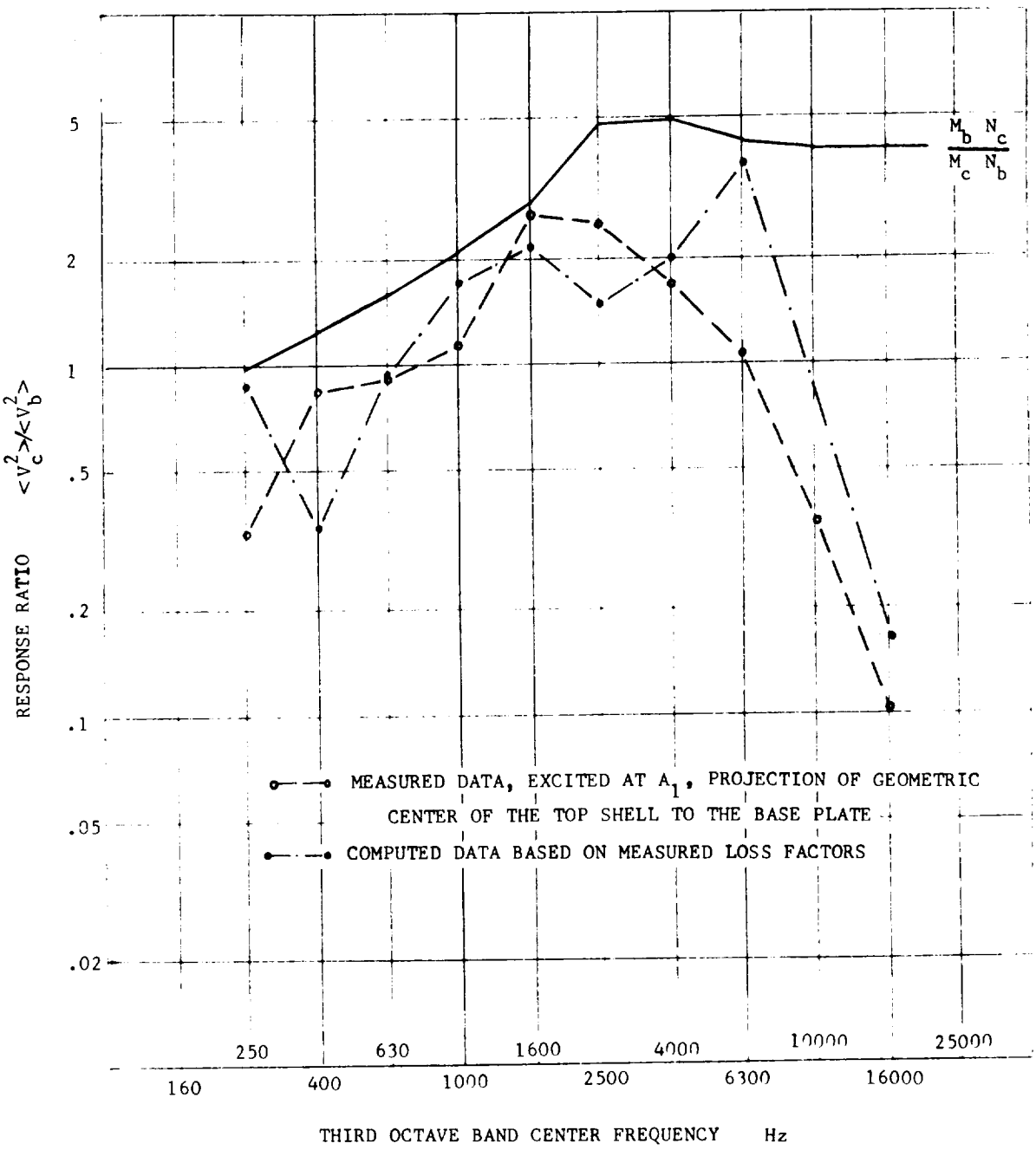

FIGURE 20 RESPONSE RATIOS OF MODEL NO. 2 WHEN BASE PLATE IS EXCITED

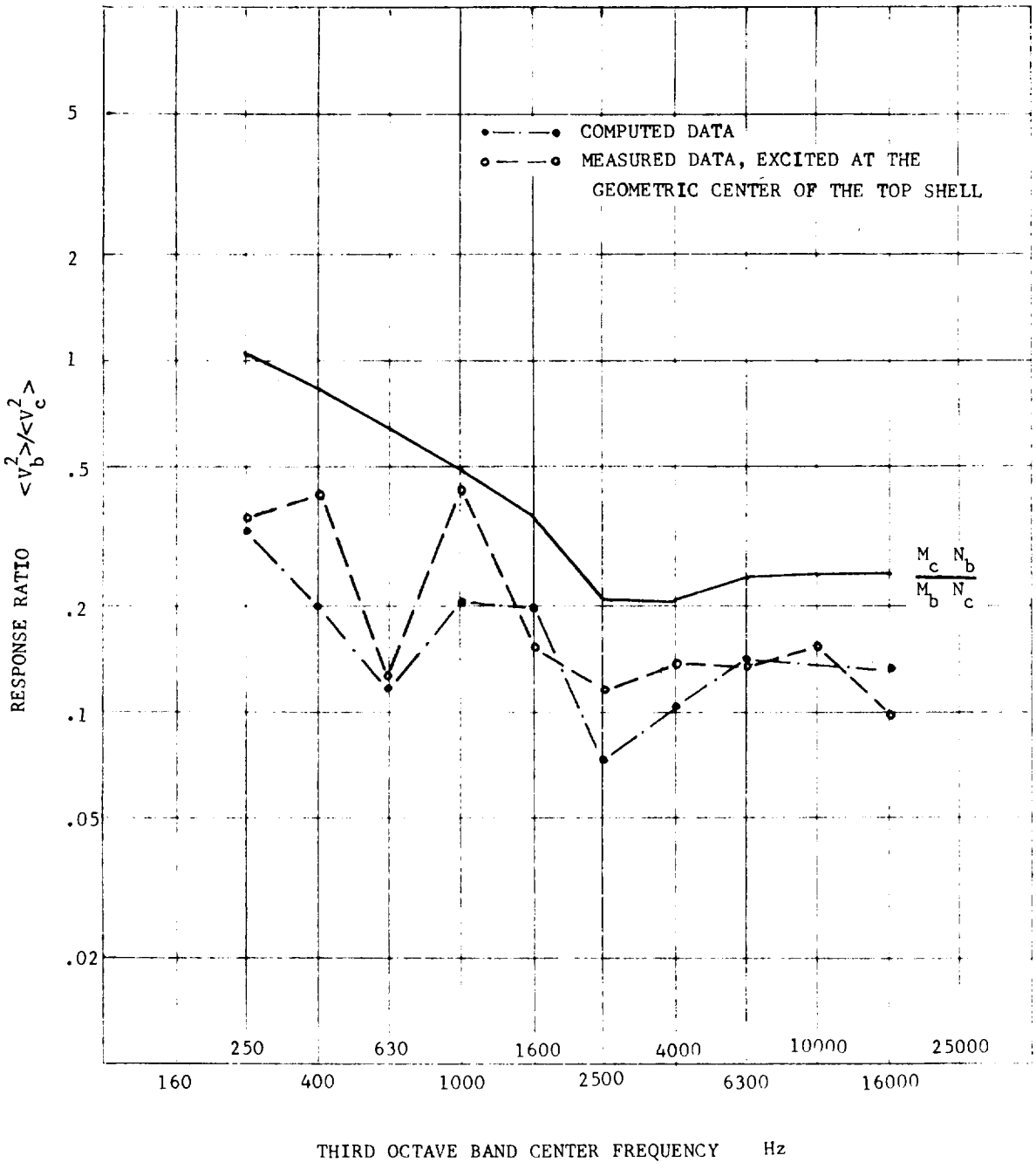

FIGURE 21 RESPONSE RATIOS OF MODEL NO. 2 WHEN TOP SHELL IS EXCITED

Work was carried out to calculate the ratio of the average transmitted power to the average input power. For this computation, use was made of Equations (III-9) to (III-13), (III-20), and (III-21), corresponding to various input bending wave frequencies and angles of incidence for Model No. 2. The results indicate a rather erratic variation of the average power based on strain energy rate in the shell with small values for some angles of incidence interspersed by very large peaks. The behavior is attributed to resonance effects in the cylindrical shell, most likely to the interaction of flexural and extensional waves. Because of the excessive oscillation of the power ratio as a function of the incidence angle, our conclusion is that it is impractical to compute the energy transfer coefficient of this model using the present analytical formulation.

The modal density of the half cylindrical shell is given in Reference 35 as:

$$n_c(f) = n_p(f) \frac{2}{\pi} \int_o^{\theta_1} \frac{d\theta}{\sqrt{1 - (f_r/f) \sin^4\theta}} \tag{82}$$

where

$n_p(f)$ = modal density of an equivalent plate, Equation (80)

$$f_r = \frac{1}{2\pi R} \sqrt{\frac{E}{\rho}} \tag{83}$$

R = radius of the cylindrical shell

$$\theta_1 = \begin{cases} \pi/2 & f \geq f_r \\ \sin^{-1} \sqrt{f/f_r} & f < f_r \end{cases}$$

The ratio n_c/n_p based on Equation (82) is shown as the solid line in Figure 22. The modal density function has a singularity at frequency f_r. As an alternate approach the total number of modes below a frequency f is

$$M(f) = n_p(f) f \frac{2}{\pi} \int_o^{\theta_1} \sqrt{1 - (f_r/f)^2 \sin^4\theta} \, d\theta \tag{84}$$

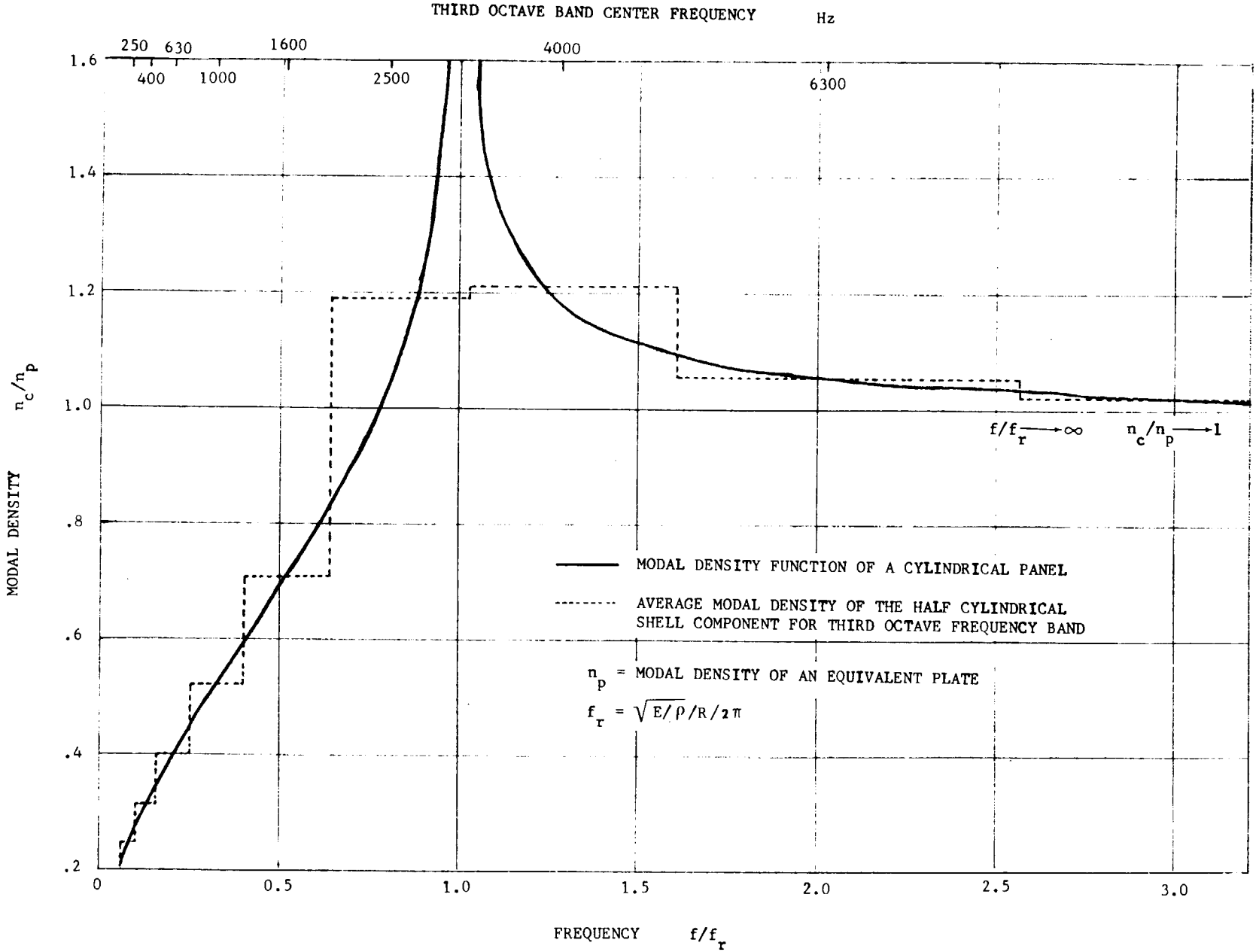

FIGURE 22 AVERAGE MODAL DENSITY OF THE HALF CYLINDRICAL SHELL OF MODEL NO. 2

The average modal density $\bar{n}_c(f_o)$ over a frequency bandwidth of Δf with center frequency f_o may be obtained as follows:

$$\bar{n}_c(f_o) = \frac{M(f_o + \frac{1}{2}\Delta f) - M(f_o - \frac{1}{2}\Delta f)}{\Delta f} \tag{85}$$

A computer program was prepared to compute the values of $\bar{n}_c(f_o)/n_p(f_o)$ for each 1/3 octave frequency band from f_o = 250 Hz to f_o = 16K Hz. The result is plotted in Figure 22 by the dotted lines. For the half cylindrical shell of model No. 2, f_r is equal to 3120 Hz. Based on the values of $\bar{n}_c(f)$, the upper limit lines for the response ratios similar to the limit line of Figure 12 are drawn in Figures 20 and 21. The limiting line corresponds to $\langle V_c^2 \rangle / \langle V_b^2 \rangle = M_b N_c / M_c N_b$ in Figure 20 and corresponds to $\langle V_b^2 \rangle / \langle V_c^2 \rangle = M_c N_b / M_b N_c$ in Figure 21. The average mode-to-mode power flow coefficients for model No. 2 are plotted in Figures 23 and 24. Similar to the two-plate system (Figures 16 and 17), the values of $\bar{g}_{bc}$, $\bar{g}_{cb}$ are computed based on the measured ratios and the dissipative loss factors using Equation (59). The values of $\bar{g}'_{bc}$ and $\bar{g}'_{cb}$ are computed based on the measured apparent and dissipative loss factors using Equations (60) and (62).

Test Data of Model No. 3

The third model features an open-end circular cylindrical shell welded to the base plate (Figure 3c). The average values of the apparent loss factor η^a_{cb} of the cylindrical shell of the model were measured and plotted in Figure 18. Since no individual cylindrical shell component was fabricated, the values of dissipative loss factor η_c of the half cylindrical component of model No. 2 (with the same thickness) were used in the computation. The average values of the apparent loss factor η^a_{bc} of the base plate of the model are plotted in Figure 19.

The response ratio plots of the model are given in Figures 25 and 26. Figure 25 shows the measured and computed values of $\langle V_c^2 \rangle / \langle V_b^2 \rangle$ when the base plate was excited. The plots of $\langle V_b^2 \rangle / \langle V_c^2 \rangle$ when the cylindrical shell was excited are illustrated in Figure 26.

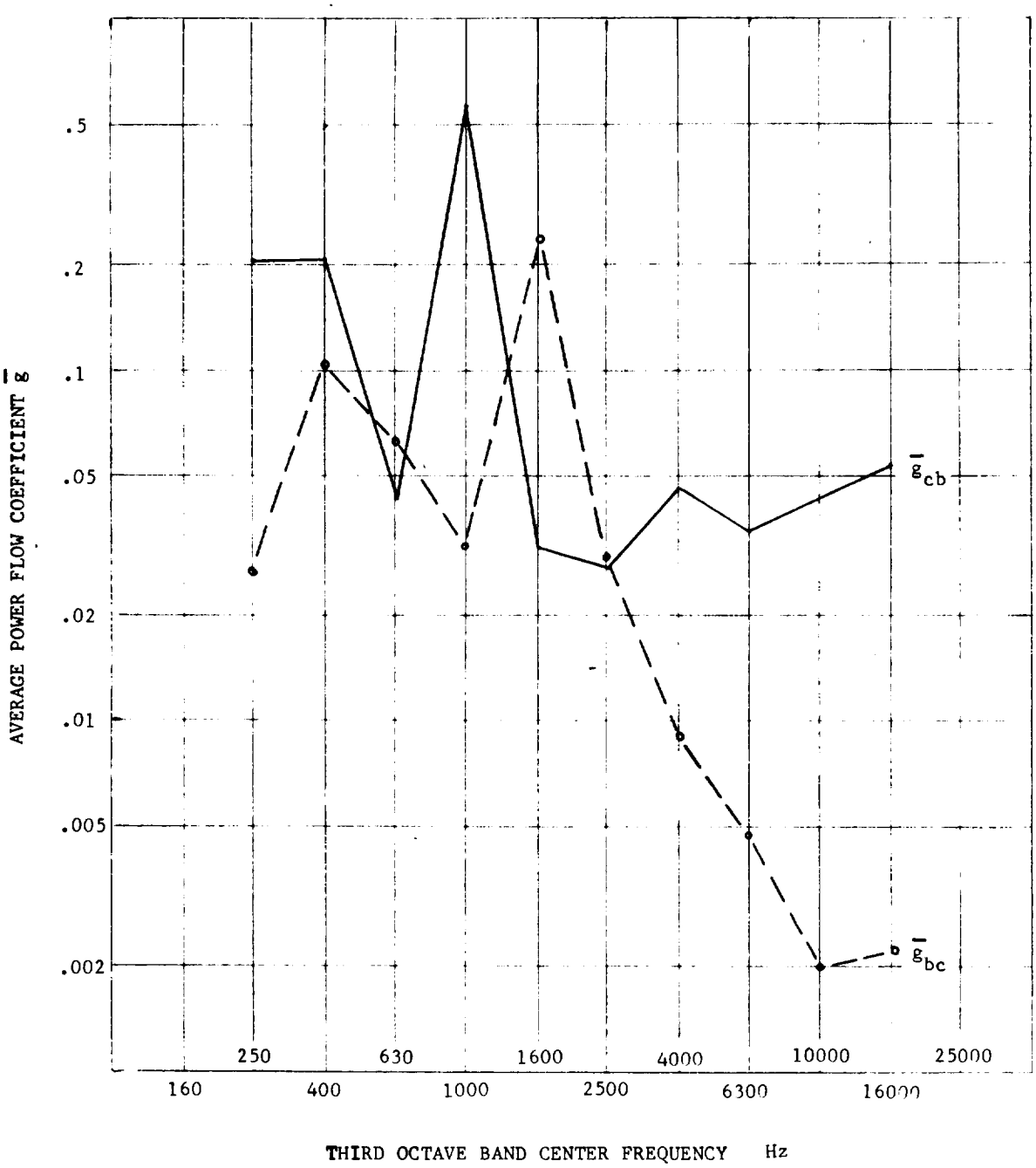

FIGURE 23 AVERAGE POWER COEFFICIENTS OF MODEL NO. 2 BASED ON MEASURED RESPONSE RATIO DATA

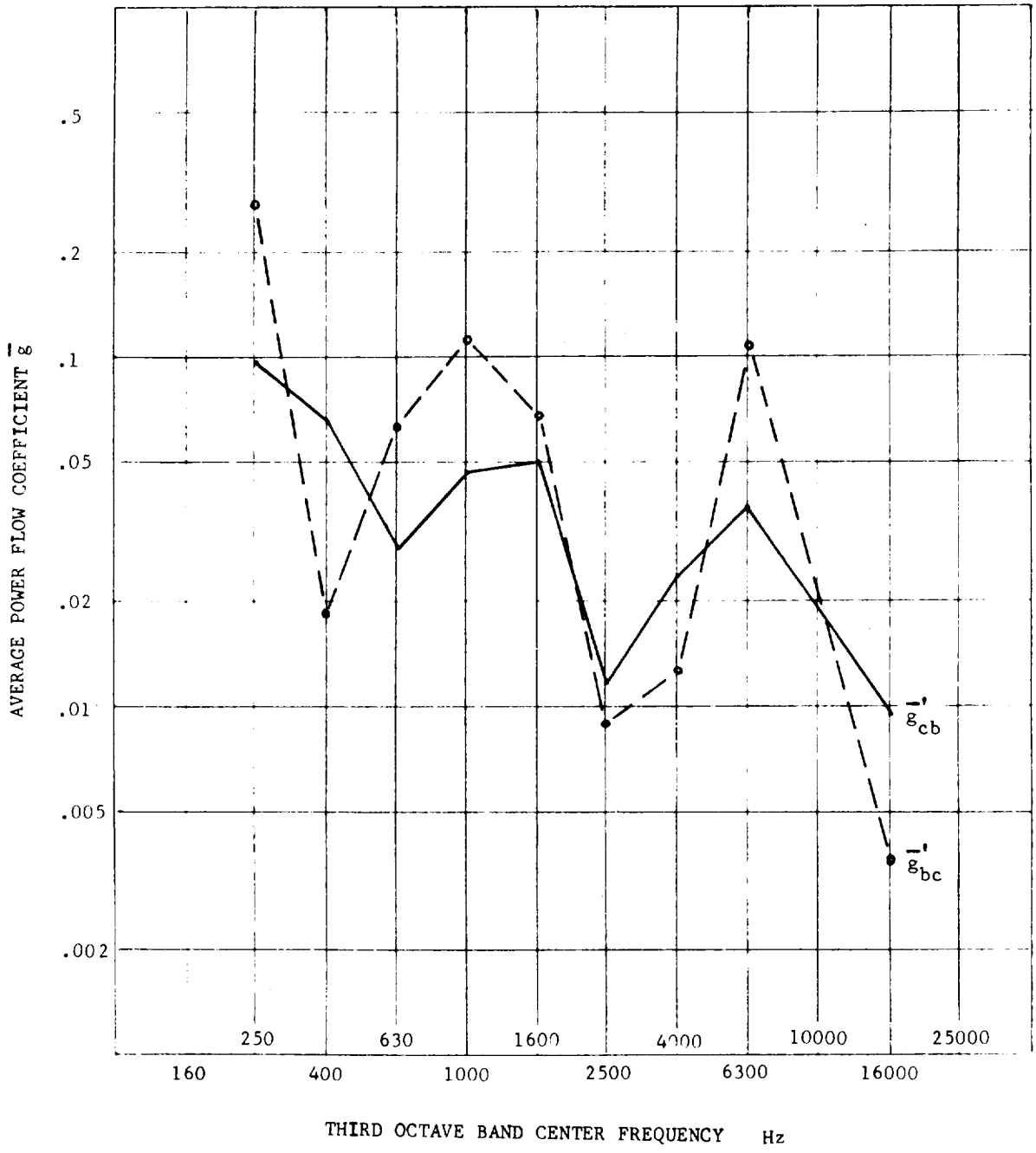

FIGURE 24 AVERAGE POWER COEFFICIENTS OF MODEL NO. 2 BASED ON COMPUTED RESPONSE RATIO DATA

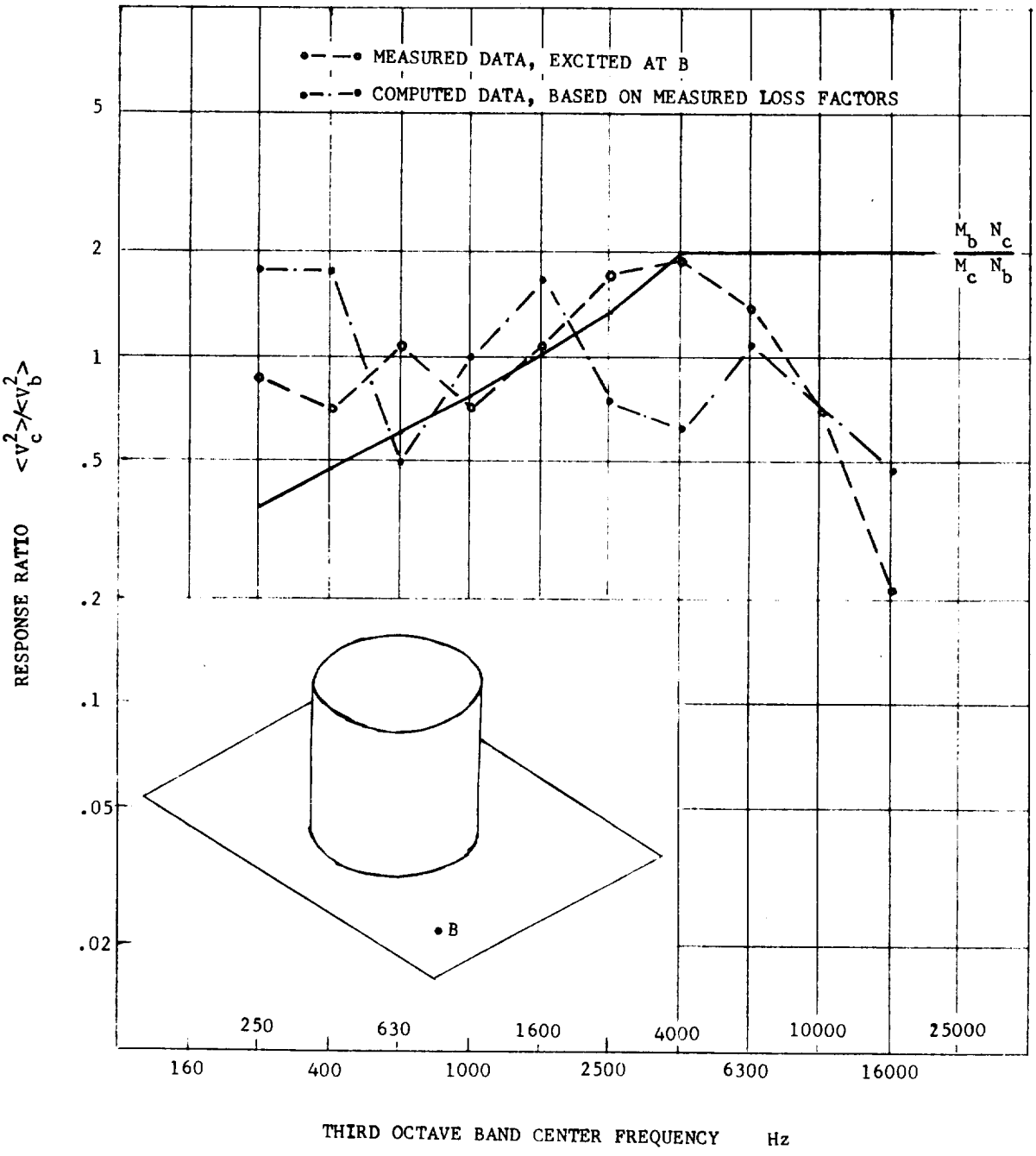

FIGURE 25. RESPONSE RATIOS OF MODEL NO. 3 WHEN BASE PLATE IS EXCITED

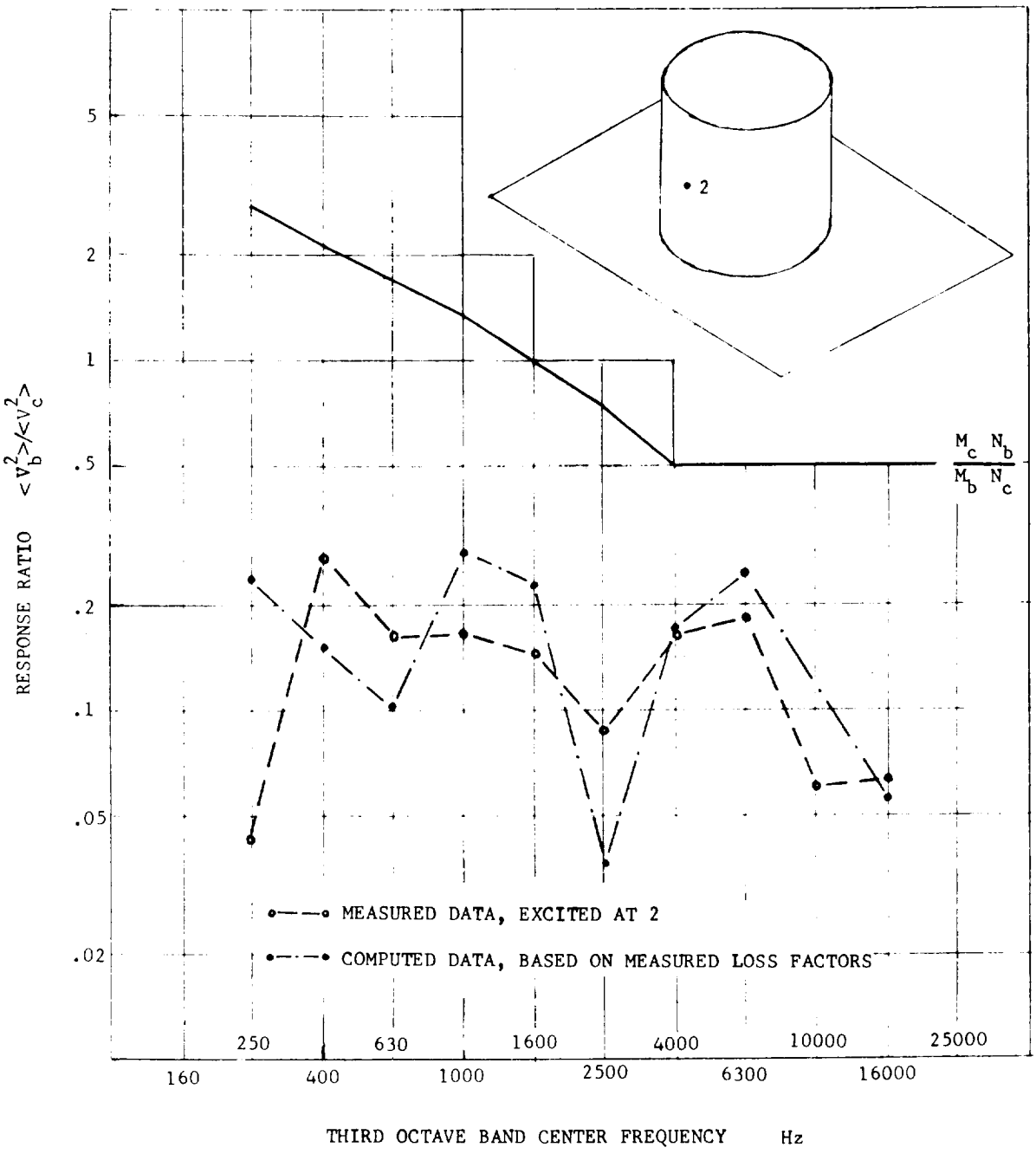

FIGURE 26 RESPONSE RATIOS TO MODEL NO. 3 WHEN TOP SHELL IS EXCITED

For a finite cylindrical shell of length ℓ, Reference 55 gives the total number of natural frequencies below a given frequency f. The formula is:

$$M(f) = \begin{cases} n_p(f)\,\frac{f_r}{\pi}\left\{\frac{(2\mu-1)}{2}\left[\frac{\pi}{2}+\sin^{-1}(2\mu-1)\right]+\sqrt{\mu-\mu^2}\right\} & \mu = f/f_r \\ & \text{for } f < f_r \\ n_p(f)\,f \qquad \text{for } f \geq f_r & \end{cases} \tag{86}$$

where f_r is the reference frequency as defined by Equation (83), and $n_p(f)$ is the modal density of a flat plate with the area $\pi R\ell$ (half the cylindrical surface). The average modal density $\bar{n}_c(f_o)$ over a frequency bandwidth Δf with center frequency of f_o may be obtained using Equation (85). With the modal density data, the upper limits of the response ratios for the sub-structures of model No. 3 are determined. These limits are plotted in Figures 25, 26. As shown in Figure 25, both the measured and computed response ratio data surpassed the upper limit curve for frequencies under 2000 Hz. This fact can be interpreted by the observation that the interface between the plate and the cylindrical shell forms a boundary which has a dominating effect on the low frequency motions of the based plate. As a result, the SEA formulation in its present form is not applicable to the structural configuration in the low frequency region.

CONCLUSIONS

In this report, the basic foundation and assumptions of the SEA method were studied in detail. A new formulation based on the strong coupling case has been generated and presented. As far as the power flow coefficient was concerned, the previous formulation based on the weak coupling case could be considered as a special case of the strong coupling case. On the other hand, in determining the kinetic energy transfer between connected substructures, the presentation of the coupling loss factors and the definition of the apparent loss factors of a connected substructure were different between the weak and strong coupling cases. This deviation in turn caused a difference in the predicted substructure response ratios based on the experimental loss factors.

In an effort to determine the power flow coefficients between two typical connected substructures, three simple models were made which included a two plate system, a plate and a half cylindrical shell system, and a plate and an end-connected cylindrical shell system. For the two plate system, the analysis was carried out to completion. The response ratio prediction based on the analytical formulation indicated that through the frequency range of interest, the analytical method was correct to within the order of magnitude of the mean square response ratios (see for instance, Figure 14). In evaluating the deviation between the experimental and analytical results, our conclusion is that part of the deviation was due to the limitation and arbitrary assumptions made in the Statistical Energy Analysis method. On the other hand, the measurement of the experimental responses was based on the averaging of the response data at a number of randomly chosen locations. Since the motion was not perfected diffused, the experimental response data was dependent on the random locations selected. The existence of a partially diffused wave motion was considered a contributing factor to the deviation between the experimental and analytical results. Our experience on the SEA method is that even

though the basic guidelines as developed in the report are satisfied, the predicted mean square values are usually only accurate to within the order of magnitude of the experimental results.

For the plate and half cylindrical shell system, analytical formulation was carried out to define wave motions at various regions of the connected substructures. In the process, a set of definitive expressions was developed for the wave motions considering the interface. Based on the wave motion equations and the response formulation of Appendices III and IV, selected computation was carried out on the ratio of power input to the cylindrical shell at various frequencies and angles of incidence. Because of the excessive variation of the power ratio as a function of the incidence angle, it has been found impractical to compute the energy transfer coefficient using the present analytical formulation. On the other hand, for this model, the computed response ratios based on the substructure loss factors and the apparent loss factors compared favorably with the measured response ratio data (Figures 20, 21). As far as the average power flow coefficients were concerned, the variations between the experimental data and the computed data again covered a band whose maximum at any one frequency might differ from the minimum value by one order of magnitude.

The third model consisted of a flat plate and a complete cylindrical shell with one end welded to the flat plate. For this structure, because of the strong interaction of the interface, it was found that the SEA method was not capable of reaching any intelligent prediction of the coupling loss factors, and the energy transfer coefficients. This fact was also confirmed by the guidelines which indicated that the SEA method in its present form was not applicable to the model under consideration.

In exploring the application of the SEA method, certain limitations were encountered. In general, for a connected structure it is not uncommon that the predicted mean square response data and the power flow data differed from the corresponding experimental data by one order of magnitude. For this reason, the SEA method seemed at best to serve the purpose of trend prediction when the guidelines were carried out and presented in this report. These derivations illustrated the vibrational energy transfer mechanisms between the specific substructures under consideration.

APPENDIX I

FLEXURAL WAVE PROPAGATION IN A TWO PLATE SYSTEM CONSIDERING ROTATORY INERTIA AND TRANSVERSE SHEAR

Mindlin (Reference 50) deduced a two-dimensional theory of flexural motions of isotropic, elastic plate from the three-dimensional equation of elasticity. The theory includes the effects of rotatory inertia and transverse shear in the same manner as Timoshenko's one-dimensional theory of bars. For this case, the three equations of motion may be expressed in terms of the plate-displacements as follows:

$$\frac{D}{2}\left[(1-\nu)\nabla^2\psi_x + (1+\nu)\frac{\partial \emptyset}{\partial x}\right] - \kappa^2 Gh\left(\psi_x + \frac{\partial w}{\partial x}\right) = \frac{\rho h^3}{12}\frac{\partial^2 \psi_x}{\partial t^2} \qquad (I\text{-}1)$$

$$\frac{D}{2}\left[(1-\nu)\nabla^2\psi_y + (1+\nu)\frac{\partial \emptyset}{\partial y}\right] - \kappa^2 Gh\left(\psi_y + \frac{\partial w}{\partial y}\right) = \frac{\rho h^3}{12}\frac{\partial^2 \psi_y}{\partial t^2} \qquad (I\text{-}2)$$

$$\kappa^2 Gh\,(\nabla^2 w + \emptyset) = \rho h \frac{\partial^2}{\partial t^2} w \qquad (I\text{-}3)$$

where

$$\nabla^2 = \frac{\partial^2}{\partial x^2} + \frac{\partial^2}{\partial y^2}$$

κ = a constant involving Poisson's ratio (see Reference 50)

G = shear modulus $\left(\frac{E}{2(1+\nu)}\right)$

D = plate bending modulus $\left(\frac{Eh^3}{12(1-\nu^2)}\right)$

ν = Poisson's ratio

h = plate thickness

ρ = density of the plate

w = transverse displacement of the plate

ψ_x, ψ_y = changes of slope

$$\emptyset = \frac{\partial \psi_x}{\partial x} + \frac{\partial \psi_y}{\partial y} \qquad \text{(I-4)}$$

$$G' = \kappa^2 G$$

The relations between the plate-stress and plate displacement components are

$$M_x = D\left(\frac{\partial \psi_x}{\partial x} + \nu \frac{\partial \psi_y}{\partial y}\right)$$

$$M_y = D\left(\frac{\partial \psi_y}{\partial y} + \nu \frac{\partial \psi_x}{\partial x}\right)$$

$$M_{yx} = \frac{1-\nu}{2} D\left(\frac{\partial \psi_y}{\partial x} + \frac{\partial \psi_x}{\partial y}\right) \qquad \text{(I-5)}$$

$$Q_x = \kappa^2 Gh\left(\frac{\partial w}{\partial x} + \psi_x\right)$$

$$Q_y = \kappa^2 Gh\left(\frac{\partial w}{\partial y} + \psi_y\right)$$

A single differential equation for w may be obtained by eliminating ψ_x and ψ_y from equations (I-1) through (I-3) to yield

$$\left(\nabla^2 - \frac{\rho}{\kappa^2 G}\frac{\partial^2}{\partial t^2}\right)\left(D\nabla^2 - \frac{\rho h^3}{12}\frac{\partial^2}{\partial t^2}\right)w + \rho h \frac{\partial^2 w}{\partial t^2} = 0 \qquad \text{(I-6)}$$

Consider a semi-infinite Plate No. 1 cantilevered to an infinite Plate No. 2 as shown in Figure I-1.

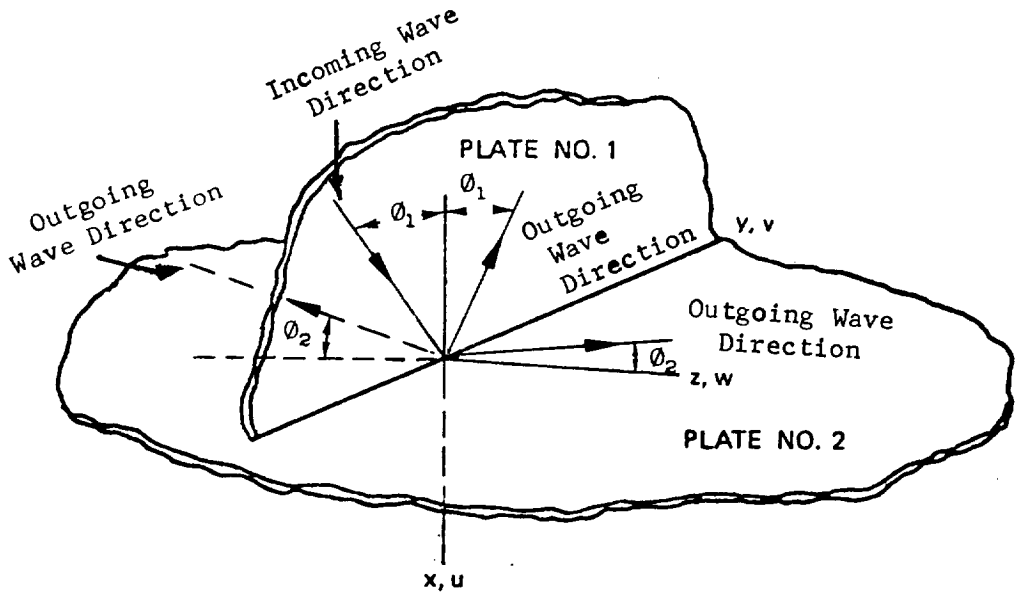

FIGURE I-1 A TWO-PLATE SYSTEM

Let the incoming wave (see Figure I-1) in Plate No. 1 be of the form

$$w_{i1} = e^{i\omega\left(t - \frac{y \sin \phi_1 + x \cos \phi_1}{c_{\omega 1}}\right)} \quad (x \leq 0) \tag{I-7a}$$

where, from equation (I-6), the wave speed $c_{\omega 1}$ is given by

$$\frac{1}{c_{\omega 1}} = \left\{ \frac{\rho_1}{2} \left[\frac{1}{G'_1} + \frac{1-\nu_1^2}{E_1} \pm \sqrt{\left(\frac{1}{G'_1} - \frac{1-\nu_1^2}{E_1}\right)^2 + \frac{48(1-\nu_1^2)}{\rho_1 E_1 h_1^2 \omega^2}} \right] \right\}^{1/2} \tag{I-7b}$$

Associated with the normal displacements are the rotation angles ψ_{xi1} and ψ_{yi1} given by equations (I-1) and (I-3) as

$$\psi_{xi1} = i\omega c_{\omega 1} \left(\frac{1}{c_{\omega 1}^2} - \frac{\rho_1}{G_1'} \right) \cos \phi_1 \; e^{i\omega\left(t - \frac{y \sin \phi_1 + x \cos \phi_1}{c_{\omega 1}}\right)} \tag{I-8a}$$

$$\psi_{yi1} = i\omega c_{\omega 1} \left(\frac{1}{c_{\omega 1}^2} - \frac{\rho_1}{G_1'} \right) \sin \phi_1 \; e^{i\omega\left(t - \frac{y \sin \phi_1 + x \cos \phi_1}{c_{\omega 1}}\right)} \tag{I-8b}$$

If

$$\omega^2 < \frac{12}{h_1^2} \frac{G_1'}{\rho_1} \tag{I-9}$$

Equation (I-7b) yields only one real wave speed, the value when the plus sign is used. In what follows, the range of ω will be assumed to be governed by equation (I-9). Then the outgoing flexural waves in Plate 1 can be represented by

$$w_{o1} = \left(A_1 \; e^{\frac{i\omega x \cos \phi_1}{c_{\omega 1}}} + B_1 \; e^{\omega \alpha_1 x} \right) e^{i\omega\left(t - \frac{y \sin \phi_1}{c_{\omega 1}}\right)} \tag{I-10a}$$

$$\psi_{xo1} = -\omega \left[i c_{\omega 1} \cos \phi_1 \left(\frac{1}{c_{\omega 1}^2} - \frac{\rho_1}{G_1'} \right) A_1 \; e^{i\omega \frac{x \cos \phi_1}{c_{\omega 1}}} \right.$$

$$\left. + \alpha_1 \left(1 + \frac{\rho_1 / G_1'}{\alpha_1^2 - \frac{\sin^2 \phi_1}{c_{\omega 1}^2}} \right) B_1 \; e^{\omega \alpha_1 x} + \sin^2 \phi_1 \; C_1 \; e^{\omega \alpha_1' x} \right] \cdot e^{i\omega\left(t - \frac{y \sin \phi_1}{c_{\omega 1}}\right)} \tag{I-10b}$$

$$\Psi_{yo1} = i\omega\, c_{\omega 1}\, \sin \phi_1 \left[\left(\frac{1}{c_{\omega 1}^2} - \frac{\rho_1}{G_1'} \right) A_1\, e^{i\omega \frac{x \cos \phi_1}{c_{\omega 1}}} \right.$$

$$\left. + \frac{1}{c_{\omega 1}^2} \left(1 + \frac{\rho_1 / G_1'}{\alpha_1^2 - \frac{\sin^2 \phi_1}{c_{\omega 1}^2}} \right) B_1\, e^{\omega \alpha_1 x} + \alpha_1'\, C_1\, e^{\omega \alpha_1' x} \right]$$

$$\cdot\, e^{i\omega \left(t - \frac{y \sin \phi_1}{c_{\omega 1}'} \right)} \qquad \text{(I-10c)}$$

where from equations (I-1) to (I-3) and (I-6)

$$\alpha_1 = \left\{ \frac{\rho_1}{2} \left[(1 + \sin^2 \phi_1) \sqrt{\left(\frac{1}{G_1'} - \frac{1-\nu_1^2}{E_1} \right)^2 + \frac{48(1-\nu_1^2)}{\rho_1 E_1 h_1^2 \omega^2}} \right. \right.$$

$$\left. \left. - \left(\frac{1}{G_1'} + \frac{1-\nu_1^2}{E_1} \right) \cos^2 \phi_1 \right] \right\}^{1/2} \qquad \text{(I-10d)}$$

$$\alpha_1' = \left(\frac{\sin^2 \phi_1}{c_{\omega 1}^2} - \frac{\rho_1}{G_1} + \frac{12\, \kappa^2}{\omega^2 h_1^2} \right)^{1/2} \qquad \text{(I-10e)}$$

Note that the terms multiplied by C_1 are the so-called thickness-shear mode and are associated with a state of zero normal displacement. In the range of frequencies considered here only one outgoing wave is harmonic while the other two are of the Rayleigh type with an exponential decrease in amplitude as the distance from the joint increases. Similarly for Plate 2 the outgoing waves are given by

$$u_2^+ = \left(A_2^+\, e^{-i\omega \frac{z \cos \phi_2}{c_{\omega 2}}} + B_2^+\, e^{-\omega \alpha_2 z} \right) e^{i\omega \left(t - \frac{y \sin \phi_2}{c_{\omega 2}} \right)} \qquad \text{(I-11a)}$$

$$\psi_{z2}^{+} = \omega \left[ic_{\omega 2} \cos \phi_2 \left(\frac{1}{c_{\omega 2}^2} - \frac{\rho_2}{G_2'} \right) A_2^{+} e^{-i\omega \frac{z \cos \phi_2}{c_{\omega 2}}} \right.$$

$$\left. + \alpha_2 \left(1 + \frac{\rho_2 / G_2'}{\alpha_2^2 - \frac{\sin^2 \phi_2}{c_{\omega 2}^2}} \right) B_2^{+} e^{-\omega \alpha_2 z} + \sin^2 \phi_2 \; C_2^{+} e^{-\omega \alpha_2' z} \right] \cdot$$

$$\cdot e^{i\omega \left(t - \frac{y \sin \phi_2}{c_{\omega 2}} \right)} \qquad \text{(I-11b)}$$

$$\psi_{y2}^{+} = i\omega c_{\omega 2} \sin \phi_2 \left[\left(\frac{1}{c_{\omega 2}^2} - \frac{\rho_2}{G_2'} \right) A_2^{+} e^{-i\omega \frac{z \cos \phi_2}{c_{\omega 2}}} \right.$$

$$\left. + \frac{1}{c_{\omega 2}^2} \left(1 + \frac{\rho_2 / G_2'}{\alpha_2^2 - \frac{\sin^2 \phi_2}{c_{\omega 2}^2}} \right) B_2^{+} e^{-\omega \alpha_2 z} + \alpha_2' C_2^{+} e^{-\omega \alpha_2' z} \right] e^{i\omega \left(t - \frac{y \sin \phi_2}{c_{\omega 2}} \right)}$$

(I-11c)

for $z > o$ and

$$u_2^{-} = \left(A_2^{-} e^{i\omega \frac{z \cos \phi_2}{c_{\omega 2}}} + B_2^{-} e^{\omega \alpha_2 z} \right) e^{i\omega \left(t - \frac{y \sin \phi_2}{c_{\omega 2}} \right)} \qquad \text{(I-12a)}$$

$$\psi_{z2}^{-} = -\omega \left[ic_{\omega 2} \cos \phi_2 \left(\frac{1}{c_{\omega 2}^2} - \frac{\rho_2}{G_2'} \right) A_2^{-} e^{i\omega \frac{z \cos \phi_2}{c_{\omega 2}}} \right.$$

$$\left. + \alpha_2 \left(1 + \frac{\rho_2 / G_2'}{\alpha_2^2 - \frac{\sin^2 \phi_2}{c_{\omega 2}^2}} \right) B_2^{-} e^{\omega \alpha_2 z} - \sin^2 \phi_2 \; C_2^{-} e^{\omega \alpha_2' z} \right] e^{i\omega \left(t - \frac{y \sin \phi_2}{c_{\omega 2}} \right)}$$

(I-12b)

$$\psi_{y2}^{-} = i\omega c_{\omega 2} \sin\phi_2 \left[\left(\frac{1}{c_{\omega 2}^2} - \frac{\rho_2}{G_2'} \right) A_2^{-} e^{i\omega \frac{z\cos\phi_2}{c_{\omega 2}}} \right.$$

$$\left. + \frac{1}{c_{\omega 2}^2} \left(1 + \frac{\rho_2 / G_2'}{\alpha_2^2 - \frac{\sin^2\phi_2}{c_{\omega 2}^2}} \right) B_2^{-} e^{\omega\alpha_2 z} - \alpha_2' C_2^{-} e^{\omega\alpha_2' z} \right] e^{i\omega \left(t - \frac{y \sin\phi_2}{c_{\omega 2}} \right)} \qquad \text{(I-12c)}$$

for $z < o$. Here

$$\frac{\sin \phi_2}{c_{\omega 2}} = \frac{\sin \phi_1}{c_{\omega 1}} \qquad \text{(I-13)}$$

and, with ω restricted also to the range

$$\omega^2 < \frac{12}{h_2^2} \frac{G_2'}{\rho_2} \qquad \text{(I-14)}$$

$$\frac{1}{c_{\omega 2}} = \left\{ \frac{\rho_2}{2} \left[\frac{1}{G_2'} + \frac{1-\nu_2^2}{E_2} + \sqrt{\left(\frac{1}{G_2'} - \frac{1-\nu_2^2}{E_2} \right)^2 + \frac{48(1-\nu_2^2)}{\rho_2 E_2 h_2^2 \omega^2}} \right] \right\}^{1/2} \qquad \text{(I-15a)}$$

$$\alpha_2 = \left\{ \frac{\rho_2}{2} \left[\left(1 + \sin^2 \phi_2 \right) \sqrt{\left(\frac{1}{G_2'} - \frac{1-\nu_2^2}{E_2} \right)^2 + \frac{48(1-\nu_2^2)}{\rho_2 E_2 h_2^2 \omega^2}} \right. \right.$$

$$\left. \left. - \left(\frac{1}{G_2'} + \frac{1-\nu_2^2}{E_2} \right) \cos^2 \phi_2 \right] \right\}^{1/2} \qquad \text{(I-15b)}$$

$$\alpha_2' = \left(\frac{\sin^2 \phi_2}{c_{\omega 2}^2} - \frac{\rho_2}{G_2} + \frac{12\,\kappa^2}{\omega^2 h_2^2} \right)^{1/2} \qquad \text{(I-15c)}$$

The nine constants of integration are determined in the present problem by the following conditions:

$$\psi_{z_2}^{+} = \psi_{z_2}^{-} = -\psi_{x_1} \tag{I-16a}$$

$$\psi_{y_2}^{+} = \psi_{y_2}^{-} \tag{I-16b}$$

$$u_2^{+} = u_2^{-} = w_1 = 0 \tag{I-16c}$$

$$M_{yz_2}^{+} = M_{yz_2}^{-} \tag{I-16d}$$

$$\psi_{y_1} = 0 \tag{I-16e}$$

$$M_{z_2}^{+} - M_{z_2}^{-} + M_{x_1} = 0 \tag{I-16f}$$

along $x = z = 0$. With the use of equations (I-5) and (I-16), equations (I-16d) and (I-16f) may also be written as

$$\frac{\partial \psi_{y_2}^{+}}{\partial z} = \frac{\partial \psi_{y_2}^{-}}{\partial z} \tag{I-16d}'$$

$$D_2 \left(\frac{\partial \psi_{z_2}^{+}}{\partial z} - \frac{\partial \psi_{z_2}^{-}}{\partial z} \right) + D_1 \frac{\partial \psi_{x_1}}{\partial x} = 0 \tag{I-16f}'$$

The quantities w_1, ψ_{x_1}, and ψ_{y_1} are the sum of the incoming and outgoing waves in Plate 1. The first of equations (I-16a) and equation (I-16b) state that Plate 2 is continuous so that lines along the y-axis originally perpendicular to the middle surface rotate the same amount. The first of equations (I-16c) and equation (I-16d) state that Plate 2 is supported along the y-axis in such a way that the normal deflection vanishes and the twisting moment is continuous. The remaining conditions imply that Plate 1 hypothetically extends to the middle surface of Plate 2 where it is fastened along the y-axis in such a way that a line originally normal to the middle surface has the same rotation in the x-z plane as a normal line in Plate 2 and remains in that plane.

Substitution of equations (I-7a), (I-8), (I-10), (I-11), and (I-12) in equations (I-16) yields the following relations for the constants of integration

$$A_1 = -(1 + B_1) \tag{I-17a}$$

$$C_1 = -\frac{\rho_1}{G_1' \alpha_1'} \frac{\alpha_1^2 + \frac{\cos^2 \phi_1}{c_{\omega 1}^2}}{\alpha_1^2 - \frac{\sin^2 \phi_1}{c_{\omega 1}^2}} B_1 \tag{I-17b}$$

$$A_2^+ = -A_2^- = -B_2^+ = B_2^- = \frac{1}{2} \frac{D_1}{D_2} \frac{\alpha_1^2 + \frac{\cos^2 \phi_1}{c_{\omega 1}^2}}{\alpha_2^2 + \frac{\cos^2 \phi_2}{c_{\omega 2}^2}} B_1 \tag{I-17c}$$

$$C_2^+ = C_2^- = \frac{1}{2} \frac{\rho_2}{G_2' \alpha_2'} \frac{D_1}{D_2} \frac{\alpha_1^2 + \frac{\cos^2 \phi}{c_{\omega 1}^2}}{\alpha_2^2 - \frac{\sin^2 \phi_2}{c_{\omega 2}^2}} B_1 \tag{I-17d}$$

$$B_1 = 2i \left[c_{\omega 1} \left(\frac{1}{c_{\omega 1}^2} - \frac{\mu_1}{G_1'} \right) \Big/ \Delta \right] \cos \phi_1 \tag{I-17e}$$

$$\Delta = \alpha_1 + \frac{\frac{\rho_1}{G_1'} \left(\alpha_1 - \frac{\alpha_1^2 + \frac{\cos^2 \phi_1}{c_{\omega 1}^2}}{\alpha_1'} \sin^2 \phi_1 \right)}{\alpha_1^2 - \sin^2 \phi_2 / c_{\omega 1}^2} + \frac{1}{2} \frac{D_1}{D_2} \frac{\alpha_1^2 + \frac{\cos^2 \phi_1}{c_{\omega 1}^2}}{\alpha_2^2 + \frac{\cos^2 \phi_2}{c_{\omega 2}^2}} \cdot$$

$$\left[\alpha_2 + \frac{\frac{\rho_2}{G_2'} \left(\alpha_2 - \frac{\alpha_2^2 + \frac{\cos^2 \phi_2}{c_{\omega 2}^2}}{\alpha_2'} \sin^2 \phi_2 \right)}{\alpha_2^2 - \sin^2 \phi_2 / c_{\omega 2}^2} \right]$$

$$- i \left[\left(\frac{1}{c_{\omega 1}^2} - \frac{\rho_1}{G_1'} \right) \cdot c_{\omega 1} \cos \phi_1 + \frac{1}{2} \frac{D_1}{D_2} \frac{\alpha_1^2 + \frac{\cos^2 \phi_1}{c_{\omega 1}^2}}{\alpha_2^2 + \frac{\cos^2 \phi_2}{c_{\omega 2}^2}} \left(\frac{1}{c_{\omega 2}^2} - \frac{\rho_2}{G_2'} \right) c_{\omega 2} \cos \phi_2 \right] \tag{I-17f}$$

If the effects of the transverse shear deformation and rotatory inertia are omitted, Equation (I-17c) will be reduced to

$$A_2^{+} = -B_2^{+} = -2i(k_1\ r/k_2)\ \cos \phi_1 \{i \cos \phi_1 - \sqrt{1 + \sin^2 \phi_1}$$

$$+ r[i \cos \phi_2 - \sqrt{1 + \sin^2 \phi_2}\ ]\}^{-1}$$

where $k_i = \omega/C_{\omega i}$

$$r = \frac{D_1}{2D_2} \frac{c_{\omega 2}}{c_{\omega 1}} \qquad \text{(I-17g)}$$

Equation (I-17g), a special case of equation (I-17c), is identical to the result obtained by Lyon and Eichler in Reference 4.

If the incoming wave is in, say, the $z > 0$ side of Plate 2, the analysis is modified by adding the incoming wave solution

$$u_{i2}^{+} = e^{i\omega \left(t - \frac{y \sin \phi_2 - z \cos \phi_2}{c_{\omega 2}} \right)} \qquad \text{(I-18a)}$$

$$\psi_{zi2}^{+} = - i\omega\ c_{\omega 2} \left(\frac{1}{c_{\omega 2}^{\ 2}} - \frac{\rho_2}{G_2'} \right) \cos \phi_2\ e^{i\omega \left(t - \frac{y \sin \phi_2 - z \cos \phi_2}{c_{\omega 2}} \right)} \qquad \text{(I-18b)}$$

$$\psi_{yi2}^{+} = i\omega\ c_{\omega 2} \left(\frac{1}{c_{\omega 2}^{\ 2}} - \frac{\rho_2}{G_2'} \right) \sin \phi_2\ e^{i\omega \left(t - \frac{y \sin \phi_2 - z \cos \phi_2}{c_{\omega 2}} \right)} \qquad \text{(I-18c)}$$

to the outgoing wave solutions for the $z > 0$ side of Plate 2 and deleting the incoming wave solution for Plate 1. Satisfaction of the boundary conditions then yields the following values of the integration constants:

$$A_1 = -B_1 = \frac{1}{\Delta}\left\{ i\, c_{\omega 2}\left(\frac{1}{c_{\omega 2}^2} - \frac{\rho_2}{G_2'}\right)\cos\phi_2 + \alpha_2\left[1 - \frac{\sin^2\phi_2}{(\alpha_2'\, c_{\omega 2})^2}\right]\cdot \left(1 + \frac{\rho_2/G_2'}{\alpha_2^2 - \frac{\sin^2\phi_2}{c_{\omega 2}^2}}\right)\right\} \qquad \text{(I-19a)}$$

$$\frac{c_1}{\rho_1/(G_1'\,\alpha_1')} = \frac{\alpha_1^2 + \frac{\cos^2\phi_1}{c_{\omega 1}^2}}{\alpha_2^2 + \frac{\cos^2\phi_2}{c_{\omega 2}^2}} \qquad A_1 = -\frac{A_2^+}{D_1/(2L_2)} \qquad \text{(I-19b)}$$

$$B_2^- = -A_2^- = A_2^+ - 1 \qquad \text{(I-19c)}$$

$$B_2^+ = -(1 + A_2^+) \qquad \text{(I-19d)}$$

$$\left.\begin{matrix} C_2^+ \\ C_2^- \end{matrix}\right\} = -\frac{1}{\alpha_2'}\left[\frac{\rho_2}{G_2'}\,\frac{\alpha_1^2 + \frac{\cos^2\phi_1}{c_{\omega 1}^2}}{\alpha_2^2 - \frac{\sin^2\phi_2}{c_{\omega 2}^2}}\,A_1 + \frac{\alpha_2/\alpha_2'}{c_{\omega 2}^2}\left(1 + \frac{\rho_2/G_2'}{\alpha_2^2 - \frac{\sin^2\phi_2}{c_{\omega 2}^2}}\right)\right] \qquad \text{(I-19e)}$$

If ω^2 exceeds the value $\frac{12G'}{h^2\rho}$ in a plate, the wave speed c_ω given by Equation (I-7b) has two real solutions, say $c_\omega^{(1)}$ and $c_\omega^{(2)}$. In addition, a real wave speed $c_\omega^{(3)}$ can be associated with the thickness-shear mode. Then the outgoing waves can be represented by

$$w_o = \sum_{j=1}^{2} A_j\, e^{i\omega\left[t - \frac{y\sin\phi^{(j)} - x\cos\phi^{(j)}}{c_\omega^{(j)}}\right]} \qquad \text{(I-20a)}$$

$$\psi_{xo} = -i\omega \sum_{j=1}^{2} c_\omega^{(j)} \cos \phi^{(j)} \left(\frac{1}{c_\omega^{(j)2}} - \frac{\rho}{G'} \right) \cdot$$

$$A_j e^{i\omega \left[t - \frac{y \sin \phi^{(j)} - x \cos \phi^{(j)}}{c_\omega^{(j)}} \right]}$$

$$+ A_3 \sin \phi^{(3)} e^{i\omega \left[t - \frac{y \sin \phi^{(3)} - x \cos \phi^{(3)}}{c_\omega^{(3)}} \right]} \qquad \text{(I-20b)}$$

$$\psi_{yo} = i\omega \sum_{j=1}^{2} c_\omega^{(j)} \sin \phi^{(j)} \left(\frac{1}{c_\omega^{(j)2}} - \frac{\rho}{G'} \right) \cdot$$

$$A_j e^{i\omega \left[t - \frac{y \sin \phi^{(j)} - x \cos \phi^{(j)}}{c_\omega^{(j)}} \right]}$$

$$+ A_3 \cos \phi^{(3)} e^{i\omega \left[t - \frac{y \sin \phi^{(3)} - x \cos \phi^{(3)}}{c_\omega^{(3)}} \right]} \qquad \text{(I-20c)}$$

with

$$\frac{\sin \phi^{(1)}}{c_\omega^{(1)}} = \frac{\sin \phi^{(2)}}{c_\omega^{(2)}} = \frac{\sin \phi^{(3)}}{c_\omega^{(3)}} \qquad \text{(I-21a)}$$

$$\left. \begin{matrix} \frac{1}{c_\omega^{(1)}} \\ \frac{1}{c_\omega^{(2)}} \end{matrix} \right\} = \left\{ \frac{\rho}{2} \left[\frac{1}{G'} + \frac{1-\nu^2}{E} \pm \sqrt{\left(\frac{1}{G'} - \frac{1-\nu^2}{E} \right)^2 + \frac{48(1-\nu^2)}{\rho E} \frac{}{h^2 \omega^2}} \right] \right\}^{1/2} \qquad \text{(I-21b)}$$

$$\frac{1}{c_{\omega}(3)} = \sqrt{\frac{\rho}{G} - \frac{12\kappa^2}{h^2\omega^2}} \qquad \text{(I-21c)}$$

Thus, different coefficient relations must be determined from the range

$$\frac{12\ G_2'}{\rho_2 h_2^2} < \omega^2 < \frac{12\ G_1'}{\rho_1 h_1^2} \qquad \text{(I-22a)}$$

and for

$$\omega^2 > \frac{12\ G_1'}{\rho_1 h_1^2} \qquad \text{(I-22b)}$$

In the range of frequency value given by equation (I-22a) the waves in Plate 1 have exponential decay and harmonic space variations while in Plate 2 the space variation is harmonic only. When the frequency is governed by Equation (I-22b) both plates have only waves with harmonic space variations.

APPENDIX II

EFFECT OF FLEXURAL AND TANGENTIAL WAVE COUPLING ON THE TRANSFER FUNCTION

In this study the effects of rotatory inertia and transverse deformation are neglected to better isolate the effects of flexural and tangential wave coupling. Consider a plate, the middle surface of which is the x-y plane. The pertinent equations of motion and force-strain relations are given by

$$D\nabla^4 w + \rho h \frac{\partial^2 w}{\partial t^2} = 0 \qquad \text{(II-1a)}$$

$$\frac{\partial^2 u}{\partial x^2} + \frac{1-\nu}{2}\frac{\partial^2 u}{\partial y^2} - \frac{(1-\nu^2)\rho}{E}\frac{\partial^2 u}{\partial t^2} + \frac{1+\nu}{2}\frac{\partial^2 v}{\partial x \partial y} = 0 \qquad \text{(II-1b)}$$

$$\frac{1+\nu}{2}\frac{\partial^2 u}{\partial x \partial y} + \frac{1-\nu}{2}\frac{\partial^2 v}{\partial x^2} + \frac{\partial^2 v}{\partial y^2} - \frac{(1-\nu^2)\rho}{E}\frac{\partial^2 v}{\partial t^2} = 0 \qquad \text{(II-1c)}$$

$$N_x = \frac{Eh}{1-\nu^2}\left(\frac{\partial u}{\partial x} + \nu\frac{\partial v}{\partial y}\right) \qquad \text{(II-1d)}$$

$$N_y = \frac{Eh}{1-\nu^2}\left(\frac{\partial v}{\partial y} + \nu\frac{\partial u}{\partial x}\right) \qquad \text{(II-1e)}$$

$$N_{xy} = \frac{Eh}{2(1+\nu)}\left(\frac{\partial u}{\partial y} + \frac{\partial v}{\partial x}\right) \qquad \text{(II-1f)}$$

$$M_x = -D\left(\frac{\partial^2 w}{\partial x^2} + \nu\frac{\partial^2 w}{\partial y^2}\right) \qquad \text{(II-1g)}$$

$$M_y = -D\left(\frac{\partial^2 w}{\partial y^2} + \nu\frac{\partial^2 w}{\partial x^2}\right) \qquad \text{(II-1h)}$$

$$M_{xy} = -D(1-\nu)\frac{\partial^2 w}{\partial x \partial y} \qquad \text{(II-1i)}$$

$$Q_x = -D \frac{\partial}{\partial x} \left(\nabla^2 w \right) \tag{II-1j}$$

$$Q_y = -D \frac{\partial}{\partial y} \left(\nabla^2 w \right) \tag{II-1k}$$

The effective transverse shear forces are given by

$$\overline{Q_x} = Q_x + \frac{\partial M_{xy}}{\partial y} = -D \frac{\partial}{\partial x} \left[\frac{\partial^2 w}{\partial x^2} + (2-\nu) \frac{\partial^2 w}{\partial y^2} \right] \tag{II-1ℓ}$$

$$\overline{Q_y} = Q_y + \frac{\partial M_{xy}}{\partial x} = -D \frac{\partial}{\partial y} \left[\frac{\partial^2 w}{\partial y^2} + (2-\nu) \frac{\partial^2 w}{\partial x^2} \right] \tag{II-1m}$$

The positive force and deformation directions are shown below.

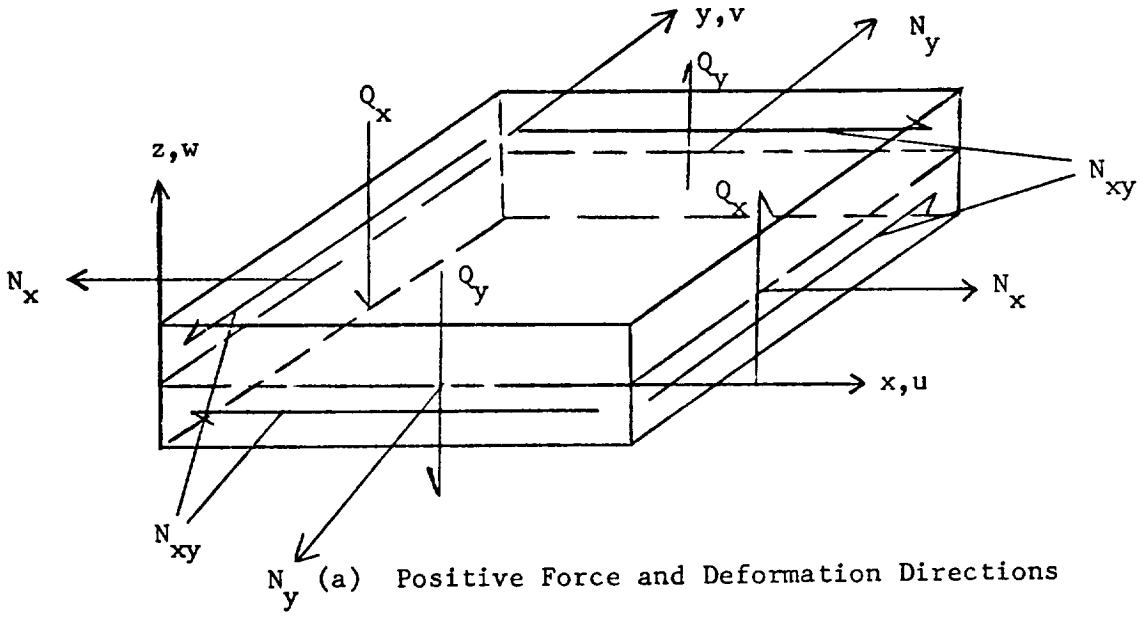

(a) Positive Force and Deformation Directions

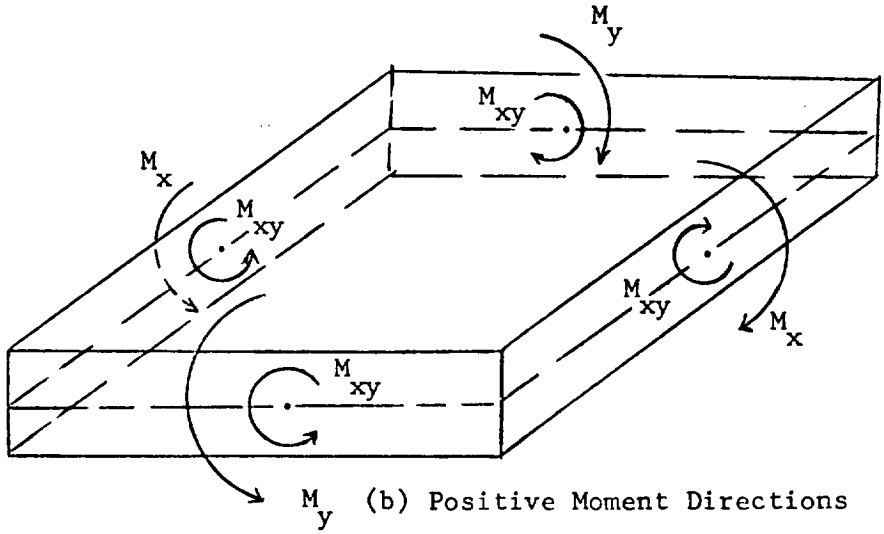

(b) Positive Moment Directions

FIGURE II-1 POSITIVE FORCE AND DEFORMATION DIRECTIONS OF A PLATE ELEMENT

An incoming flexural wave can be expressed as

$$w_i = e^{i\omega\left(t - \frac{y\sin\phi - x\cos\phi}{c}\right)} \tag{II-2a}$$

where $$\frac{1}{c} = \sqrt[4]{\frac{\rho h}{D\omega^2}} \tag{II-2b}$$

Outgoing flexural waves are given by

$$w_o = \left(A\, e^{-i\omega\frac{x\cos\phi}{c}} + \bar{A}\, e^{-\omega\alpha\frac{x}{c}}\right) e^{i\omega\left(t - \frac{y\sin\phi}{c}\right)} \tag{II-3a}$$

with $$\alpha = \sqrt{1+\sin^2\phi} \tag{II-3b}$$

Outgoing tangential waves can be written as

$$u_o = \left(B\, e^{-\lambda\omega x} + \bar{B}\, e^{-\bar{\lambda}\omega x}\right) e^{i\omega\left(t - \frac{y\sin\phi}{c}\right)} \tag{II-4a}$$

$$v_o = i\left(\frac{\sin\phi}{\lambda c}\, B\, e^{-\lambda\omega x} + \frac{\bar{\lambda} c}{\sin\phi}\, \bar{B}\, e^{-\bar{\lambda}\omega x}\right) e^{i\omega\left(t - \frac{y\sin\phi}{c}\right)} \tag{II-4b}$$

with $$\lambda = \sqrt{\left(\frac{\sin\phi}{c}\right)^2 - \frac{(1-\nu^2)\rho}{E}} \tag{II-4c}$$

$$\bar{\lambda} = \sqrt{\left(\frac{\sin\phi}{c}\right)^2 - \frac{\rho}{G}} \tag{II-4d}$$

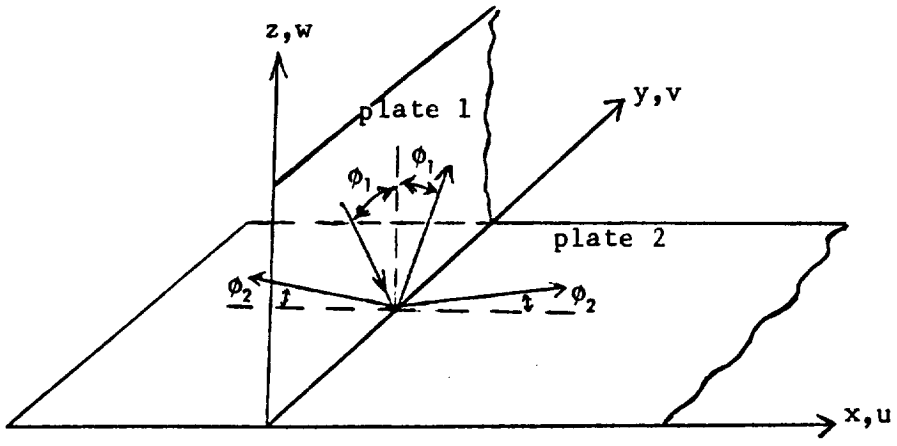

FIGURE II-2 INTEGRALLY JOINED PERPENDICULAR PLATES

Consider now an imcoming flexural wave in Plate 1 of the form

$$u_{1i} = -e^{i\omega\left(t - \frac{y \sin\phi_1 - z\cos\phi_1}{c_1}\right)} \tag{II-5a}$$

Outgoing wave displacements in Plate 1 are

$$u_{1o} = \left(A_1 e^{-i\omega \frac{z\cos\phi_1}{c_1}} + \bar{A}_1 e^{-\omega\alpha_1 \frac{z}{c_1}}\right) e^{i\omega\left(t - \frac{y\sin\phi_1}{c_1}\right)} \tag{II-5b}$$

$$v_{1o} = i\left(\frac{\sin\phi_1/c_1}{\lambda_1} B_1 e^{-\lambda_1\omega z} + \frac{\bar{\lambda}_1}{\sin\phi_1/c_1} \bar{B}_1 e^{-\bar{\lambda}_1\omega z}\right) e^{i\omega\left(t - \frac{y\sin\phi_1}{c_1}\right)} \tag{II-5c}$$

$$w_{1o} = \left(B_1 e^{-\lambda_1\omega z} + \bar{B}_1 e^{-\bar{\lambda}_1\omega z}\right) e^{i\omega\left(t - \frac{y\sin\phi_1}{c_1}\right)} \tag{II-5d}$$

For the $x > o$ and $x < o$ sides of Plate 2, the outgoing displacements are given by

$$u_2^+ = \left(B_2^+ e^{-\lambda_2\omega x} + \bar{B}_2^+ e^{-\bar{\lambda}_2\omega x}\right) e^{i\omega\left(t - \frac{y\sin\phi_2}{c_2}\right)} \tag{II-6a}$$

$$v_2^+ = i\left(\frac{\sin\phi_2/c_2}{\lambda_2} B_2^+ e^{-\lambda_2\omega x} + \frac{\bar{\lambda}_2}{\sin\phi_2/c_2} \bar{B}_2^+ e^{-\bar{\lambda}_2\omega x}\right) e^{i\omega\left(t - \frac{y\sin\phi_2}{c_2}\right)} \tag{II-6b}$$

$$w_2^+ = \left(A_2^+ e^{-i\omega x\frac{\cos\phi_2}{c_2}} + \bar{A}_2^+ e^{-\omega\alpha_2 \frac{x}{c_2}}\right) e^{i\omega\left(t - \frac{y\sin\phi_2}{c_2}\right)} \tag{II-6c}$$

and

$$u_2^- = \left(B_2^- e^{\lambda_2\omega x} + \bar{B}_2^- e^{\bar{\lambda}_2\omega x}\right) e^{i\omega\left(t - \frac{y\sin\phi_2}{c_2}\right)} \tag{II-7a}$$

$$v_2^- = -i\left(\frac{\sin\phi_2/c_2}{\lambda_2} B_2^- e^{\lambda_2\omega x} + \frac{\bar{\lambda}_2}{\sin\phi_2/c_2} \bar{B}_2^- e^{\bar{\lambda}_2\omega x}\right) e^{i\omega\left(t - \frac{y\sin\phi_2}{c_2}\right)} \tag{II-7b}$$

$$w_2^- = \left(A_2^- e^{i\omega x \frac{\cos\phi_2}{c_2}} + \bar{A}_2^- e^{\omega\alpha_2 \frac{x}{c_2}}\right) e^{i\omega\left(t - \frac{y\sin\phi_2}{c_2}\right)} \tag{II-7c}$$

with

$$\frac{\sin\phi_1}{c_1} = \frac{\sin\phi_2}{c_2} \qquad \text{(II-8)}$$

Note that if $\frac{c_2}{c_1} \sin \phi_1 > 1$, there are two Rayleigh waves rather than one plane wave and one Rayleigh wave.

At the joint the displacements and rotations must be continuous. Then at $x = z = 0$

$$u_1 = u_2^+ = u_2^- \qquad \text{(II-9a,b)}$$

$$v_1 = v_2^+ = v_2^- \qquad \text{(II-9c,d)}$$

$$w_1 = w_2^+ = w_2^- \qquad \text{(II-9e,f)}$$

$$-\frac{\partial u_1}{\partial z} = \frac{\partial w_2^+}{\partial x} = \frac{\partial w_2^-}{\partial x} \qquad \text{(II-9g,h)}$$

These eight deformation continuity conditions are supplemented by four force and moment continuity conditions (see Figure II-3)

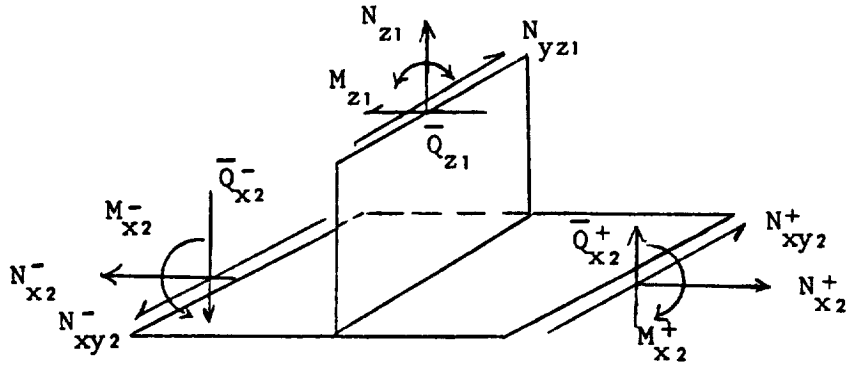

FIGURE II-3 JOINT FORCES

$$M_{x2}^{+} - M_{x2}^{-} + M_{z1} = 0 \qquad \text{(II-10a)}$$

$$N_{x2}^{+} - N_{x2}^{-} - \bar{Q}_{z1} = 0 \qquad \text{(II-10b)}$$

$$N_{xy2}^{+} - N_{xy2}^{-} + N_{yz1} = 0 \qquad \text{(II-10c)}$$

$$\bar{Q}_{x2}^{+} - \bar{Q}_{x2}^{-} + N_{z1} = 0 \qquad \text{(II-10d)}$$

which can be expressed with the aid of the deformation continuity conditions as

$$- D_2\left(\frac{\partial^2 w_2^{+}}{\partial x^2} - \frac{\partial^2 w_2^{-}}{\partial x^2}\right) + D_1\left(\frac{\partial^2 u_1}{\partial z^2} + \nu \frac{\partial^2 u_1}{\partial y^2}\right) = 0 \qquad \text{(II-11a)}$$

$$\frac{E_2 h_2}{1-\nu_2^2}\left(\frac{\partial u_2^{+}}{\partial x} - \frac{\partial u_2^{-}}{\partial x}\right) - D_1 \frac{\partial}{\partial z}\left[\frac{\partial^2 u_1}{\partial z^2} + (2-\nu)\frac{\partial^2 u_1}{\partial y^2}\right] = 0 \qquad \text{(II-11b)}$$

$$\frac{E_2 h_2}{2(1+\nu_2)}\left(\frac{\partial v_2^{+}}{\partial x} - \frac{\partial v_2^{-}}{\partial x}\right) + \frac{E_1 h_1}{2(1+\nu_1)}\left(\frac{\partial w_1}{\partial y} + \frac{\partial v_1}{\partial z}\right) = 0 \qquad \text{(II-11c)}$$

$$- D_2 \frac{\partial}{\partial x}\left(\frac{\partial^2 w_2^{+}}{\partial x^2} - \frac{\partial w_2^{-}}{\partial x^2}\right) + \frac{E_1 h_1}{1-\nu_1^2}\left(\frac{\partial w_1}{\partial z} + \nu \frac{\partial v_1}{\partial y}\right) = 0 \qquad \text{(II-11d)}$$

The substitution of equations (II-5), (II-6), and (II-7) into equations (II-9) and (II-11) yields twelve simultaneous equations for the determination of the integration constants.

$$1 + A_1 + \bar{A}_1 = B_2^{+} + \bar{B}_2^{+} = B_2^{-} + \bar{B}_2^{-} \qquad \text{(II-12a,b)}$$

$$\frac{\sin\phi_1/c_1}{\lambda_1} B_1 + \frac{\bar{\lambda}_1}{\sin\phi_1/c_1}\bar{B}_1 = \frac{\sin\phi_2/c_2}{\lambda_2} B_2^{+} + \frac{\bar{\lambda}_2}{\sin\phi_2/c_2}\bar{B}_2^{+} =$$

$$= - \left(\frac{\sin\phi_2/c_2}{\lambda_2} B_2^{-} + \frac{\bar{\lambda}_2}{\sin\phi_2/c_2}\bar{B}_2^{-}\right) \qquad \text{(II-12c,d)}$$

$$B_1 + \bar{B}_1 = A_2^{+} + \bar{A}_2^{+} = A_2^{-} + \bar{A}_2^{-} \qquad \text{(II-12e,f)}$$

$$-i\ \frac{\cos\phi_1}{c_1}\left(1 - A_1\right) + \frac{\alpha_1}{c_1}\bar{A}_1 = -\left(i\ \frac{\cos\phi_2}{c_2}\ A_2^+ + \frac{\alpha_2}{c_2}\ \bar{A}_2^+\right) =$$

$$= i\ \frac{\cos\phi_2}{c_2}\ A_2^- + \frac{\alpha_2}{c_2}\ \bar{A}_2^- \qquad \text{(II-12g,h)}$$

$$\frac{D_1}{c_1^2}\left\{\left[1 - (1-\nu)\ \sin^2\phi_1\right]\ \left(1 + A_1\right) - \left[1 + (1-\nu)\ \sin^2\phi_1\right]\bar{A}_1\right\}$$

$$- \frac{D_2}{c_2^2}\left[(1-\sin^2\phi_2)\ (A_2^+ - A_2^-) -\right.$$

$$\left.(1 + \sin^2\phi_2)\ (\bar{A}_2^+ - \bar{A}_2^-)\right] = 0 \qquad \text{(II-12i)}$$

$$\frac{D_1\omega^2}{c_1^3}\left\{i\left[1 + (1-\nu)\ \sin^2\phi_1\right]\ \left(1 - A_1\right)\ \cos\phi_1 + \left[1 - (1-\nu)\ \sin^2\phi_1\right]\bar{A}_1\ \alpha_1\right\}$$

$$- \frac{E_2 h_2}{1-\nu_2^2}\left[\lambda_2\left(B_2^+ + B_2^-\right) + \bar{\lambda}_2\left(\bar{B}_2^+ + \bar{B}_2^-\right)\right] = 0 \qquad \text{(II-12j)}$$

$$\frac{E_1 h_1}{2(1+\nu)}\left[2\ \frac{\sin\phi_1}{c_1}\ B_1 + \left(\frac{\bar{\lambda}_1^2}{\sin\phi_1/c_1} + \sin\phi_1 c_1\right)\bar{B}_1\right]$$

$$+ \frac{E_2 h_2}{2(1+\nu)}\left[\frac{\sin\phi_2}{c_2}\left(B_2^+ + B_2^-\right) + \frac{\bar{\lambda}_2^2}{\sin\phi_2/c_2}\left(\bar{B}_2^+ + \bar{B}_2^-\right)\right] = 0 \qquad \text{(II-12k)}$$

$$\frac{E_1 h_1}{1-\nu_1^2}\left[\left(\lambda_1 - \nu_1\frac{\sin^2\phi_1/c_1^2}{\lambda_1}\right) B_1 + (1-\nu)\bar{\lambda}_1\bar{B}_1\right] +$$

$$\frac{D_2\omega^2}{c_2^3}\left[i\left(A_2^+ + A_2^-\right)\cos^3\phi_2 - \alpha_2^3\left(\bar{A}_2^+ + \bar{A}_2^-\right)\right] = 0 \qquad \text{(II-12ℓ)}$$

The solution of these equations can be expressed as

$$\bar{A}_2^+ + \bar{A}_2^- = -\tfrac{1}{2}\left(1 + \frac{i\cos\phi_2}{\alpha_2}\right)\left(A_2^+ + A_2^-\right) \qquad \text{(II-13a)}$$

$$\bar{A}_2^+ - \bar{A}_2^- = -\left(A_2^+ - A_2^-\right) \tag{II-13b}$$

$$B_2^+ + B_2^- = -\frac{\lambda_2 \bar{\lambda}_2}{\left(\sin \phi_2/c_2\right)^2}\left(\bar{B}_2^+ + \bar{B}_2^-\right) = -\kappa\left(A_2^+ + A_2^-\right) \tag{II-13c}$$

$$B_2^+ - B_2^- = -\left(\bar{B}_2^+ - \bar{B}_2^-\right) = \eta\left(A_2^+ + A_2^-\right) \tag{II-13d}$$

$$1 + A_1 = \frac{D_2}{D_1}\left(\frac{c_1}{c_2}\right)^2 \left(A_2^+ - A_2^-\right) - \frac{1 + (1-\nu_1)\sin^2\phi_1}{4}\left[1 - \frac{\left(\sin \phi_2/c_2\right)^2}{\lambda_2 \bar{\lambda}_2}\right]\kappa\left(A_2^+ + A_2^-\right) \tag{II-13e}$$

$$\bar{A}_1 = -\left\{\frac{D_2}{D_1}\left(\frac{c_1}{c_2}\right)\left(A_2^+ - A_2^-\right) + \frac{1-(1-\nu_1)\sin^2\phi_1}{4}\left[1 - \frac{\left(\sin \phi_2/c_2\right)^2}{\lambda_2 \bar{\lambda}_2}\right]\kappa\left(A_2^+ + A_2^-\right)\right\} \tag{II-13f}$$

$$\kappa\left(A_2^+ + A_2^-\right) = -\left(A_2^+ - A_2^-\right)\frac{c_1}{c_2}\,\frac{\left[\frac{1 + (1-\nu_1)\sin^2\phi_1}{2}\,\frac{\alpha_2 - i\cos\phi_2}{\alpha_1} + \frac{2D_2}{D_1}\frac{c_1}{c_2}\right]\zeta}{\left[1 - \frac{\left(\sin \phi_2/c_2\right)^2}{\lambda_2 \bar{\lambda}_2}\right]\left[1 + \frac{1-(1-\nu_1)\sin^2\phi_1}{2}\,\zeta\right]} \tag{II-13g}$$

$$A_2^+ - A_2^- = -4i\frac{c_2}{c_1}\cos\phi_1\left[1 + \frac{1-(1-\nu_1)\sin^2\phi_1}{2}\,\zeta\right]\Bigg(\alpha_2 - i\cos\phi_2 + \frac{2D_2}{D_1}\frac{c_1}{c_2}\left(\alpha_1 - i\cos\phi_1\right) + \zeta\Bigg\langle\left(\alpha_2 - i\cos\phi_2\right)\Bigg|\left[\frac{1-(1-\nu_1)\sin^2\phi_1}{2}\right]^2 - i\frac{\cos\phi_1}{\alpha_1}\left[\frac{1+(1-\nu_1)\sin^2\phi_1}{2}\right]^2\Bigg| - i\frac{2D_2}{D_1}\frac{c_1}{c_2}\cos\phi_1\Bigg\rangle\Bigg)^{-1} \tag{II-13h}$$

$$\zeta = \frac{(1-\nu_2^2)\,D_1\,\omega^2\alpha_1}{c_1^3\,E_2 h_2\,\lambda_2}\,\frac{1 - \frac{\left(\sin\phi_2/c_2\right)^2}{\lambda_2\bar{\lambda}_2}}{1 - \left(\frac{\sin\phi_2/c_2}{\lambda_2}\right)^2} \tag{II-13i}$$

$$K = \frac{G_1 h_1}{G_2 h_2} \left\langle \tfrac{1}{2}\left(1-i\,\frac{\cos\phi_2}{\alpha_2}\right)\left\{\left[\left(\frac{\bar{\lambda}_1}{\sin\phi_{1/c_1}}\right)^2 + 1\right]\left[1-\nu_1\left(\frac{\sin\phi_{1/c_1}}{\lambda_1}\right)^2\right] - 2\,(1-\nu_1)\frac{\bar{\lambda}_1}{\lambda_1}\right\}\right.$$
$$\left. + 2i\,\frac{(1-\nu_1^2)\,D_2\omega^2\cos\phi_2}{c_2^3\;E_1 h_1 \lambda_1}\left[\left(\frac{\bar{\lambda}_1}{\sin\phi_{\gamma_{c_1}}}\right)^2 - 1\right]\right\rangle \cdot$$
$$\left(1-\frac{\bar{\lambda}_2}{\lambda_2}\right)^{-1}\left[1-\nu_1\left(\frac{\sin\phi_{\gamma_{c_1}}}{\lambda_1}\right)^2 - (1-\nu_1)\,\frac{\bar{\lambda}_1}{\lambda_1}\right]^{-1} \qquad \text{(II-13j)}$$

$$\eta = \left[\left(1-i\,\frac{\cos\phi_2}{\alpha_2}\right)\frac{\bar{\lambda}_1}{\lambda_1}\left(\frac{\lambda_1}{\sin\phi_{1/c_1}} - \frac{\sin\phi_{1/c_1}}{\lambda_1}\right) + 4i\,\frac{(1-\nu_1^2)\,D_2\omega^2\cos\phi_2}{c_2^3\;E_1 h_1 \lambda_1}\cdot\right.$$
$$\left.\left(\frac{\bar{\lambda}_1}{\sin\phi_{1/c_1}} - \frac{\sin\phi_{1/c_1}}{\lambda_1}\right)\right]\left(\frac{\sin\phi_{2/c_2}}{\lambda_2} - \frac{\bar{\lambda}_2}{\sin\phi_{2/c_2}}\right)^{-1}\cdot$$
$$\left[1-\nu\left(\frac{\sin\phi_{1/c_1}}{\lambda_1}\right)^2 - (1-\nu_1)\,\frac{\bar{\lambda}_1}{\lambda_1}\right]^{-1} \qquad \text{(II-13k)}$$

The effect of flexural and tangential wave coupling depends on the parameter ζ. The results for uncoupled motion are obtained with ζ equal to zero. If ζ is large, however, the effects of coupling can be significant. In order to get a better idea of the magnitude of ζ, let it be rewritten as .

$$\zeta = -\frac{\rho_1 h_1}{\rho_2 h_2}\,\alpha_1 \sin\phi_1 \left(1-\frac{1-\nu_2}{2}\mu\right)^{\frac{1}{2}}\left[1-\frac{1}{\left(1-\frac{1-\nu_2}{2}\mu\right)^{\frac{1}{2}}\left(1-\mu\right)^{\frac{1}{2}}}\right] \qquad \text{(II-14a)}$$

with

$$\mu = \frac{\omega h_2 \csc^2\phi_2}{\sqrt{3\;\frac{1-\nu_2}{1+\nu_2}\;\frac{E_2}{\rho_2}}} \qquad \text{(II-14b)}$$

If μ is small, ζ can be approximated by

$$\zeta \approx -\frac{3-\nu_2}{2}\;\frac{\rho_1 h_1}{\rho_2 h_2}\,\mu\;\alpha_1\;\sin\phi_1 \qquad \text{(II-15)}$$

so that ζ will also be small if the mass ratio is of the order of unity. However, ζ becomes large when μ is in the vicinity of unity. This is possible in the range of values of ω of interest for a certain range of values of ϕ_2. For example, for a steel plate with

$$E_2 = 30 \times 10^6 \text{ psi} = 20.69 \times 10^6 \text{ N/cm}^2$$
$$\nu_2 = 0.3$$
$$\rho_2 = 0.00777 \ ^{\#\text{sec}^2}/_{\text{in}^4} = 6.813 \text{ gm/cm}^3$$
$$h_2 = 0.062 \text{ in} = 0.158 \text{ cm}$$
$$\omega = 2\pi \times 10^4 \ ^{\text{rad}}/_{\text{sec}}$$

μ is equal to unity if ϕ_2 is equal to 7.18°. The magnitude of the coupling effect is very sensitive to angle, however, for if ϕ_2 vanishes (implying large μ), then

$$\zeta = -i \frac{\rho_1 h_1}{\rho_2 h_2} \left[\frac{\omega h_2 \sqrt{12}}{\sqrt{\frac{E_2/(1-\nu_2^2)}{\rho_2}}} \right]^{\frac{1}{2}} \qquad \text{(II-16)}$$

which is small again.

APPENDIX III

TRANSMISSION OF A FLEXURAL WAVE IN AN INFINITE FLAT PLATE WITH AN INTEGRALLY ATTACHED HALF CIRCULAR CYLINDRICAL SHELL

INTRODUCTION

The structure under consideration consists of an infinite flat plate to which an infinite half circular cylindrical shell is integrally joined along the diametrically opposite generators (Figure III-1). A harmonic flexural wave is produced in the plate and is scattered by the half cylinder. The object of the investigation is to determine the scattered wave distribution in the plate-cylinder combination. In what follows rotatory inertia and transverse shear deformations are neglected in both the plate and the cylinder. Flexural and extensional wave coupling is considered, however. The effects of transverse shear and rotatory inertia in the cylinder can be considered with the use of Reference 53, if necessary.

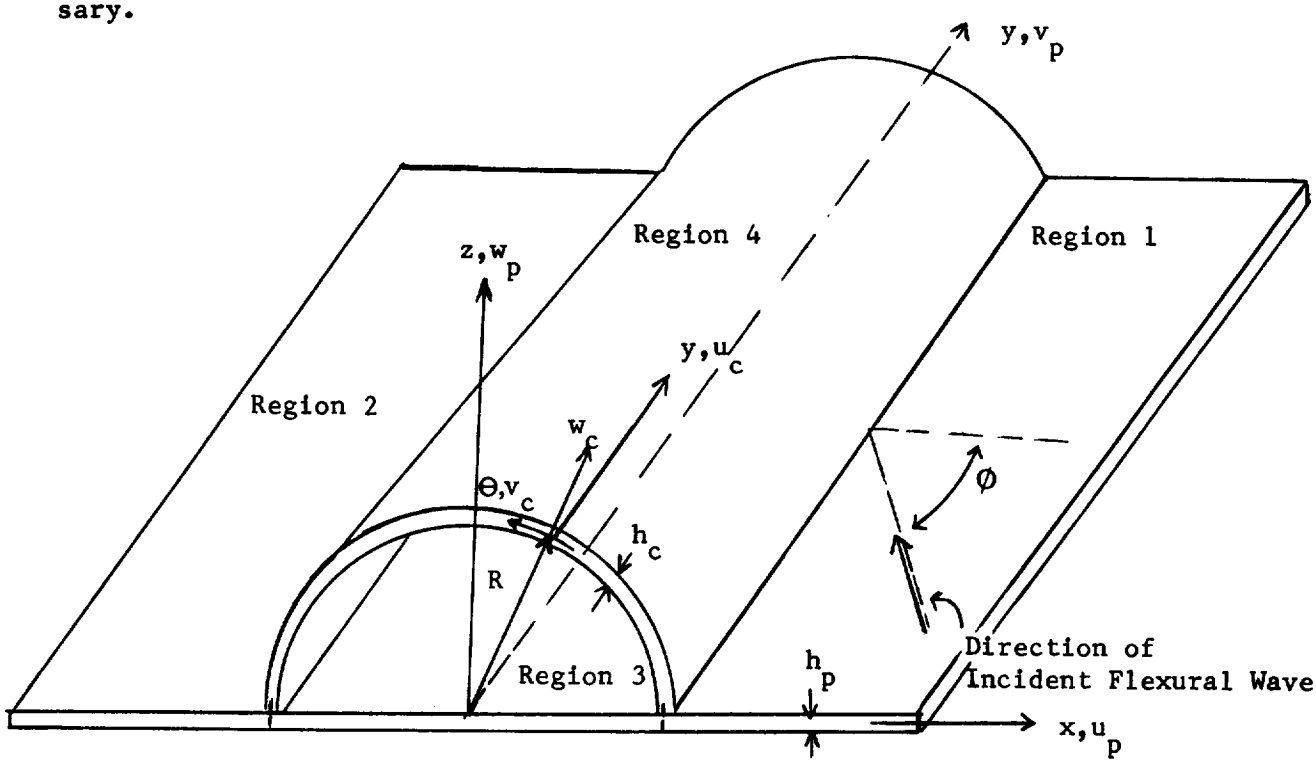

FIGURE III-1 PLATE-CYLINDER COMBINATION

FLAT PLATE ANALYSIS

The plate is considered to be divided into three regions, region 1 for which $x > R$, region 2 for which $x < -R$, and region 3 for which $-R < x < R$. In region 1 the incident and reflected wave deformations are given by the following equations (see Appendix II):

$$u_p^+ = \left[B^+ e^{-\lambda\omega(x-R)} + \bar{B}^+ e^{-\bar{\lambda}\omega(x-R)} \right] e^{i\omega\left(t - \frac{y \sin\phi}{c}\right)} \qquad \text{(III-1a)}$$

$$v_p^+ = i\left[\frac{\sin\phi/c}{\lambda} B^+ e^{-\lambda\omega(x-R)} + \frac{\bar{\lambda}}{\sin\phi/c} \bar{B}^+ e^{-\bar{\lambda}\omega(x-R)} \right] e^{i\omega\left(t - \frac{\sin\phi}{c}\right)} \qquad \text{(III-1b)}$$

$$w_p^+ = \left[e^{i\omega\frac{\cos\phi}{c}(x-R)} + A^+ e^{-i\omega\frac{\cos\phi}{c}(x-R)} + \bar{A}^+ e^{-\omega\frac{\alpha}{c}(x-R)} \right] \cdot e^{i\omega\left(t - \frac{y \sin\phi}{c}\right)} \qquad \text{(III-1c)}$$

In region 2, the outgoing wave deformations are given by

$$u_p^- = \left[B^- e^{\lambda\omega(x+R)} + \bar{B}^- e^{\bar{\lambda}\omega(x+R)} \right] e^{i\omega\left(t - \frac{y \sin\phi}{c}\right)} \qquad \text{(III-2a)}$$

$$v_p^- = -i\left[\frac{\sin\phi/c}{\lambda} B^- e^{\lambda\omega(x+R)} + \frac{\bar{\lambda}}{\sin\phi/c} \bar{B}^- e^{\bar{\lambda}\omega(x+R)} \right] \cdot e^{i\omega\left(t - \frac{y \sin\phi}{c}\right)} \qquad \text{(III-2b)}$$

$$w_p^- = \left[A^- e^{i\omega\frac{\cos\phi}{c}(x+R)} + \bar{A}^- e^{\omega\frac{\alpha}{c}(x+R)} \right] e^{i\omega\left(t - \frac{y \sin\phi}{c}\right)} \qquad \text{(III-2c)}$$

Finally in region 3, waves are directed into the interior from both boundaries so that the deflections may be written as

$$u_p^\circ = \left[B^\circ \; e^{-\lambda\omega(x+R)} + C^\circ \; e^{\lambda\omega(x-R)} + \bar{B}^\circ \; e^{-\bar{\lambda}\omega(x+R)} + \bar{C}^\circ \; e^{\bar{\lambda}\omega(x-R)} \right] e^{i\omega\left(t - \frac{y \sin\phi}{c}\right)} \qquad \text{(III-3a)}$$

$$v_p^\circ = i \left\{ \frac{\sin\phi/c}{\lambda} \left[B^\circ \; e^{-\lambda\omega(x+R)} - C^\circ \; e^{\lambda\omega(x-R)} \right] + \frac{\bar{\lambda}}{\sin\phi/c} \left[\bar{B}^\circ \; e^{-\bar{\lambda}\omega(x+R)} - \bar{C}^\circ \; e^{\bar{\lambda}\omega(x-R)} \right] \right\} e^{i\omega\left(t - \frac{y \sin\phi}{c}\right)} \qquad \text{(III-3b)}$$

$$w_p^\circ = \left[A^\circ \; e^{-i\omega \frac{\cos\phi}{c}(x+R)} + D^\circ \; e^{i\omega \frac{\cos\phi}{c}(x-R)} + \bar{A}^\circ \; e^{-\omega\frac{\alpha}{c}(x+R)} + \bar{D}^\circ \; e^{\omega\frac{\alpha}{c}(x-R)} \right] e^{i\omega\left(t - \frac{y \sin\phi}{c}\right)} \qquad \text{(III-3c)}$$

with

$$c = \sqrt{\frac{D_p \omega^2}{\rho_p h_p}} \qquad \text{(III-4a)}$$

$$\alpha = \sqrt{1 + \sin^2\phi} \qquad \text{(III-4b)}$$

$$\lambda = \sqrt{\left(\frac{\sin\phi}{c}\right)^2 - \frac{(1-\nu_p^2)\rho_p}{E_p}} \qquad \text{(III-4c)}$$

$$\bar{\lambda} = \sqrt{\left(\frac{\sin\phi}{c}\right)^2 - \frac{2(1+\nu_p)\rho_p}{E_p}} \qquad \text{(III-4d)}$$

CYLINDRICAL SHELL ANALYSIS

The equations of motion of a cylindrical shell with transverse shear deformation and rotatory inertia neglected may be written as (Reference 54)

$$\frac{\partial^2 u_c}{\partial \xi^2} + \frac{1-\nu_c}{2}(1+k)\frac{\partial^2 u_c}{\partial \theta^2} - \frac{\rho_c h_c R^2}{K_c}\frac{\partial^2 u_c}{\partial t^2} + \frac{1+\nu_c}{2}\frac{\partial^2 v_c}{\partial \xi \partial \theta} + \nu_c \frac{\partial w_c}{\partial \xi} - k\left(\frac{\partial^3 w_c}{\partial \xi^3} - \frac{1-\nu_c}{2}\frac{\partial^3 w_c}{\partial \xi \partial \theta^2}\right) = 0 \qquad \text{(III-5a)}$$

$$\frac{1+\nu_c}{2}\frac{\partial^2 u_c}{\partial \xi \partial \theta} + \frac{1-\nu_c}{2}(1+3k)\frac{\partial^2 v_c}{\partial \xi^2} + \frac{\partial^2 v_c}{\partial \theta^2} - \frac{\rho_c h_c R^2}{K_c}\frac{\partial^2 v_c}{\partial t^2} + \frac{\partial w_c}{\partial \theta} - \frac{3-\nu_c}{2}k\frac{\partial^3 w_c}{\partial \xi^2 \partial \theta} = 0 \qquad \text{(III-5b)}$$

$$\nu_c \frac{\partial u_c}{\partial \xi} - k\left(\frac{\partial^3 u_c}{\partial \xi^3} - \frac{1-\nu_c}{2}\frac{\partial^3 u_c}{\partial \xi \partial \theta^2}\right) + \frac{\partial v_c}{\partial \theta} - \frac{3-\nu_c}{2}k\frac{\partial^3 v_c}{\partial \xi^2 \partial \theta} + w_c + k\left(\frac{\partial^4 w_c}{\partial \xi^4} + 2\frac{\partial^4 w_c}{\partial \xi^2 \partial \theta^2} + \frac{\partial^4 w_c}{\partial \theta^4} + 2\frac{\partial^2 w_c}{\partial \theta^2} + w_c\right) + \frac{\rho_c h_c R^2}{K_c}\frac{\partial^2 w_c}{\partial t^2} = 0 \qquad \text{(III-5c)}$$

with

$$\xi = y/R \qquad \text{(III-6a)}$$

$$k = \frac{1}{12}\left(\frac{h_c}{R}\right)^2 \qquad \text{(III-6b)}$$

$$K_c = \frac{E_c h_c}{1-\nu_c^2} \qquad \text{(III-6c)}$$

The forces needed are those on the straight generators of the cylindrical shell (Figure III-2) which are given by Reference 54.

$$N_\theta = \frac{K_c}{R}\left[\frac{\partial v_c}{\partial \theta} + w_c + \nu\frac{\partial u_c}{\partial \xi} + k\left(\frac{\partial^2 w_c}{\partial \theta^2} + w_c\right)\right] \qquad \text{(III-7a)}$$

$$N_{\theta\xi} = \frac{1-\nu_c}{2}\,\frac{K_c}{R}\left[\frac{\partial u_c}{\partial \theta} + \frac{\partial v_c}{\partial \xi} + k\left(\frac{\partial u_c}{\partial \theta} + \frac{\partial^2 w_c}{\partial \xi \partial \theta}\right)\right] \qquad \text{(III-7b)}$$

$$M_\theta = k\,K_c\left(\frac{\partial^2 w_c}{\partial \theta^2} + w_c + \nu_c\frac{\partial^2 w_c}{\partial \xi^2}\right) \qquad \text{(III-7c)}$$

$$\bar{Q}_\theta = \frac{kK_c}{R}\left[\frac{\partial^3 w_c}{\partial \theta^3} + \frac{\partial w_c}{\partial \theta} + (2-\nu_c)\frac{\partial^3 w_c}{\partial \xi^2 \partial \theta} + \frac{1-\nu_c}{2}\left(\frac{\partial^2 u_c}{\partial \xi \partial \theta} - 3\frac{\partial^2 v_c}{\partial \xi^2}\right)\right] \qquad \text{(III-7d)}$$

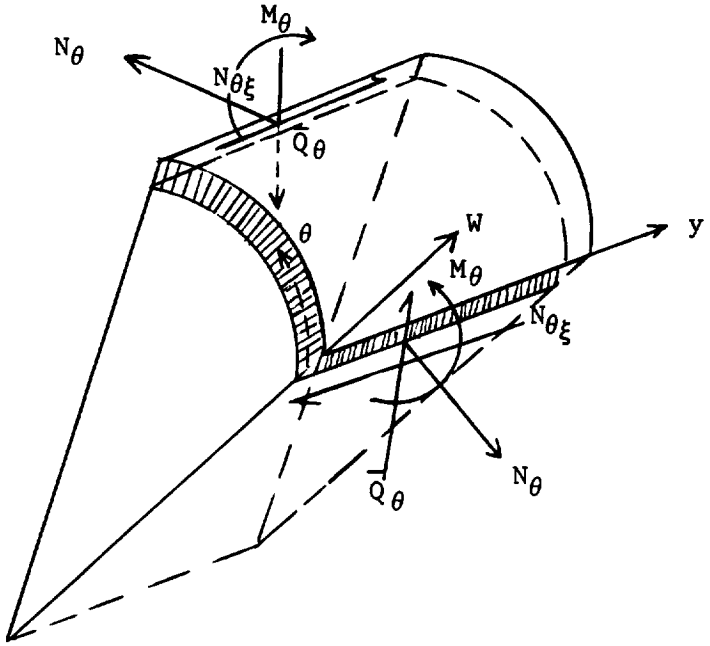

FIGURE III-2 STRESS - RESULTANTS ON GENERATORS OF CYLINDRICAL SHELL

Let the solution of Equations (III-5) be of the form

$$u_c = U\, e^{\gamma\theta + i\omega\left(t - \frac{y \sin\phi}{c}\right)} \tag{III-8a}$$

$$v_c = V\, e^{\gamma\theta + i\omega\left(t - \frac{y \sin\phi}{c}\right)} \tag{III-8b}$$

$$w_c = W\, e^{\gamma\theta + i\omega\left(t - \frac{y \sin\phi}{c}\right)} \tag{III-8c}$$

with U, V, and W constants. Then the substitution of Equations (III-8) into Equations (III-5) yields the following set of equations to be satisfied.

$$\begin{bmatrix} \frac{1-\nu_c}{2}(1+k)\gamma^2 - \psi^2 + \Omega^2 & -\frac{1+\nu_c}{2} i\psi\gamma & -i\psi\left(\frac{1-\nu_c}{2} k\gamma^2 + \nu_c + k\psi^2\right) \\ -\frac{1+\nu_c}{2} i\psi\gamma & \gamma^2 + \Omega^2 - \frac{1-\nu_c}{2}(1+3k)\psi^2 & \left(1 + \frac{3-\nu_c}{2} k\psi^2\right)\gamma \\ -i\psi\left(\frac{1-\nu_c}{2} k\gamma^2 + \nu_c + k\psi^2\right) & \left(1 + \frac{3-\nu_c}{2} k\psi^2\right)\gamma & k\gamma^4 + 2(1-\psi^2)k\gamma^2 \\ & & + 1 - \Omega^2 + k(1+\psi^4) \end{bmatrix} \begin{Bmatrix} U \\ V \\ W \end{Bmatrix} = 0 \tag{III-9a}$$

with

$$\psi = \frac{\omega R \sin\phi}{c} \tag{III-9b}$$

$$\Omega = \sqrt{\frac{\rho_c h_c}{K}}\, \omega R \tag{III-9c}$$

Thus, for Equations (III-9) to be satisfied γ must be a solution of the biquartic equation

$$\alpha_1 \gamma^8 + (2\alpha_1 - \alpha_2\psi^2 + \alpha_3\Omega^2)\gamma^6$$
$$+ \left[\alpha_1 - \alpha_4\psi^2 + \alpha_5\psi^4 - (\alpha_6 + \alpha_7\psi^2)\Omega^2 + \alpha_8\Omega^4\right]\gamma^4$$
$$+ \left[\alpha_2 - \alpha_4 + \alpha_9\psi^2 - \alpha_{10}\psi^4 + (\alpha_{11} + 2\alpha_{12}\psi^2 + \alpha_{13}\psi^4)\Omega^2\right.$$
$$\left. - (\alpha_{14} + 2\alpha_8\psi^2)\Omega^4\right]\gamma^2 + (\alpha_{15} - \alpha_{16}\psi^2 + \alpha_{17}\psi^4)\psi^4$$
$$- (\alpha_{18} + \alpha_{19}\psi^2 + \alpha_{20}\psi^4)\psi^2\Omega^2 + (\alpha_{21} + \alpha_{22}\psi^2 + \alpha_8\psi^4)\Omega^4 = 0 \qquad \text{(III-10)}$$

where

$$\alpha_1 = 1 + k \qquad \text{(III-11a)}$$

$$\alpha_2 = 4 + \frac{7 - 3\nu_c}{2} k + 3\frac{1 - \nu_c}{2} k^2 \qquad \text{(III-11b)}$$

$$\alpha_3 = \frac{3 - \nu_c}{1 - \nu_c} + k \qquad \text{(III-11c)}$$

$$\alpha_4 = 2(4 - \nu_c) + (7 - 5\nu_c) k + 3(1 - \nu_c) k^2 \qquad \text{(III-11d)}$$

$$\alpha_5 = 6 + 3(2 - \nu_c) k - \nu_c^2 k^2 \qquad \text{(III-11e)}$$

$$\alpha_6 = \frac{1}{k} - \frac{5 - \nu_c}{1 - \nu_c} - 2k \qquad \text{(III-11f)}$$

$$\alpha_7 = 3\frac{3 - \nu_c}{1 - \nu_c} + \frac{9 - \nu_c}{2} k \qquad \text{(III-11g)}$$

$$\alpha_8 = \frac{2}{1 - \nu_c} \qquad \text{(III-11h)}$$

$$\alpha_9 = 6 + 3(2 - \nu_c + \nu_c^2)\, k \qquad \text{(III-11i)}$$

$$\alpha_{10} = 4 + \frac{11 - 3\nu_c}{2}\, k + 9\, \frac{1 - \nu_c}{2}\, k^2 \qquad \text{(III-11j)}$$

$$\alpha_{11} = \frac{1}{k} + 2\, \frac{2 - \nu_c}{1 - \nu_c} + k \qquad \text{(III-11k)}$$

$$\alpha_{12} = \frac{1}{k} - \frac{5 + \nu_c - 2\nu_c^2}{1 - \nu_c} - 3\, \frac{3 - \nu_c}{4}\, k \qquad \text{(III-11}\ell\text{)}$$

$$\alpha_{13} = 3\, \frac{3 - \nu_c}{1 - \nu_c} + \frac{5 - 8\nu_c - \nu_c^2}{2(1 - \nu_c)}\, k \qquad \text{(III-11m)}$$

$$\alpha_{14} = \frac{3 - \nu_c}{1 - \nu_c}\, \frac{1}{k} - \frac{3 + \nu_c}{1 - \nu_c} \qquad \text{(III-11n)}$$

$$\alpha_{15} = (1 + 3k)\left[1 + (1 - \nu_c^2)/k\right] \qquad \text{(III-11o)}$$

$$\alpha_{16} = 2\nu_c(1 + 3k) \qquad \text{(III-11p)}$$

$$\alpha_{17} = (1 - k)(1 + 3k) \qquad \text{(III-11q)}$$

$$\alpha_{18} = \frac{3 + 2\nu_c}{k} + 2\, \frac{3 - 2\nu_c}{1 - \nu_c} + 3k \qquad \text{(III-11r)}$$

$$\alpha_{19} = \frac{1}{k} + \frac{3 - 7\nu_c}{1 - \nu_c} \qquad \text{(III-11s)}$$

$$\alpha_{20} = \frac{3 - \nu_c}{1 - \nu_c} + \frac{1 - 3\nu_c}{1 - \nu_c}\, k \qquad \text{(III-11t)}$$

$$\alpha_{21} = \frac{2(1 + k)}{(1 - \nu_c)\, k} \qquad \text{(III-11u)}$$

$$\alpha_{22} = \frac{3 - \nu_c}{(1 - \nu_c)k} + 3 \qquad \text{(III-11v)}$$

Equation (III-10) has eight solutions which are denoted by

$$\gamma = \pm \gamma_n \qquad n = 1, 2, 3, 4 \tag{III-12}$$

The ratios of A and B to C for each value of γ are given by

$$\frac{U}{W} = i\psi\delta \tag{III-13a}$$

$$\frac{V}{W} = -\gamma\epsilon \tag{III-13b}$$

with

$$\delta = \frac{1}{\Delta}\left\{\frac{1-\nu_c}{2} k \gamma^4 - \frac{1-\nu_c}{2}\left(1 - k\Omega^2 + 3\frac{1-\nu_c}{2} k^2\psi^2\right)\gamma^2 + (\nu_c + k\psi^2)\left[\Omega^2 - \frac{1-\nu_c}{2}(1+3k)\psi^2\right]\right\} \tag{III-13c}$$

$$\epsilon = \frac{1}{\Delta}\left\{\frac{1-\nu_c}{2}\gamma^2\left[1 + k + 2\left(1 + \frac{3-\nu_c}{4} k\right) k\psi^2\right] - (1-\nu_c)\cdot\left(\frac{2+\nu_c}{2} + k\psi^2\right)\psi^2 + \left(1 + \frac{3-\nu_c}{2} k\psi^2\right)\Omega^2\right\} \tag{III-13d}$$

$$\Delta = \frac{1-\nu_c}{2}(1+k)\gamma^4 + \gamma^2\left[\left(\frac{3-\nu_c}{2} + \frac{1-\nu_c}{2} k\right)\Omega^2 - (1-\nu_c)\cdot\left(1 + \frac{1-\nu_c}{2}\frac{4+3k}{2} k\right)\psi^2\right] + (\Omega^2 - \psi^2)\left[\Omega^2 - \frac{1-\nu_c}{2}(1+3k)\psi^2\right] \tag{III-13e}$$

Then the expressions for the displacements, slope change, and pertinent stress-resultants may be expressed as

$$u_c = i\psi \sum_{n=1}^{4} \delta_n \left(A_n e^{\gamma_n \theta} + B_n e^{-\gamma_n \theta} \right) \qquad \text{(III-14a)}$$

$$v_c = - \sum_{n=1}^{4} \epsilon_n \gamma_n \left(A_n e^{\gamma_n \theta} - B_n e^{-\gamma_n \theta} \right) \qquad \text{(III-14b)}$$

$$w_c = \sum_{n=1}^{4} \left(A_n e^{\gamma_n \theta} + B_n e^{-\gamma_n \theta} \right) \qquad \text{(III-14c)}$$

$$\frac{1}{R} \left(\frac{\partial w_c}{\partial \theta} - v_c \right) = \frac{1}{R} \sum_{n=1}^{4} \gamma_n \left(1 + \epsilon_n \right) \left(A_n e^{\gamma_n \theta} - B_n e^{-\gamma_n \theta} \right) \qquad \text{(III-14d)}$$

$$N_\theta = \frac{K_c}{R} \sum_{n=1}^{4} \left[1 - \lambda_n^2 \epsilon_n + \nu_c \psi^2 \delta_n + k \left(1 + \gamma_n^2 \right) \right] \left(A_n e^{\gamma_n \theta} + B_n e^{-\gamma_n \theta} \right) \qquad \text{(III-14e)}$$

$$N_{\theta\xi} = \frac{1 - \nu_c}{2} \frac{K_c}{R} i\psi \sum_{n=1}^{4} \gamma_n \left[(1 + k) \delta_n + \epsilon_n - k \right] \left(A_n e^{\gamma_n \theta} - B_n e^{-\gamma_n \theta} \right) \qquad \text{(III-14f)}$$

$$M_\theta = K_c k \sum_{n=1}^{4} \left(1 + \gamma_n^2 - \nu_c \psi^2 \right) \left(A_n e^{\gamma_n \theta} + B_n e^{-\gamma_n \theta} \right) \qquad \text{(III-14g)}$$

$$\overline{Q}_\theta = \frac{K_c k}{R} \sum_{n=1}^{4} \gamma_n \left[1 - (2 - \nu_c) \psi^2 + \gamma_n^2 - \frac{1 - \nu_c}{2} \psi^2 \left(3\epsilon_n - \delta_n \right) \right] \cdot \left(A_n e^{\gamma_n \theta} - B_n e^{-\gamma_n \theta} \right) \qquad \text{(III-14h)}$$

The common factor $e^{i\omega \left(t - \frac{y \sin \phi}{c} \right)}$ has been omitted from each of Equations (III-14) for simplicity.

BOUNDARY CONDITIONS

The 24 constants of integration in the preceding equations are determined by the boundary conditions that must be satisfied at the two lines of contact of the plate and the half cylinder. These are (Figures III-1 and III-3)

$$u_p^+ = u_p^\circ = w_c \qquad \text{(III-15a,b)}$$

$$v_p^+ = v_p^\circ = u_c \qquad \text{(III-15c,d)}$$

$$w_p^+ = w_p^\circ = v_c \qquad \text{(III-15e,f)}$$

$$\frac{\partial w_p^+}{\partial x} = \frac{\partial w_p^\circ}{\partial x} = -\frac{1}{R}\left(\frac{\partial w_c}{\partial \theta} - v_c\right) \qquad \text{(III-15g,h)}$$

$$Q_x^+ - Q_x^\circ + N_\theta = 0 \qquad \text{(III-15i)}$$

$$N_x^+ - N_x^\circ - \bar{Q}_\theta = 0 \qquad \text{(III-15j)}$$

$$N_{xy}^+ - N_{xy}^\circ + N_{\theta\xi} = 0 \qquad \text{(III-15k)}$$

$$M_x^+ - M_x^\circ + M_\theta = 0 \qquad \text{(III-15}\ell\text{)}$$

at $x = R$, $\theta = -\pi/2$ and

$$u_p^\circ = u_p^- = -w_c \qquad \text{(III-16a,b)}$$

$$v_p^\circ = v_p^- = u_c \qquad \text{(III-16c,d)}$$

$$w_p^\circ = w_p^- = -v_c \qquad \text{(III-16e,f)}$$

$$\frac{\partial w_p^\circ}{\partial x} = \frac{\partial w_p^-}{\partial x} = -\frac{1}{R}\left(\frac{\partial w_c}{\partial \theta} - v_c\right) \qquad \text{(III-16g,h)}$$

$$Q_x^o - Q_x^- + N_\theta = 0 \qquad \text{(III-16i)}$$

$$N_x^o - N_x^- - \bar{Q}_\theta = 0 \qquad \text{(III-16j)}$$

$$N_{xy}^o - N_{xy}^- - N_{\theta\xi} = 0 \qquad \text{(III-16k)}$$

$$M_x^o - M_x^- - M_\theta = 0 \qquad \text{(III-16}\ell\text{)}$$

at $x = -R$, $\theta = \pi/2$. From the force-strain relations (see Appendix II) and the continuity conditions for displacements, the last four of Equations (III-15) and of Equations (III-16) may be expressed as

$$D_p \frac{\partial^3}{\partial x^3}\left(w_p^+ - w_p^o\right) - N_\theta = 0 \qquad \text{(III-17a)}$$

$$\frac{E_p h_p}{1-\nu_p^2} \frac{\partial}{\partial x}\left(u_p^+ - u_p^o\right) - \bar{Q}_\theta = 0 \qquad \text{(III-17b)}$$

$$\frac{E_p h_p}{2(1+\nu_p)} \frac{\partial}{\partial x}\left(v_p^+ - v_p^o\right) + N_{\theta\xi} = 0 \qquad \text{(III-17c)}$$

$$D_p \frac{\partial^2}{\partial x^2}\left(w_p^+ - w_p^o\right) - M_\theta = 0 \qquad \text{(III-17d)}$$

at $x = R$, $\theta = -\frac{\pi}{2}$ and

$$D_p \frac{\partial^3}{\partial x^3}\left(w_p^o - w_p^-\right) - N_\theta = 0 \qquad \text{(III-18a)}$$

$$\frac{E_p h_p}{1-\nu_p^2} \frac{\partial}{\partial x}\left(u_p^o - u_p^-\right) - \bar{Q}_\theta = 0 \qquad \text{(III-18b)}$$

$$\frac{E_2 h_2}{2(1+\nu_p)} \frac{\partial}{\partial x}\left(v_p^o - v_p^-\right) - N_{\theta\xi} = 0 \qquad \text{(III-18c)}$$

$$D_p \frac{\partial^2}{\partial x^2}\left(w_p^o - w_p^-\right) + M_\theta = 0 \qquad \text{(III-18d)}$$

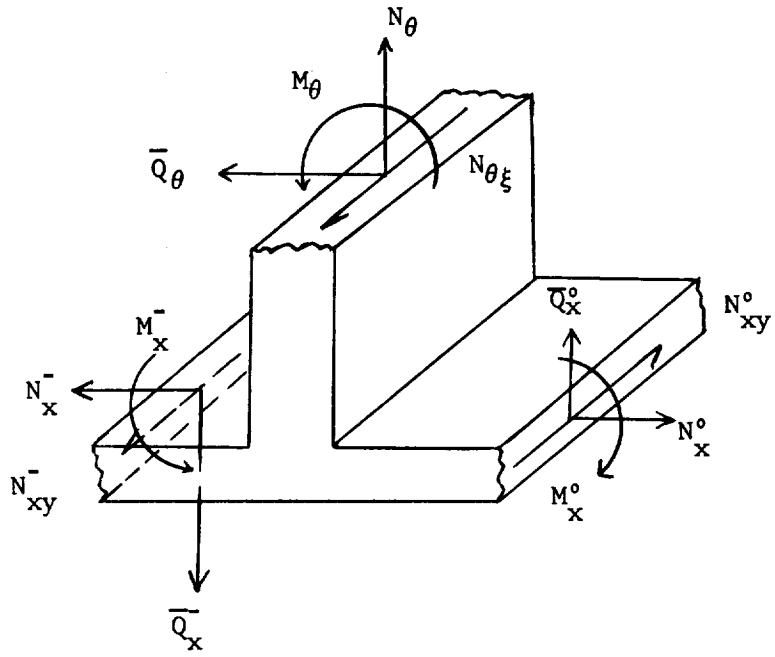

(a) $x = -R,\ \theta = \frac{\pi}{2}$

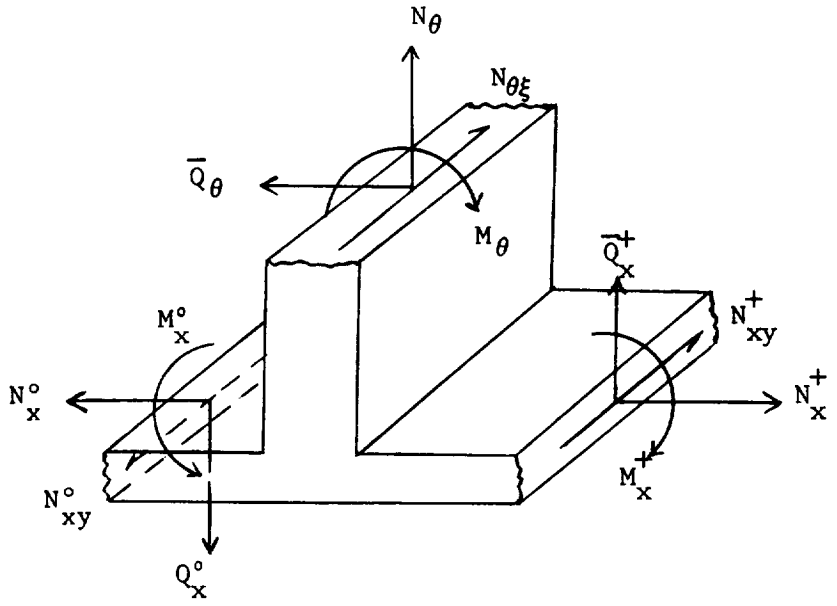

(b) $x = R,\ \theta = -\frac{\pi}{2}$

FIGURE III-3 JOINT FORCES

Substitution of Equations (III-1 - III-3) and (III-14) into Equations (III-15a-h), (III-16a-h), (III-17) and (III-18) and manipulation of the resulting expressions then yields the following set of equations

$$B^+ \pm B^- = \left(e^{-2\lambda\omega R} \pm \frac{1+\delta}{1-\delta}\right)\left(B^\circ \pm C^\circ\right) \pm \frac{2}{1-\delta}\left(\bar{B}^\circ \pm \bar{C}^\circ\right)$$

(III-19a,b)

$$\bar{B}^+ \pm \bar{B}^- = \mp \frac{2\delta}{1-\delta}\left(B^\circ \pm C^\circ\right) + \left(e^{-2\lambda\omega R} \mp \frac{1+\delta}{1-\delta}\right)\left(\bar{B}^\circ \pm \bar{C}^\circ\right)$$

(III-19c,d)

$$A^+ \pm A^- = \left(e^{-\frac{2i\omega R\cos\phi}{c}} \pm \frac{1+\eta}{1-\eta}\right)\left(A^\circ \pm D^\circ\right) \pm \frac{2}{1-\eta}\left(\bar{A}^\circ \pm \bar{D}^\circ\right)$$

(III-19e,f)

$$- \frac{1+\eta}{1-\eta}$$

$$\bar{A}^+ \pm \bar{A}^- = \mp \frac{2\eta}{1-\eta}\left(A^\circ \pm D^\circ\right) + \left(e^{-\frac{2\omega R\alpha}{c}} \mp \frac{1+\eta}{1-\eta}\right)\left(\bar{A}^\circ \pm \bar{D}^\circ\right) + \frac{2\eta}{1-\eta}$$

(III-19g,h)

$$B^\circ + C^\circ = \frac{2}{\Delta_1} \sum_{n=1}^{4} \left[\frac{\bar{\lambda}}{\sin\phi_c}\left(1 - e^{-2\bar{\lambda}\omega R}\right) + \psi\,\delta_n\left(1 + e^{-2\bar{\lambda}\omega R}\right)\right] \cdot$$

$$\left(A_n - B_n\right)\sinh\left(\gamma_n \frac{\pi}{2}\right) = -\frac{\left(1+\nu_p\right)K_c}{E_p h_p R\omega} \sum_{n=1}^{4} \gamma_n \left\{\frac{(1-\nu_c)\,\psi\left[(1+k)\delta_n + \epsilon_n - k\right]}{\frac{\sin\phi}{c}\left[1 - \left(\frac{\bar{\lambda}}{\sin\phi_c}\right)^2\right]}\right.$$

$$\left. + \frac{(1-\nu_p)\,k\left[1 + \gamma_n^2 - (2-\nu_c)\psi^2 + \frac{1-\nu_c}{2}\left(\delta_n - 3\epsilon_n\right)\psi^2\right]}{\lambda\left[1 - \left(\frac{\sin\phi_c}{\lambda}\right)^2\right]}\right\} \cdot \left(A_n - B_n\right)\cosh\left(\gamma_n \frac{\pi}{2}\right)$$

(III-20a,b)

$$\bar{B}^{\circ} + \bar{C}^{\circ} = -\frac{2}{\Delta_1} \sum_{n=1}^{4} \left[\frac{\sin\phi/c}{\lambda} \left(1 - e^{-2\lambda\omega R}\right) + \psi\delta_n \left(1 + e^{-2\lambda\omega R}\right) \right].$$

$$\left(A_n - B_n\right) \sinh\left(\gamma_n \frac{\pi}{2}\right) = \frac{(1+\nu_p)K_c}{E_p h_p R\omega} \sum_{n=1}^{4} \left\{ \frac{(1-\nu_c)\psi\left[\left(1+k\right)\delta_n + \epsilon_n - k\right]}{\frac{\sin\phi}{c}\left[1 - \left(\frac{\lambda}{\sin\phi/c}\right)^2\right]} \right.$$

$$\left. + \frac{\left(\sin\phi/c\right)^2 (1-\nu_p)k\left[1 + \gamma_n^2 - (2-\nu_c)\psi^2 + \frac{1-\nu}{2}\left(\delta_n - \epsilon_n\right)\psi^2\right]}{\lambda^2 \bar{\lambda}\left[1 - \left(\frac{\sin\phi/c}{\lambda}\right)^2\right]} \right\}$$

$$\cdot \left(A_n - B_n\right) \cosh\left(\gamma_n \frac{\pi}{2}\right) \qquad \text{(III-20c,d)}$$

$$A^{\circ} - D^{\circ} = \frac{2}{\Delta_4} \sum_{n=1}^{4} \left[\frac{\omega R\alpha}{c} \left(1 + e^{-2\omega\alpha R/c}\right)\epsilon_n - \left(1 - e^{-2\omega\alpha R/c}\right)\left(1 + \epsilon_n\right) \right].$$

$$\gamma_n \left(A_n - B_n\right) \cosh\left(\gamma_n \frac{\pi}{2}\right) = -1 - \frac{K_c}{2D_p\left(\frac{\omega}{c}\right)^2} \sum_{n=1}^{4}$$

$$\left\{ \left(1 + \gamma_n^2 - \nu_c \psi^2\right)k - \frac{ic}{\omega R \cos\phi}\left[1 - \gamma_n^2 \epsilon_n + \nu_c \psi^2 \delta_n + k(1+\gamma_n^2)\right] \right\}.$$

$$\left(A_n - B_n\right) \sinh\left(\gamma_n \frac{\pi}{2}\right) \qquad \text{(III-20e,f)}$$

$$\bar{A}^{\circ} - \bar{D}^{\circ} = -\frac{2}{\Delta_4} \sum_{n=1}^{4} \left[\frac{i\omega R \cos\phi}{c} \left(1 + e^{\frac{-2i\omega R \cos\phi}{c}}\right)\epsilon_n - \left(1 - e^{\frac{-2i\omega R \cos\phi}{c}}\right)\left(1 + \epsilon_n\right)\right] \gamma_n \left(A_n - B_n\right) \cosh\left(\gamma_n \frac{\pi}{2}\right)$$

$$= \frac{K_c}{2D_p\left(\frac{\omega}{c}\right)^2} \sum_{n=1}^{4} \left\{ \left(1 + \gamma_n^2 - \nu_c \psi^2\right)k + \frac{c}{\omega R \alpha}\left[1 - \gamma_n^2 \epsilon_n + \nu_c \psi^2 \delta_n + k\left(1 + \gamma_n^2\right)\right]\right\} \cdot$$

$$\left(A_n - B_n\right) \sinh\left(\gamma_n \frac{\pi}{2}\right) \qquad \text{(III-20g,h)}$$

$$B^{\circ} - C^{\circ} = -\frac{2}{\Delta_2} \sum_{n=1}^{4} \frac{\bar{\lambda}}{\sin\phi/c}\left[\left(1 + e^{-2\bar{\lambda}\omega R}\right) + \psi\delta_n \left(1 - e^{-2\bar{\lambda}\omega R}\right)\right] \cdot$$

$$\left(A_n + B_n\right) \cosh\left(\gamma_n \frac{\pi}{2}\right) = \frac{(1+\nu_p)K_c}{E_p h_p R \omega} \sum_{n=1}^{4} \gamma_n \cdot$$

$$\left\{ \frac{(1-\nu_c)\psi\left[(1+k)\delta_n + \epsilon_n - k\right]}{\frac{\sin\phi}{c}\left[1 - \left(\frac{\bar{\lambda}}{\sin\phi/c}\right)^2\right]} + \frac{k(1-\nu_p)\left[1 + \gamma_n^2 - (2-\nu_c)\psi^2 + \frac{1-\nu_c}{2}\left(\delta_n - 3\epsilon_n\right)\psi^2\right]}{\lambda\left[1 - \left(\frac{\sin\phi/c}{\lambda}\right)^2\right]} \right\} \cdot$$

$$\left(A_n + B_n\right) \sinh\left(\gamma_n \frac{\pi}{2}\right) \qquad \text{(III-21a,b)}$$

$$\bar{B}^\circ - \bar{C}^\circ = \frac{2}{\Delta_2} \sum_{n=1}^{4} \left[\frac{\sin\phi/c}{\lambda} \left(1 + e^{-2\lambda\omega R}\right) + \psi\delta_n \left(1 - e^{-2\lambda\omega R}\right) \right].$$

$$\left(A_n + B_n\right) \cosh\left(\gamma_n \frac{\pi}{2}\right) = -\frac{(1+\nu_p)K_c}{E_p h_p R \omega} \sum_{n=1}^{4} \gamma_n \left\{ \frac{(1-\nu_c)\psi\left[(1+k)\delta_n + \epsilon_n - k\right]}{\frac{\sin\phi}{c}\left[1 - \left(\frac{\bar{\lambda}}{\sin\phi/c}\right)^2\right]} \right.$$

$$\left. + \frac{\left(\sin\phi/c\right)^2 (1-\nu_p)k \left[1 + \gamma_n^2 - (2-\nu_c)\psi^2 + \frac{1-\nu_c}{2}\left(\delta_n - 3\epsilon_n\right)\psi^2\right]}{\lambda^2 \bar{\lambda}\left[1 - \left(\frac{\sin\phi/c}{\lambda}\right)^2\right]} \right\}.$$

$$\left(A_n + B_n\right) \sinh\left(\gamma_n \frac{\pi}{2}\right) \qquad \text{(III-21c,d)}$$

$$A^\circ + D^\circ = -\frac{2}{\Delta_3} \sum_{n=1}^{4} \left[\frac{\omega R\alpha}{c} \left(1 - e^{-2\omega\alpha R/c}\right) \epsilon_n - \left(1 + e^{-2\omega\alpha R/c}\right)\left(1 + \epsilon_n\right) \right].$$

$$\gamma_n \left(A_n + B_n\right) \sinh\left(\gamma_n \frac{\pi}{2}\right) = 1 + \frac{K_c}{2D_p\left(\frac{\omega}{c}\right)^2} \cdot$$

$$\sum_{n=1}^{4} \left\{ \left(1 + \gamma_n^2 - \nu_c \psi^2\right)k - \frac{ic}{\omega R \cos\phi}\left[1 - \gamma_n^2 \epsilon_n + \nu_c \psi^2 \delta_n + k\left(1 + \gamma_n^2\right)\right] \right\}.$$

$$\left(A_n + B_n\right) \cosh\left(\gamma_n \frac{\pi}{2}\right) \qquad \text{(III-21e,f)}$$

$$\bar{A}^{\circ} + \bar{D}^{\circ} = \frac{2}{\Delta_3} \sum_{n=1}^{4} \left[\frac{i\omega R \cos\phi}{c} \left(1 - e^{-2i\omega R \cos\phi/c}\right) \epsilon_n \right.$$

$$\left. - \left(1 + e^{-2i\omega R \cos\phi/c}\right)\left(1 + \epsilon_n\right)\right] \gamma_n \left(A_n + B_n\right) \sinh\left(\gamma_n \frac{\pi}{2}\right)$$

$$= - \frac{K_c}{2D_p\left(\frac{\omega}{c}\right)^2} \sum_{n=1}^{4} \left\{ \left(1 + \gamma_n^2 - \nu_c \psi^2\right)k + \frac{c}{\omega R \alpha} \cdot \right.$$

$$\left. \left[1 - \gamma_n^2 \epsilon_n + \nu_c \psi^2 \delta_n + k\left(1 + \gamma_n^2\right)\right] \right\} \left(A_n + B_n\right) \cosh\left(\gamma_n \frac{\pi}{2}\right) \qquad \text{(III-21g,h)}$$

with

$$\delta = \frac{\left(\sin\phi/c\right)^2}{\lambda \bar{\lambda}} \qquad \text{(III-22a)}$$

$$\eta = \frac{i \cos\phi}{\alpha} \qquad \text{(III-22b)}$$

$$\left.\begin{matrix}\Delta_1 \\ \Delta_2\end{matrix}\right\} = \frac{\bar{\lambda}}{\sin\phi/c} \left(1 \pm e^{-2\lambda\omega R}\right)\left(1 \mp e^{-2\lambda\omega R}\right)$$

$$- \frac{\sin\phi/c}{\lambda} \left(1 \mp e^{-2\lambda\omega R}\right)\left(1 \pm e^{-2\bar{\lambda}\omega R}\right) \qquad \text{(III-22c,d)}$$

$$\left.\begin{matrix}\Delta_3 \\ \Delta_4\end{matrix}\right\} = \frac{\omega R}{c} \left[\alpha \left(1 \mp e^{-2\omega\alpha R/c}\right)\left(1 \pm e^{-2i\omega R \cos\phi/c}\right)\right.$$

$$\left. - i \cos\phi \left(1 \pm e^{-2\omega\alpha R/c}\right)\left(1 \mp e^{-2i\omega R \cos\phi/c}\right)\right] \qquad \text{(III-22e,f)}$$

It will be seen that Equations (III-20a, d, f, and h) constitute four equations for the coefficients $(A_n - B_n)$ $(n = 1, 2, 3, 4)$ while Equations (III-21b, d, f, and h) constitute four equations for the coefficients $(A_n + B_n)$ $(n = 1, 2, 3, 4)$. Thus, the solution of the problem has been reduced to the solution of two independent sets of four equations.

APPENDIX IV

ENERGY TRANSFER IN VARIOUS STRUCTURAL SYSTEMS

TIME AVERAGES OF HARMONIC COMPLEX QUANTITIES

In what follows we shall be dealing with time averages of quantities of the form $\left(\text{Re } A\, e^{i\omega t}\right)\left(\text{Re } B\, e^{i\omega T}\right)$, where A and B are complex numbers. The integration of the quantities are carried out for one period $T = \frac{2\pi}{\omega}$.

$$\frac{1}{T}\int_0^T \left(\text{Re } Ae^{i\omega t}\right)\left(\text{Re } Be^{i\omega t}\right) dt = \frac{1}{4T}\int_0^T \left(Ae^{i\omega t} + \tilde{A}e^{-i\omega t}\right)\cdot$$

$$\left(Be^{i\omega t} + \tilde{B}e^{-i\omega t}\right) dt = \frac{1}{4T}\int_0^T \left[A\,Be^{2i\omega t} + \tilde{A}\,\tilde{B}e^{-2i\omega t}\right.$$

$$\left. + \left(A\,\tilde{B} + \tilde{A}\,B\right)\right] dt = \frac{1}{4}\left(A\,\tilde{B} + \tilde{A}\,B\right) \qquad \text{(IV-1)}$$

where the tilde over a quantity indicates the complex conjugate of that quantity. If A is equal to B, the right-hand-side of Equation (IV-1) becomes $\frac{1}{2}\,A\,\tilde{A}$.

AVERAGE INPUT POWER

The average input power per unit width for a flat plate governed by a Kirchhoff plate theory is given by (Figure IV-19 and Appendix II)

$$P_i = \frac{1}{T}\int_0^T \left(\bar{Q}_x \frac{\partial w}{\partial t} - M_x \frac{\partial^2 w}{\partial x \partial t}\right) dt$$

$$= \frac{D}{T}\int_0^T \left\{\left(\frac{\partial^2 w}{\partial x^2} + \nu\frac{\partial^2 w}{\partial y^2}\right)\frac{\partial^2 w}{\partial x \partial t} - \left[\frac{\partial^3 w}{\partial x^3} + (2-\nu)\frac{\partial^3 w}{\partial x \partial y^2}\right]\frac{\partial w}{\partial t}\right\} dt$$

(IV-2)

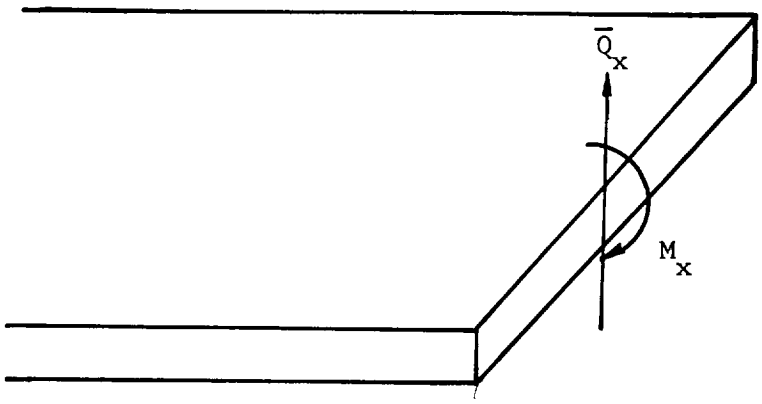

(a)

Kirchhoff Theory Plate Forces

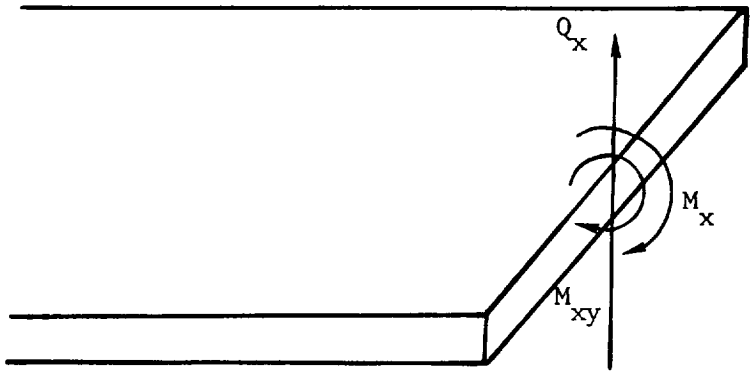

(b)

Mindlin Theory Plate Forces

FIGURE IV-1 STRESS RESULTANTS ALONG A PLATE BOUNDARY

with w_i given by

$$w = \text{Re } e^{i\omega\left(t + \frac{x}{c}\right)} \qquad \text{(IV-3)}$$

equation (IV-2) becomes

$$P_i = \frac{\omega^4 D}{c^3 T} \int_0^T \left\{ \left[\text{Re } e^{i\omega\left(t + \frac{x}{c}\right)} \right]^2 + \left[\text{Re } ie^{i\omega\left(t + \frac{x}{c}\right)} \right]^2 \right\} dt$$

$$= \frac{\omega^4 D}{c^3} \qquad \text{(IV-4a)}$$

It should be noted that the input power is actually constant in this case. Since c is given by

$$c = c^* = \sqrt[4]{\frac{\omega^2 D}{\rho h}} \qquad \text{(IV-4b)}$$

equation (IV-4a) may be written as

$$P_i = \rho h \omega^2 c^* \qquad \text{(IV-4c)}$$

If shear deformations are included, the input power is given by (see Figure IV-1b and Appendix I)

$$P_i = \frac{1}{T} \int_0^T \left(M_x \frac{\partial \psi_x}{\partial t} + M_{xy} \frac{\partial \psi_y}{\partial t} + Q_x \frac{\partial w}{\partial t} \right) dt$$

$$= \frac{1}{T} \int_0^T \left\{ D\left[\left(\frac{\partial \psi_x}{\partial x} + \nu \frac{\partial \psi_y}{\partial y} \right) \frac{\partial \psi_x}{\partial t} + \frac{1-\nu}{2} \left(\frac{\partial \psi_y}{\partial x} + \frac{\partial \psi_x}{\partial y} \right) \frac{\partial \psi_y}{\partial t} \right] \right.$$

$$\left. + G' h \left(\frac{\partial w}{\partial x} + \psi_x \right) \frac{\partial w}{\partial t} \right\} dt \qquad \text{(IV-5)}$$

With the deformations given by (Appendix I)

$$w = e^{i\omega\left(t + \frac{x}{c}\right)} \qquad \text{(IV-6a)}$$

$$\psi_x = \frac{-i\omega}{c} \left(1 - \frac{\rho c^2}{G'}\right) e^{i\omega\left(t + \frac{x}{c}\right)} \qquad \text{(IV-6b)}$$

$$\psi_y = 0$$

Equation (IV-5) becomes

$$P_i = \frac{\omega^4 D}{c^3 T}\int_o^T \left\{ \left(1 - \frac{\rho c^2}{G'}\right)^2 \left[\text{Re } e^{i\omega\left(t + \frac{x}{c}\right)}\right]^2 + \frac{\rho h c^4}{\omega^2 D}\left[\text{Re } ie^{i\omega\left(t + \frac{x}{c}\right)}\right]^2 \right\} dt$$

$$= \frac{\omega^4 D}{2c^3}\left[\left(1 - \frac{\rho c^2}{G'}\right)^2 + \frac{\rho h c^4}{\omega^2 D}\right] \qquad \text{(IV-7)}$$

The wave speed c in this case is given by

$$\frac{1}{c} = \frac{1}{c^*}\left\{\sqrt{1 + \left[\tfrac{1}{2}\left(1 - \frac{1-\nu}{2}\kappa^2\right)\Phi\right]^2} + \tfrac{1}{2}\left(1 + \frac{1-\nu}{2}\kappa^2\right)\Phi\right\}^{\frac{1}{2}} \qquad \text{(IV-8a)}$$

with

$$\Phi = \left(\frac{c^*}{\sqrt{G'/\rho}}\right)^2 \qquad \text{(IV-8b)}$$

Then Equation (IV-7) becomes

$$\frac{P_i}{\rho h \omega^2 c^*} = \frac{1 - \tfrac{1}{2}\left(1 - \frac{1-\nu}{2}\kappa^2\right)\Phi\sqrt{1 + \left[\tfrac{1}{2}\left(1 - \frac{1-\nu}{2}\kappa^2\right)\Phi\right]^2} + \left[\tfrac{1}{2}\left(1 - \frac{1-\nu}{2}\kappa^2\right)\Phi\right]^2}{\sqrt{\sqrt{1 + \left[\tfrac{1}{2}\left(1 - \frac{1-\nu}{2}\kappa^2\right)\Phi\right]^2} + \tfrac{1}{2}\left(1 + \frac{1-\nu}{2}\kappa^2\right)\Phi}}$$

(IV-9)

The quantity given is thus the ratio of the power required for the Mindlin and Kirchhoff plate theories to yield a flexural wave having a given transverse amplitude. The ratio is less than unity for all values of Φ, ranging from approximately $1 - \frac{3}{4}\Phi$ for every small Φ to $\frac{1}{2\sqrt{\Phi}}$ for large Φ. It should be noted, however, that Equation (IV-9) is valid only for $\Phi < \sqrt{\frac{2}{(1-\nu)\kappa^2}}$ (Appendix I).

ORTHOGONALITY RELATIONSHIPS FOR AVERAGE POWER EXPRESSIONS

We can show generally that the average power involved in the forces of one mode of motion moving through the displacements of another mode is zero. For the Kirchhoff flat plate, for example, with

$$w_o = \text{Re } F(x)\ e^{i\omega\left(t - \frac{y \sin\phi}{c}\right)} \tag{IV-10}$$

with the average output flexural power given by an equation of the form of Equation (IV-2), and with use of Equation (IV-1) we have

$$\begin{aligned} P_{BK} = \frac{i\omega D}{4} \Bigg\{ & \left[\frac{d^2\tilde{F}}{dx^2} - \nu\left(\frac{\omega \sin\phi}{c}\right)^2 \tilde{F} \right] \frac{dF}{dx} \\ & - \left[\frac{d^2F}{dx^2} - \nu\left(\frac{\omega \sin\phi}{c}\right)^2 F \right] \frac{d\tilde{F}}{dx} \\ & - \left[\frac{d^3\tilde{F}}{dx^3} - (2-\nu)\left(\frac{\omega \sin\phi}{c}\right)^2 \frac{d\tilde{F}}{dx} \right] F \\ & + \left[\frac{d^3F}{dx^3} - (2-\nu)\left(\frac{\omega \sin\phi}{c}\right)^2 \frac{dF}{dx} \right] \tilde{F} \Bigg\} \\ = \frac{i\omega D}{4} \Bigg[& \frac{d^3F}{dx^3} \tilde{F} - \frac{d^3\tilde{F}}{dx^3} F - \frac{d^2F}{dx^2} \frac{d\tilde{F}}{dx} \\ & + \frac{d^2\tilde{F}}{dx^2} \frac{dF}{dx} - 2\left(\frac{\omega \sin\phi}{c}\right)^2 \left(\frac{dF}{dx} \tilde{F} - \frac{d\tilde{F}}{dx} F \right) \Bigg] \end{aligned} \tag{IV-11}$$

However, F and $\tilde{F}$ satisfy the equation (Appendix II)

$$\frac{d^4(F,\tilde{F})}{dx^4} - 2\left(\frac{\omega \sin\phi}{c}\right)^2 \frac{d^2(F,\tilde{F})}{dx^2} - \frac{\omega^4}{c^4}(1 - \sin^4\phi)(F,\tilde{F}) = 0 \tag{IV-12}$$

If we multiply the equation for F by $\tilde{F}$, the equation for $\tilde{F}$ by F, and subtract the two we have, after some manipulation

$$\frac{d}{dx}\left[\tilde{F}\frac{d^3F}{dx^3} - F\frac{d^3\tilde{F}}{dx^3} - \frac{d^2F}{dx^2}\frac{d\tilde{F}}{dx} + \frac{d^2\tilde{F}}{dx^2}\frac{dF}{dx}\right.$$

$$\left. - 2\left(\frac{\omega \sin\phi}{c}\right)^2\left(\frac{dF}{dx}\tilde{F} - \frac{d\tilde{F}}{dx}F\right)\right] = 0 \qquad \text{(IV-13)}$$

which states, then, that the average power is a constant and thus is independent of x. The implication of this result is that any product terms in Equation (IV-11) which are functions of x can be ignored. This further implies that the modes are orthogonal and that only exponential solutions having pure imaginary characteristics contribute to the average power.

For the Mindlin plate the deformations are given by (Appendix I)

$$w = \text{Re } W(x)\ e^{i\omega\left(t - \frac{y \sin\phi}{c}\right)} \qquad \text{(IV-14a)}$$

$$\psi_x = \text{Re } X(x)\ e^{i\omega\left(t - \frac{y \sin\phi}{c}\right)} \qquad \text{(IV-14b)}$$

$$\psi_y = \text{Re } Y(x)\ e^{i\omega\left(t - \frac{y \sin\phi}{c}\right)} \qquad \text{(IV-14c)}$$

with the average output flexural energy given by an equation of the form of Equation (IV-5), the use of Equation (IV-1) yields

$$P_{BM} = \frac{i\omega D}{4}\left\{\left(\frac{d\tilde{X}}{dx} + i\nu\frac{\omega \sin\phi}{c}\tilde{Y}\right)X - \left(\frac{dX}{dx}\right.\right.$$

$$\left. - i\nu\frac{\omega \sin\phi}{c}Y\right)\tilde{X} + \frac{1-\nu}{2}\left[\left(\frac{d\tilde{Y}}{dx} + i\frac{\omega \sin\phi}{c}\tilde{X}\right)Y\right.$$

$$\left.\left. - \left(\frac{dY}{dx} - i\frac{\omega \sin\phi}{c}X\right)\tilde{Y}\right] + \frac{G'h}{D}\left[\left(\frac{d\tilde{W}}{dx} + \tilde{X}\right)W\right.\right.$$

$$- \left(\frac{dW}{dx} + X \right) \tilde{W} \Bigg| = \frac{i\omega D}{4} \left[X \frac{d\tilde{X}}{dx} - \tilde{X} \frac{dX}{dx} + \frac{1-\nu}{2} \left(Y \frac{d\tilde{Y}}{dx} \right.\right.$$

$$\left. - \tilde{Y} \frac{dY}{dx} \right) + \frac{1+\nu}{2} i \frac{\omega \sin\phi}{c} \left(\tilde{X}Y + X\tilde{Y} \right)$$

$$\left. + \frac{G'h}{D} \left(W \frac{d\tilde{W}}{dx} - \tilde{W} \frac{dW}{dx} + \tilde{X}W - X\tilde{W} \right) \right] \qquad \text{(IV-15)}$$

But W, X, and Y satisfy the equations (Appendix I)

$$\frac{d^2X}{dx^2} + \left[\frac{\rho\omega^2}{E/(1-\nu^2)} - \frac{G'h}{D} - \frac{1-\nu}{2} \left(\frac{\omega \sin\phi}{c} \right)^2 \right] X - i \frac{1+\nu}{2}$$

$$\frac{\omega \sin\phi}{c} \frac{dY}{dx} - \frac{G'h}{D} \frac{dW}{dx} = 0 \qquad \text{(IV-16a)}$$

$$- i \frac{1+\nu}{2} \frac{\omega \sin\phi}{c} \frac{dX}{dx} + \frac{1-\nu}{2} \frac{d^2Y}{dx^2} + \left[\frac{\rho\omega^2}{E/(1-\nu^2)} - \frac{G'h}{D} - \right.$$

$$\left. - \left(\frac{\omega \sin\phi}{c} \right)^2 \right] Y + i \frac{G'h}{D} \frac{\omega \sin\phi}{c} W = 0 \qquad \text{(IV-16b)}$$

$$\frac{G'h}{D} \left[\frac{dX}{dx} - i \frac{\omega \sin\phi}{c} Y + \frac{d^2W}{dx^2} - \left(\frac{\sin^2\phi}{c} - \frac{\rho}{G'} \right) \omega^2 W \right] = 0$$

and $\tilde{X}$, $\tilde{Y}$, and $\tilde{W}$ satisfy the complex conjugates of Equations (IV-16). Now multiply the three equations of the first set respectively by $\tilde{X}$, $\tilde{Y}$, and $\tilde{W}$, add the three resulting expressions, and subtract from it the sum of the three equations of the second set multiplied by X, Y, and W respectively to obtain the result that the derivative of Equation (IV-15) is zero. Thus, conclusions similar to those for the Kirchhoff plate hold.

For inplane motion of either a Kirchhoff or Mindlin plate the average power involved in extensional motion is given by (Appendix II)

$$P_E = \frac{K}{T}\int_0^T \left[\left(\frac{\partial u}{\partial x} + \frac{\partial v}{\partial y}\right)\frac{\partial u}{\partial t} + \frac{1-\nu}{2}\left(\frac{\partial u}{\partial y} + \frac{\partial v}{\partial x}\right)\frac{\partial v}{\partial t}\right] dt \qquad \text{(IV-17)}$$

with u and v given by (Appendix II)

$$u = \mathrm{Re}\, U(x)\ e^{i\omega\left(t - \frac{y\sin\phi}{c}\right)} \qquad \text{(IV-18a)}$$

$$v = \mathrm{Re}\, V(x)\ e^{i\omega\left(t - \frac{y\sin\phi}{c}\right)} \qquad \text{(IV-18b)}$$

Equation (IV-17) becomes

$$P_E = \frac{iK\omega}{4}\left\{\left(\frac{d\tilde{U}}{dx} + i\nu\frac{\omega\sin\phi}{c}\tilde{V}\right)U - \left(\frac{dU}{dx} - i\nu\frac{\omega\sin\phi}{c}V\right)\tilde{U} + \frac{1-\nu}{2}\left[\left(\frac{d\tilde{V}}{dx} + i\frac{\omega\sin\phi}{c}\tilde{U}\right)V - \left(\frac{dV}{dx} - i\frac{\omega\sin\phi}{c}U\right)\tilde{V}\right]\right\}$$

$$= \frac{iK\omega}{4}\left[U\frac{d\tilde{U}}{dx} - \tilde{U}\frac{dU}{dx} + \frac{1+\nu}{2}i\frac{\omega\sin\phi}{c}\left(U\tilde{V} + \tilde{U}V\right) + \frac{1-\nu}{2}\left(V\frac{d\tilde{V}}{dx} - \tilde{V}\frac{dV}{dx}\right)\right] \qquad \text{(IV-19)}$$

But U and V satisfy the equations (Appendix II)

$$\frac{d^2U}{dx^2} - \frac{1-\nu}{2}\omega^2\left(\frac{\sin^2\phi}{c^2} - \frac{\rho}{G}\right)U - \frac{1+\nu}{2}i\frac{\omega\sin\phi}{c}\frac{dV}{dx} = 0 \qquad \text{(IV-20a)}$$

$$- \frac{1+\nu}{2} i \frac{\omega \sin\phi}{c} \frac{dU}{dx} + \frac{1-\nu}{2} \frac{d^2V}{dx^2} - \omega^2 \left[\frac{\sin^2\phi}{c^2} - \frac{(1-\nu^2)\rho}{E} \right] V = 0 \qquad \text{(IV-20b)}$$

while $\tilde{U}$ and $\tilde{V}$ satisfy the complex conjugates of Equation (IV-20).

Then multiplying Equations (IV-20) by $\tilde{U}$ and $\tilde{V}$ respectively, adding the two equations and subtracting the sum of the complex conjugates multiplied by U and V respectively yields the result that the derivative of Equation (IV-19) is zero. Thus, the same conclusions apply as for the Kirchhoff and Mindlin plate average bending power.

Finally the case of the integrally connected half cylindrical shell and flat plate combination can be shown to yield similar results. The average power per unit length of the half cylinder is given by (Appendix III)

$$P_o = \frac{1}{T} \int_0^T \left[\frac{M_\theta}{R} \frac{\partial}{\partial t} \left(\frac{\partial w_c}{\partial \theta} - v_c \right) - \bar{Q}_\theta \frac{\partial w_c}{\partial t} + N_{\theta\xi} \frac{\partial u_c}{\partial t} + N_\theta \frac{\partial v_c}{\partial t} \right] dt$$

$$= \frac{K_c}{TR} \int_0^T \left\{ k \left(\frac{\partial^2 w_c}{\partial \theta^2} + w_c + \nu_c \frac{\partial^2 w_c}{\partial \xi^2} \right) \frac{\partial}{\partial t} \left(\frac{\partial w_c}{\partial \theta} - v_c \right) \right.$$

$$- k \left[\frac{\partial^3 w_c}{\partial \theta^3} + \frac{\partial w_c}{\partial \theta} + (2 - \nu_c) \frac{\partial^3 w_c}{\partial \xi^2 \partial \theta} + \frac{1-\nu_c}{2} \left(\frac{\partial^2 u_c}{\partial \xi \partial \theta} - 3 \frac{\partial^2 v_c}{\partial \xi^2} \right) \right] \frac{\partial w_c}{\partial t} + \frac{1-\nu_c}{2} \left[\frac{\partial u_c}{\partial \theta} + \frac{\partial v_c}{\partial \xi} + k \left(\frac{\partial u_c}{\partial \theta} + \frac{\partial^2 w_c}{\partial \xi \partial \theta} \right) \right] \frac{\partial u_c}{\partial t}$$

$$\left. + \left[\frac{\partial v_c}{\partial \theta} + w_c + \nu_c \frac{\partial u_c}{\partial \xi} + k \left(\frac{\partial^2 w_c}{\partial \theta^2} + w_c \right) \right] \frac{\partial v_c}{\partial t} \right\} dt \qquad \text{(IV-21)}$$

With u_c, v_c, and w_c given by (Appendix III)

$$u_c = U(\theta)\ e^{i\,(\omega t - \psi\xi)} \tag{IV-22a}$$

$$v_c = V(\theta)\ e^{i(\omega t - \psi\xi)} \tag{IV-22b}$$

$$W_c = W(\theta)\ e^{i(\omega t - \psi\xi)} \tag{IV-22c}$$

Equation (IV-21) becomes, with the use of Equation (IV-1),

$$\begin{aligned} P_o = \frac{iK_c\omega}{4R} \Bigg\{ k \Bigg[& \frac{dW}{d\theta}\ \frac{d^2\tilde{W}}{d\theta^2} - \frac{d\tilde{W}}{d\theta}\ \frac{d^2W}{d\theta^2} - W\frac{d^3\tilde{W}}{d\theta^3} + \tilde{W}\frac{d^3W}{d\theta^3} \\ & - 2(1-\psi^2)\left(W\frac{d\tilde{W}}{d\theta} - \tilde{W}\frac{dW}{d\theta}\right) - \frac{1-\nu_c}{2} i\psi \left(\frac{Wd\tilde{U}}{d\theta}\right. \\ & \left. - \frac{\tilde{U}dW}{d\theta} - \frac{Ud\tilde{W}}{d\theta} + \frac{\tilde{W}dU}{d\theta}\right) \Bigg] + \left(1 + \frac{3-\nu_c}{2} k\psi^2\right)\left(V\tilde{W} - W\tilde{V}\right) \\ & + \frac{1-\nu_c}{2}(1+k)\left(U\frac{d\tilde{U}}{d\theta} - \tilde{U}\frac{dU}{d\theta}\right) \\ & + \frac{1+\nu_c}{2} i\psi\left(U\tilde{V} + V\tilde{U}\right) + V\frac{d\tilde{V}}{d\theta} - \tilde{V}\frac{dV}{d\theta} \Bigg\} \end{aligned} \tag{IV-23}$$

Now U, V, and W satisfy the Equations (Appendix III)

$$\frac{1-\nu_c}{2}(1+k)\ \frac{d^2U}{d\theta^2} + (\Omega^2 - \psi^2)U - \frac{1+\nu_c}{2} i\psi\frac{dV}{d\theta}$$

$$- \frac{1-\nu_c}{2} i\psi\ \frac{d^2W}{d\theta^2} - i\psi\left(\nu_c + k\psi^2\right)W = 0 \tag{IV-24a}$$

$$- \frac{1+\nu_c}{2} i\psi \frac{dU}{d\theta} + \frac{d^2V}{d\theta^2} + \left[\Omega^2 - \frac{1-\nu_c}{2}(1+3k)\psi^2\right] V$$

$$+ \left(1 + \frac{3-\nu_c}{2} k\psi^2\right) \frac{dW}{d\theta} = 0 \qquad \text{(IV-24b)}$$

$$- \frac{1-\nu_c}{2} i\psi \frac{d^2U}{d\theta^2} - i\psi \left(\nu_c + k\psi^2\right) U + \left(1 + \frac{3-\nu_c}{2} k\psi^2\right) \frac{dV}{d\theta}$$

$$+ k \frac{d^4W}{d\theta^4} + 2(1-\psi^2) k \frac{d^2W}{d\theta^2} + \left[1 + k(1+\psi^4) - \Omega^2\right] W = 0$$

$$\text{(IV-24c)}$$

and $\tilde{U}$, $\tilde{V}$ and $\tilde{W}$ satisfy the complex conjugates of Equations (IV-24). Multiply Equation (IV-24c) by $\tilde{W}$ and subtract from it the sum of Equation (IV-24a) multiplied by $\tilde{U}$ and (IV-24b) multiplied by $\tilde{V}$. Subtract the complex conjugate of the resulting expression from it to obtain the result that the derivative of Equation (IV-23) with respect to θ vanishes. The usual conclusions follow.

AVERAGE TRANSMITTED POWER

The results of the preceding section can be applied to obtain expressions for the average output power in the various structural systems under consideration.

a) Perpendicular Kirchhoff Plates with no Motion of the Joint Line

For this problem the outgoing wave displacement function is given by (Reference 49).

$$W_o = \text{Re}\, C_2' \left(e^{-i\omega|x|} \frac{\cos\phi_2}{c_2^*} - e^{-\omega\alpha_2|x|/c_2^*} \right) e^{i\omega\left(t - \frac{y \sin\phi_2}{c_2^*}\right)}$$

$$\text{(IV-25a)}$$

for $x > 0$ and by the negative of the expression for $x < 0$, with

$$\alpha_2 = \sqrt{1 + \sin^2\phi_2} \qquad \text{(IV-25b)}$$

$$c_2^* = \sqrt[4]{\frac{\omega^2 D_2}{\rho_2 h_2}} \qquad \text{(IV-25c)}$$

The average outgoing power is given by Equation (IV-2), for $x > 0$ and by the negative of Equation (IV-2) for $x < 0$. Then Equations (IV-11) and (IV-13) yield the total output power in both parts of plate 2 as

$$P_o = -2\rho_2 h_2 \omega^2 c_2^* \; C_2' \widetilde{C}_2' \cos\phi_2 \qquad \text{if } \sin\phi_2 = c_2^*/c_1^* \sin\phi_1 < 1$$

$$= 0 \qquad \text{if } \sin\phi_2 = c_2^*/c_1^* \sin\phi_1 > 1 \qquad \text{(IV-26)}$$

b) Perpendicular Kirchhoff Plates with Motion of the Joint Line

For this problem the outgoing wave displacements are (Appendix II)

$$u_2^+ = \mathrm{Re}\left[\left(B_2^+ e^{-\lambda_2\omega x} + \bar{B}_2^+ e^{-\bar{\lambda}_2\omega x}\right) e^{i\omega\left(t - \frac{y\sin\phi_2}{c_2^*}\right)}\right] \qquad \text{(IV-27a)}$$

$$v_2^+ = \mathrm{Re}\left[i\left(\frac{\sin\phi_2/c_2^*}{\lambda_2} B_2^+ e^{-\lambda_2\omega x} + \frac{\bar{\lambda}_2}{\sin\phi_2/c_2^*} \bar{B}_2^+ e^{-\bar{\lambda}_2\omega x}\right) \cdot e^{i\omega\left(t - \frac{y\sin\phi_2}{c_2^*}\right)}\right] \qquad \text{(IV-27b)}$$

$$w_2^+ = \mathrm{Re}\left[\left(A_2^+ e^{-i\omega x\cos\phi_2/c_2^*} + \bar{A}_2^+ e^{-\omega\alpha_2 x/c_2^*}\right) e^{i\omega\left(t - \frac{y\sin\phi_2}{c_2^*}\right)}\right] \qquad \text{(IV-27c)}$$

and for $x < 0$ by

$$u_2^- = \mathrm{Re}\left[\left(B_2^- e^{\lambda_2\omega x} + \bar{B}_2^- e^{\bar{\lambda}_2\omega x}\right) e^{i\omega\left(t - \frac{y\sin\phi_2}{c_2^*}\right)}\right] \qquad \text{(IV-28a)}$$

$$v_2^- = - \mathrm{Re}\left[i\left(\frac{\sin\phi_2/c_2^*}{\lambda_2} B_2^- e^{\lambda_2 \omega x} + \frac{\bar{\lambda}_2}{\sin\phi_2/c_2^*} \bar{B}_2^- e^{\lambda_2 \omega x} \right) e^{i\omega\left(t - \frac{y \sin\phi_2}{c_2^*}\right)} \right] \qquad \text{(IV-28b)}$$

$$w_2^- = \mathrm{Re}\left[\left(A_2^- e^{i\omega x \cos\phi_2/c_2^*} + \bar{A}_2 e^{\omega\alpha_2 x/c_2^*} \right) e^{i\omega\left(t - \frac{y \sin\phi_2}{c_2^*}\right)} \right] \qquad \text{(IV-28c)}$$

The average output power is given by the sum of Equations (IV-2) and (IV-17) for $x > 0$ and by the negative of these expressions for $x < 0$. Then the use of Equations (IV-11) and (IV-19) and the conclusions reached in the preceding section yield

$$P_o = - \left(P_B + P_S \right) \qquad \text{(IV-29a)}$$

where

$$P_B = \rho_2 h_2 \omega^2 c_2^* \cos\phi_2 \left(A_2^+ \tilde{A}_2^+ + A_2^- \tilde{A}_2^- \right) \quad \text{if} \quad \sin\phi_2 = \frac{c_2^*}{c_1^*} \sin\phi_1 < 1 \qquad \text{(IV-29b)}$$

$$= 0 \quad \text{if} \quad \sin\phi_2 = \frac{c_2^*}{c_1^*} \sin\phi_1 > 1$$

and

$$P_S = 0 \quad \text{if} \quad \omega h_2/\sqrt{12} < \frac{1 - \nu}{2} \sqrt{\frac{E_2/(1-\nu_2^2)}{\rho_2}} \sin^2\phi_2$$

$$= \tfrac{1}{2} \omega^2 \rho_2 h_2 \frac{|\bar{\lambda}_2|}{(\sin\phi_2/c_2)^2} \left(\bar{B}_2^+ \tilde{\bar{B}}_2^+ + \bar{B}_2^- \tilde{\bar{B}}_2^- \right)$$

$$\text{if} \quad \frac{1 - \nu_2}{2} \sqrt{\frac{E_2/(1-\nu_2^2)}{\rho_2}} \sin^2\phi_2 < \omega h_2/\sqrt{12} < \sqrt{\frac{E_2/(1-\nu_2^2)}{\rho_2}} \sin^2\phi_2$$

$$= \frac{1}{2}\omega^2\rho_2 h_2 \left[\frac{|\bar{\lambda}_2|}{(\sin\phi_2/c_2)^2} \left(\bar{B}_2^+ \tilde{\bar{B}}_2^+ + \bar{B}_2^- \tilde{\bar{B}}_2^- \right) + \frac{1}{|\lambda_2|} \left(B_2^+ \tilde{B}_2^+ + B_2^- \tilde{B}_2^- \right) \right]$$

$$\text{if} \quad \frac{\omega h_2}{\sqrt{12}} > \sqrt{\frac{E_2/(1-\nu_2^2)}{\rho_2}} \sin^2\phi_2 \qquad \text{(IV-29c)}$$

c) Perpendicular Mindlin Plates with no Motion of the Joint Line

The average outgoing power per unit plate width for a plate edge with $x > 0$ is given by Equation (IV-5) and by the negative of Equation (IV-5) for a plate edge with $x < 0$. The deformations are given by Appendix I, in the case when $\sin\phi_2 = \frac{c_2}{c_1} \sin\phi_1 < 1$, as

$$w_2^+ = \left(A_2^+ e^{-i\omega \frac{|x|\cos\phi_2}{c_2}} + B_2^+ e^{-\omega\alpha_2|x|} \right) e^{i\omega\left(t - \frac{y \sin\phi_2}{c_2}\right)} \qquad \text{(IV-30a)}$$

$$\psi_{x2}^+ = \omega \left[ic_2 \cos\phi_2 \left(\frac{1}{c_2^2} - \frac{\rho_2}{G_2'} \right) A_2^+ e^{-i\omega \frac{|x|\cos\phi_2}{c_2}} + \left(1 + \frac{\rho_2/G_2'}{\alpha_2^2 - \frac{\sin^2\phi_2}{c_2^2}} \right) B_2^+ e^{-\omega\alpha_2|x|} + C_2^+ \sin^2\phi_2 \, e^{-\omega\alpha_2'|x|} \right] \cdot$$

$$e^{i\omega\left(t - \frac{y \sin\phi_2}{c_2}\right)} \qquad \text{(IV-30b)}$$

$$\psi_{y2}^+ = i\omega c_2 \sin\phi_2 \left[\left(\frac{1}{c_2^2} - \frac{\rho_2}{G_2'} \right) A_2^+ e^{-i\omega |x| \cos\phi_2/c_2} + \frac{1}{c_2^2} \left(1 + \frac{\rho_2/G_2'}{\alpha_2^2 - \frac{\sin^2\phi_2}{c_2^2}} \right) B_2^+ e^{-\omega\alpha_2|x|} \right.$$

$$+ \quad \alpha_2' \; C_2^+ \; e^{-\omega \alpha_2' |x|} \Big] e^{i\omega\left(t - \frac{y \sin\phi_2}{c_2}\right)} \qquad \text{(IV-30c)}$$

with, provided $\omega h/\sqrt{12} < \sqrt{\frac{G_2'}{\rho_2}}$,

$$\frac{1}{c_2} = \sqrt[4]{\frac{\rho_2 h_2}{\omega^2 D_2}} \left\{ \sqrt{1 + \left[\tfrac{1}{2} \left(1 - \frac{1-\nu_2}{2} \kappa^2 \right) \Phi_2 \right]^2} + \tfrac{1}{2} \left(1 + \frac{1-\nu_2}{2} \kappa^2 \right) \Phi_2 \right\}^{\frac{1}{2}} \qquad \text{(IV-31a)}$$

$$\alpha_2 = \sqrt[4]{\frac{\rho_2 h_2}{\omega^2 D_2}} \left\{ \sqrt{1 + \left[\tfrac{1}{2} \left(1 - \frac{1-\nu_2}{2} \kappa^2 \right) \Phi_2 \right]^2} \left(1 + \sin^2\phi_2 \right) - \tfrac{1}{2} \left(1 + \frac{1-\nu_2}{2} \kappa^2 \right) \Phi_2 \cos^2\phi_2 \right\}^{\frac{1}{2}} \qquad \text{(IV-31b)}$$

$$\alpha_2' = \sqrt[4]{\frac{\rho_2 h_2}{\omega^2 D_2}} \left\langle \left\{ \sqrt{1 + \left[\tfrac{1}{2} \left(1 - \frac{1-\nu_2}{2} \kappa^2 \right) \Phi_2 \right]^2} + \tfrac{1}{2} \left(1 + \frac{1-\nu_2}{2} \kappa^2 \right) \Phi_2 \right\} \sin^2\phi_2 - \kappa^2 \Phi_2 + \frac{2}{1-\nu_2} \frac{1}{\Phi_2} \right\rangle^{\frac{1}{2}} \qquad \text{(IV-31c)}$$

$$\Phi_2 = \sqrt{\frac{\omega^2 D_2}{\rho_2 h_2}} \Big/ \left(G_2' / \rho_2 \right) \qquad \text{(IV-31d)}$$

Then it can be shown from Equations (IV-15) and the conclusions of the preceding section that

$$P_o = -2\rho_2 h_2 \omega^2 c_2^* \cos\phi_2 \; A_2^+ \tilde{A}_2^+ \cdot \frac{1 - \tfrac{1}{2}\left(1 - \frac{1-\nu_2}{2} \kappa^2\right) \Phi_2 \sqrt{1 + \left[\tfrac{1}{2} \left(1 - \frac{1-\nu_2}{2} \kappa^2 \right) \Phi_2 \right]^2} + \left[\tfrac{1}{2} \left(1 - \frac{1-\nu_2}{2} \kappa^2 \right) \Phi_2 \right]^2}{\sqrt{\sqrt{1 + \left[\tfrac{1}{2} \left(1 - \frac{1-\nu_2}{2} \kappa^2 \right) \Phi_2 \right]^2} + \tfrac{1}{2} \left(1 + \frac{1-\nu_2}{2} \kappa^2 \right) \Phi_2}} \qquad \text{(IV-32)}$$

If $\sin\phi_2 = \frac{c_2}{c_1}\sin\phi_1 > 1$, the outgoing power vanishes.

d) Integrally Joined Half Cylindrical Shell and Flat Plate

For this problem the shell displacements are given by (Appendix III)

$$u_c = i\psi \sum_{n=1}^{4} \delta_n \left(A_n e^{\gamma_n\theta} + B_n e^{-\gamma_n\theta} \right) e^{i(\omega t - \psi\xi)} \qquad \text{(IV-33a)}$$

$$v_c = - \sum_{n=1}^{4} \epsilon_n \gamma_n \left(A_n e^{\gamma_n\theta} - B_n e^{-\gamma_n\theta} \right) e^{i(\omega t - \psi\xi)} \qquad \text{(IV-33b)}$$

$$w_c = \sum_{n=1}^{4} \left(A_n e^{\gamma_n\theta} + B_n e^{-\gamma_n\theta} \right) e^{i(\omega t - \psi\xi)} \qquad \text{(IV-33c)}$$

from Equation (IV-23) and the conclusions reached in the preceding section we have

$$P_o = \sum_n \frac{K_c\omega}{R} i\gamma_n \left\{ \left[1 + \gamma_n^2 - \psi^2\left(1 - \frac{1-\nu}{2}\delta_n + \frac{3-\nu}{4}\epsilon_n\right)\right] k \right.$$

$$\left. - \tfrac{1}{2}\epsilon_n \left(1 + \frac{1+\nu}{2}\psi^2\delta_n - \gamma_n^2\epsilon_n\right) - \frac{1-\nu}{4}(1+k)\psi^2\delta_n^2 \right\}$$

$$\cdot \left(A_n \tilde{A}_n - B_n \tilde{B}_n \right) \qquad \text{(IV-34)}$$

where the summation is over all values of n for which γ_n is pure imaginary.

REFERENCES

1. Lyon, R.H., and Maidanik, G., "Power Flow Between Linearly Coupled Oscillators," J. Acoust. Soc. Am. 34, 623-639, May 1962.

2. Smith, P.W., Jr., "Response and Radiation of Structural Modes Excited by Sound," J. Acoust. Soc. Am. 34, 827, 1962.

3. Maidanik, G., "Response of Ribbed Panels to Reverberant Acoustic Fields," J. Acoust. Soc. Am. 34, 809-826, 1962.

4. Lyon, R.H., and Eichler, E., "Random Vibration of Connected Structures," J. Acoust. Soc. Am. 36, 1344-1354, July 1964.

5. Crocker, M.J., and Price, A.J., "Sound Transmission Using Statistical Energy Analysis," J. Sound and Vibration, 9 (3), 469-486, September 1969.

6. Lyon, R.H., "An Energy Method for Prediction of Noise and Vibration Transmission," Shock, Vibr. and Assoc. Environments, Bull. No. 33, Pt. II, pp. 13-25, 1964.

7. Lyon, R.H., and Maidanik, G., "Statistical Methods in Vibration Analysis," AIAA Journal 2, 1015-1024, June 1964.

8. Smith, P.W., Jr., and Lyon, R.H., "Sound and Structural Vibration," NASA CR-160, March 1965.

9. Lyon, R.H., and Scharton, T.D., "Vibrational-Energy Transmission in a Three-Element Structure," J. Acoust. Soc. Am. 38, 253-261, August 1965.

10. Eichler, E., "Thermal Circuit Approach to Vibrations in Coupled Systems and the Noise Reduction of a Rectangular Box," J. Acoust. Soc. Am. 37, 995-1007, 1965.

11. Ungar, E.E., "Fundamentals of Statistical Energy Analysis of Vibrating Systems," AFFDL-TR-66-52, May 1966.

12. Ungar, E.E., "Mechanical Vibrations," Sec. 6 of Mechanical Design and Systems Handbook, McGraw-Hill Book Co., Inc., New York, 1964.

13. Ungar, E. E., "Statistical Energy Analysis of Vibrating Systems," J. Eng. Ind. 89, No. 4, 626-632, 1967.

14. Lyon, R. H., "Statistical Analysis of Power Injection and Response in Structures and Rooms," J. Acoust. Soc. Am. 45, 545-565, March 1969.

15. Noiseux, D. U., "Measurement of Power Flow in Uniform Beams and Plates," J. Acoust. Soc. Am. 47, 238-247, January 1970.

16. Zeman, J. L., and Bogdanoff, J. L., "A Comment on Complex Structural Response to Random Vibrations," AIAA Journal 7, 7, 1225-1231, July 1969.

17. Newland, D. E., "Calculation of Power Flow Between Coupled Oscillators," J. Sound Vib. 3, 262-276, 1966.

18. Newland, D. E., "Power Flow Between a Class of Coupled Oscillators," J. Acoust. Soc. Am. 43, 553-565, March 1968.

19. Heckl, M. A., "Wave Propagation on Beam-Plate Systems," J. Acoust. Soc. Am. 33, 640-651, 1961.

20. Ungar, E. E., "Transmission of Plate Flexural Waves through Reinforcing Beams; Dynamic Stress Concentrations," J. Acoust. Soc. Am. 33, 633-639, 1961.

21. Manning, J. E., and Maidanik, G., "Radiation Properties of Cylindrical Shells," J. Acoust. Soc. Am. 36, 1691-1698, 1964.

22. Lyon, R. H., "Spatial Response Concentrations in Extended Structures," Trans. ASME, J. Eng. for Ind., Series B, 1967.

23. Dyer, I., "Response of Space Vehicle Structures to Rocket Engine Noise," Ch. 7 of Random Vibration, Vol. 2, Ed. by S. H. Crandall, The MIT Press, Cambridge, Massachusetts, 1963.

24. Skudrzyk, E., "Vibrations of a System with a Finite or an Infinite Number of Resonances," J. Acoust. Soc. Am. 30, 1140-1152, 1958.

25. Kronauer, R. E., and Musa, S. A., "Exchange of Energy Between Oscillations in Weakly Nonlinear Conservative Systems," J. Appl. Mech. 33, No. 2, 451-452, 1966.

26. Franken, P. A., and Lyon, R. H., "Estimation of Sound-Induced Vibrations by Energy Methods, with Applications to the Titan Missile," Shock, Vibration, and Associated Environments, Bull. No. 31, Part III, pp. 12-26, 1963.

27. Heckl, M.A., "Measurements of Absorption Coefficients on Plates," J. Acoust. Soc. Am. 34, 803-808, 1962.

28. Lyon, R.H., "What Good Is Statistical Energy Analysis, Anyway?" Shock and Vibration Digest, Vol. 2, No. 6, June 1970.

29. Ungar, E.E., Koronaios, N., Manning, J.E., "Application of Statistical Energy Analysis to Vibrations of Multipanel Structures" AFFDL-TR-67-79, 1967.

30. Cobble, M.H., "Finite Transform Solution of the Damped Clamped-Clamped Beam Having Distributed Load and Elastic Support, J. Acoust. Soc. Am. 40, 1529-1533, December 1966.

31. Hurty, W.C., and Rubinstein, M.F., Dynamics of Structures, Prentice-Hall, Inc., Englewood Cliffs, New Jersey, First Edition, 1965.

32. Nowacki, W., Dynamics of Elastic Systems, John Wiley and Sons, New York, First Edition, 1963.

33. Hwang, C., and Pi, W.S., "Random Acoustic Response of a Cylindrical Shell," AIAA Journal 7, 12, 2204-2210, December 1969.

34. Kana, D.D., Chu, W.H., and Bessey, R.L., "The Response of Cylindrical Shells to Random Acoustic Excitation Over Broad Frequency Ranges," AIAA Paper 71-331, April 1971.

35. Bolotin, V.V., "On the Density of the Distribution of Natural Frequencies of Thin Elastic Shells," J. Appl. Math. and Mech. 27, No. 2, 538-543 (Transl. from Soviet Journal: Prikhadnaya Matematika y Mekhanika, 27, No. 2, pp. 362-364), 1963.

36. Bolotin, V.V., "The Density of Eigenvalues in Vibration Problems of Elastic Plates and Shells," Proc. of Vibration Problems, Warsaw 4, No. 6, 341-351, 1965.

37. Wilkinson, J.P.D., "Modal Densities of Certain Shallow Structural Elements," J. Acoust. Soc. Am., Vol. 43, No. 2, pp. 245-251, February 1968.

38. Sneddon, I.N., Fourier Transforms, McGraw-Hill Company, New York, 1951.

39. Bendat, J.S., and Piersol, J.S., Measurement and Analysis of Random Data, J. Wiley and Sons, Inc., New York, 1966.

40. Powell, A., "On the Response of Structures to Random Pressures and to Jet Noise in Particular," Ch. 8 of Random Vibration, Vol. I, Ed. by S.H. Crandall, The MIT Press, Cambridge, Massachusetts, 1963.

41. Bolotin, V.V., "The Edge Effect in the Oscillations of Elastic Shells," PMM 24, No. 5, pp. 831-834 (translation pp. 1257-1272), 1960.

42. Bolotin, V.V., Makarov, B.P., Mishenkov, G.V., and Shveiko, Iu. Iu., "An Asymptotic Method for the Study of Natural Frequencies of Elastic Plates," Sbornik Raschety na Prochnost," Vol. 6, Mashgiz, 1960 (in Russian).

43. Hart, F.D., and Desai, V.D., "Additive Property of Modal Density for a Composite Structure," J. Acoust. Soc. Am. 42, 1203, November 1967.

44. Jacobs, L.D., and Lagerquist, D.R., "Finite Element Analysis of Complex Panel Response to Random Loads," AFFDL-TR-68-44, October 1968.

45. Morse, P.M., and Ingard, K.U., Theoretical Acoustics, McGraw-Hill Book Co., New York, 1968.

46. Pope, L.D., "On the Transmission of Sound through Finite Closed Shells: Statistical Energy Analysis, Modal Coupling, and Nonresonant Transmission," J. Acoust. Soc. Am., Vol. 50, No. 3, 1971, pp. 1004-1018.

47. Zeman, J.L., and Bogdanoff, J.L., "Statistical Approach to Complex Random Vibration," J. Acoust. Soc. Am., Vol. 50, No. 3, 1971, pp. 1019-1027.

48. Chen, K.K., and Soong, T.T., "Covariance Properties of Waves Propagating in a Random Medium," J. Acoust, Soc. Am., Vol. 49, No. 5, 1971, pp. 1639-1642.

49. Hwang, C., and Pi, W.S., "Evaluation of Three Analytical Methods for Structures under Random Acoustic Excitation," NASA Contract Report NAS8-26195, Northrop Report NOR-71-102, August 1971.

50. Mindlin, R.D., "Influence of Rotationary Inertia and Shear on Flexural Motions of Isotropic, Elastic Plates," J. Applied Mechanics, 18, 3, pp. 31-38, March 1951.

51. Faran, J.J., and Hill, R. Jr., "Correlations for Signal Reception," Tech. Memo 27, Harvard University Acoustics Research Lab, Cambridge, Mass., Sept 1952.

52. Noiseux, D.U., and Meyer, E.B., "Application of Impedance Theory and Measurements to Structural Vibration," AFFDL-TR-67-182, pp. 146-165, Jan. 1968.

53. Naghdi, P. M., and Cooper, R. M., "Propagation of Elastic Waves in Cylindrical Shells, Including the Effects of Transverse Shear and Rotatory Inertia," J.Acoust. Soc. Am. 28, 56-63, January 1956.

54. Flugge, W., Stresses in Shells, Springer-Verlag, 208-216, 218-219, 245, 1960.

55. Hechl, M., "Vibrations of Point-Driven Cylindrical Shells," J. Acoust. Soc. Am. 34, p. 1553, October 1962.